Tarek Al-Arbi Omar Ganat

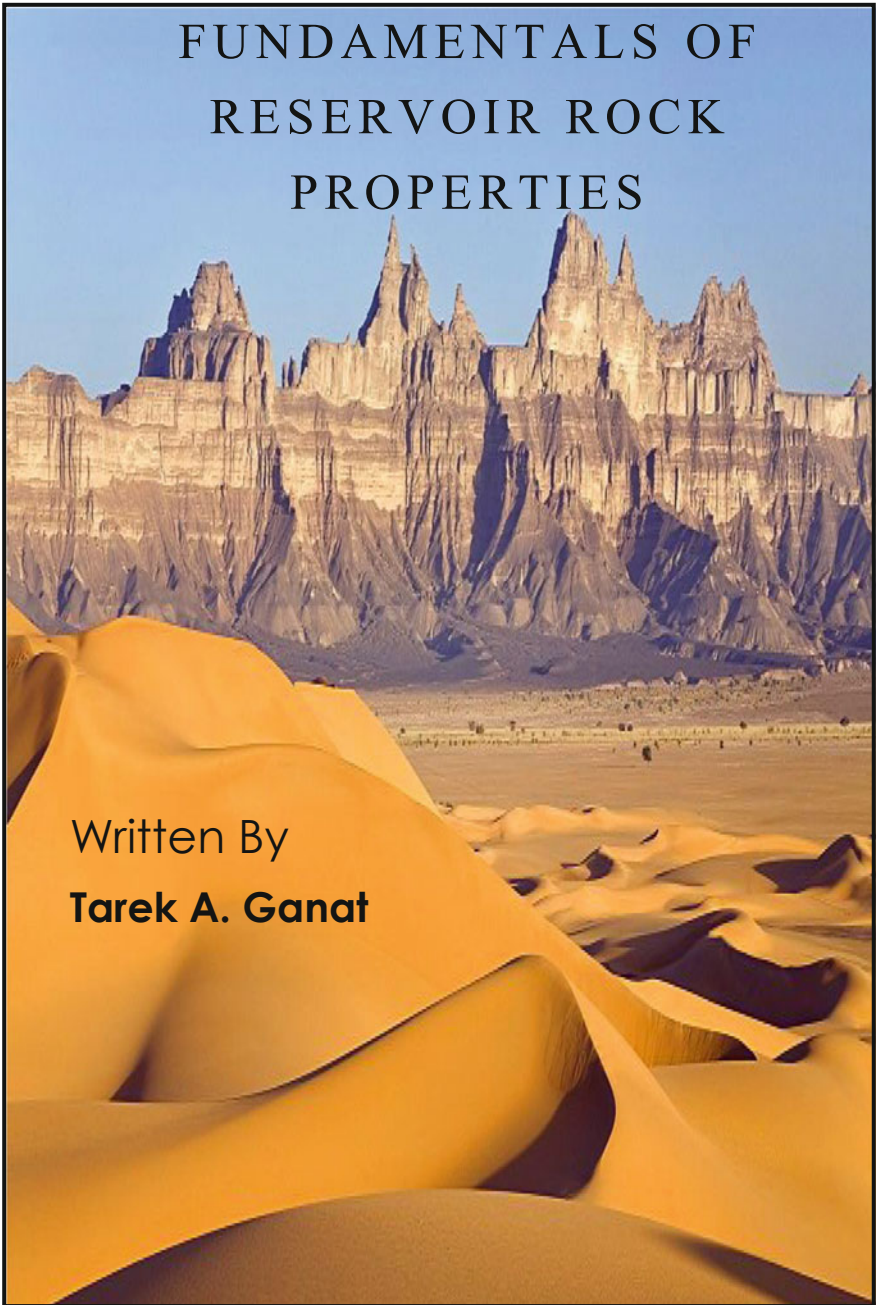# Fundamentals of Reservoir Rock Properties

# Fundamentals of Reservoir Rock Properties

# FUNDAMENTALS OF RESERVOIR ROCK PROPERTIES

Written By

**Tarek A. Ganat**

Tarek Al-Arbi Omar Ganat

# Fundamentals of Reservoir Rock Properties

Springer

Tarek Al-Arbi Omar Ganat ⓘ
Department of Petroleum Engineering
Universiti Teknologi Petronas
Seri Iskender, Malaysia

# Introduction

In general, naturally occurring rocks are saturated with fluids, water, oil, or gas (Amyx et al. 1960). Any formation rock can produce oil, gas, and water which are considered as reservoir rock. A reservoir rock is a rock has an adequate permeability and porosity to permit fluids flow, to accumulate and to extract in viable volumes (Daniel and Lapedes 1978).

Normally, hydrocarbons exist in sandstones, carbonate, and shales formations and also are present in metamorphic and igneous rocks (basement rock). The principal reservoir rocks are sandstone and carbonate formations. Typically, the physical properties and the composition of the sandstone and carbonate reservoir rocks are varying (Cecil 1949). Therefore, known the physical properties of reservoir rocks, reservoir engineers can estimate the hydrocarbon reserve and identified the ultimate reservoir recovery and determine the best effective production that is economically viable under the existing condition.

The scale of investigation used in reservoir studies is microscopic (geological thin section), macroscopic (wireline log, core plug), megascopic (reservoir modelling grid cell), and gigascopic (well test). In this section, the focus will be on microscopic and megascopic scales to characterise the reservoir. By studying a core sample of any reservoir rock under telescopic equipments, to determine the reservoir rock and the reservoir textures either solid or brittle. The reservoir pore space is generally known as voidage space (pores media), where the fluids can either move in and fill in the apertures or pass throughout the void space if the pores are connected. From the shape and size of the connected apertures in a reservoir, the estimation of the ability of the reservoir rock to store and transfer the fluids can be evaluated. Hence, the reservoir rock physical properties are very reliant on the composition and the rock texture.

The following are the main important characteristics of oil reservoir properties that control the overall reservoir performance and production potential:

1. The reservoir rock porosity, permeability, and compressibility;
2. The capillary pressure, phase saturation, relative permeability, wettability properties;
3. The net to gross of reservoir hydrocarbons and fluid mixture composition.

The objective of this book is to understand the fundamentals and the definitions of the petrophysical properties and their laboratory measurements. The main purpose of reservoir description is to make 3D images' petrophysical properties of the reservoir rocks.

## Reservoir Rocks

The reservoir rock is permeable rock formation capable of retaining the hydrocarbon reserves. It consists of one or more subsurface lithological units of either sedimentary or carbonate origin. Reservoir rocks are described by good permeability and porosity and confined by sealed layers that trap the hydrocarbons. A reservoir cross section is depicted in Fig. 1. Hydrocarbon is produced from underground permeable rock formations throughout production wells optimally drilled around the reservoir area.

Usually, reservoir rocks contain pores media and the fraction of pores in the total rock volume is known as effective porosity. The pores need to be interconnecting and permit the hydrocarbons to flow everywhere. The lack of impediment in the reservoir enhances the permeability which is the ability of the fluid to transfer within the pore space of the reservoir rock.

The geological trap is rocks that confine hydrocarbons in the subsurface. Above the trap, there is an impermeable rock layer that prevents the hydrocarbons from migrating to the shallower layers or to the surface. Below the reservoir rock, there is a plane surface that splits it from the underlying fluid, usually briny water. A reservoir rock may contain liquid, gas, or both, and the vertical occurrence of
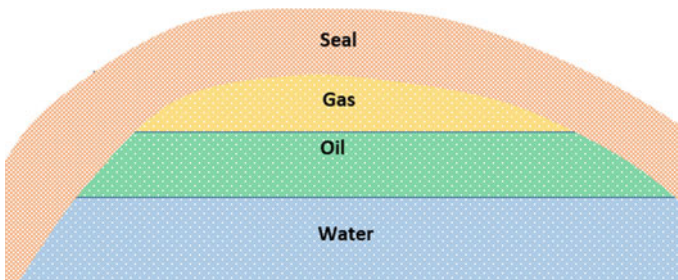


**Fig. 1** Cross-sectional view of a simple reservoir oil and gas accumulation in an anticline trap

fluids in the structure is governed by the gravitational separation. If the three phases exist in the reservoir rock, then the reservoir fluids are stacked on the top of each other, due to the difference in densities, gas on top, oil in the middle, and water on the bottom.

# References

Amyx J, Bass D, Whiting RL (1960) Petroleum reservoir engineering physical properties. ISBN:9780070016002, 0070016003

Cecil GL (1949) Principles of petroleum geology. In: The century earth science series. Appleton-Century-Crofts, Inc., New York

Lapedes DN (1978) McGraw-Hill encyclopedia of the geological sciences. McGraw-Hill

# Contents

# Chapter 1
# Physical Properties of Reservoir Rocks

The most prominent features of reservoir rock are porosity, permeability, and fluid saturations. These properties related to the pore media system and its fluid distribution and flow forms. By carrying out laboratory analyses, using core samples, reservoir rock properties can be investigated.

Once the core samples are collected from the reservoir and transported to the laboratory to be evaluated, many rock properties might have been changed due to many reasons. Therefore, there are many chemical and physical processes that changing the composition of a core sample at the surface condition. Common physical processes which may degrade a sample are adsorption, volatilization, and diffusion. Therefore, the sample must be representative of the subsurface environment. Caution and care must be taken to minimize sample degradation to attain the original conditions as much as possible.

The influence of these alterations on the reservoir rock properties may vary from small to major, reliant on rock property and the physical characteristics of the reservoir rock. However, Core study is of paramount importance to obtain reservoir rock data to help the reservoir engineers in evaluating the hydrocarbon accumulation. The sources of the engineering data obtained from field tests and laboratory tests are shown in Fig. 1.1. Typically, experimental data are used to compare with field measurements data which might be performed under some certain conditions.

Principally, two main available techniques of core analysis assessment are as follows:

1. Routine Core Analysis (RCA).
2. Special Core Analysis (SCAL).
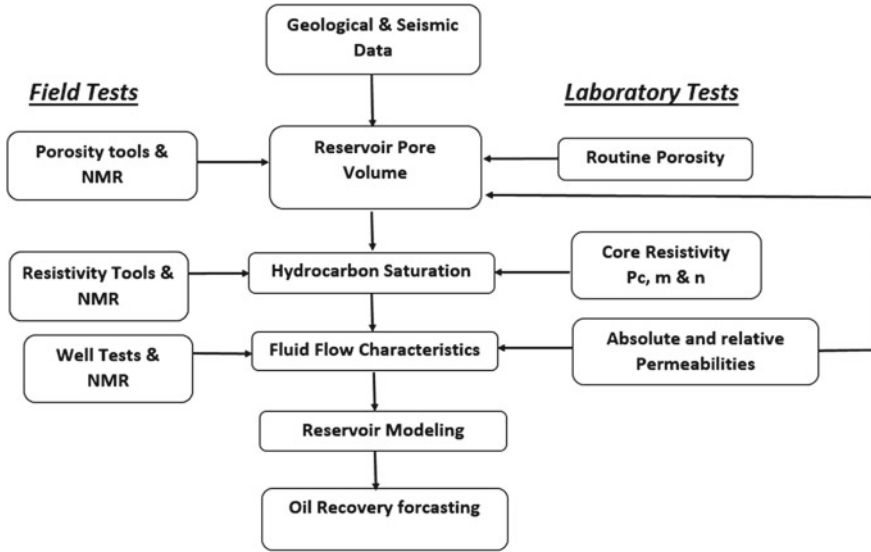
**Fig. 1.1**  Sources of reservoir engineering data

## 1.1  Routine Core Analysis (RCA)

To determine the main reservoir petrophysical properties, routine core analysis technique is applied on the surface core samples (outcrop) or on the subsurface core samples (at reservoir depth). Reservoir core samples are collected in either a horizontal or vertical alignment with regard to the surface. The basic rock parameters are permeability, porosity, grain density, and water saturation. Data collected is considered valuable information about the well and reservoir performance. The advantages of the RCA data is considered inexpensive, and provide a great dataset representing reservoir core properties. Figure 1.2 is a schematic diagram shows the common RCA measurements.

The obtained porosity data are very reliable, being slightly influenced by interfaces between reservoir fluids and minerals. Occasionally the measured permeability does not represent the reservoir condition if reservoir fluids react with the existing minerals in the pores. As the compressibility of gases is used to determine the permeability, then, Klinkenberg correction factor (KL) are utilized to account for the changes in gas permeability to equivalent liquid permeability, however, still considering no fluid-rock interface.
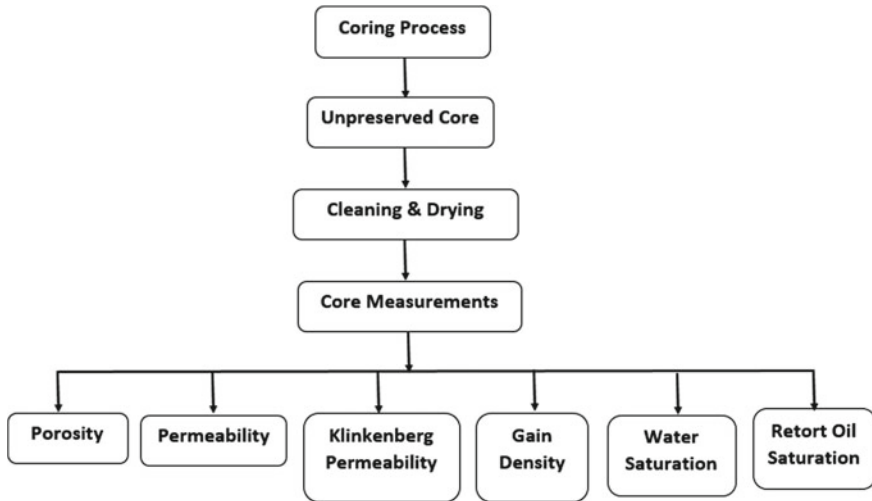
**Fig. 1.2**   Schematic diagram of the common RCA measurement

## 1.2   Special Tests Core Analysis (SCAL)

Special Core Analysis a rigorous measurement provides more representative reservoir rock properties data at reservoir conditions. The obtained SCAL data along with the well test and log data to characterise the whole reservoir performance. Though, the cost of the SCAL measurements is more expensive than RCA measurements, where the core samples are carefully selected. Several tests are conducted to determine fluid distribution, electrical properties, and fluid flow features in either two or three phase condition, and are performed on well-maintained core samples. Figure 1.3 shows a schematic diagram of a wide range of valuable data that can be obtained from SCAL measurements as follows:

- Capillary Pressure
- Wettability
- Reservoir Condition Core floods
- Relative Permeability
- Relative Permeability Effects
- Surface and interfacial tension
- Pore Volume Compressibility
- Fluid Compatibility
- Steady-state and Unsteady state
- Archie Exponents—a, m, n
- CT Scan Evaluation
- Overburden pressure
- And more.
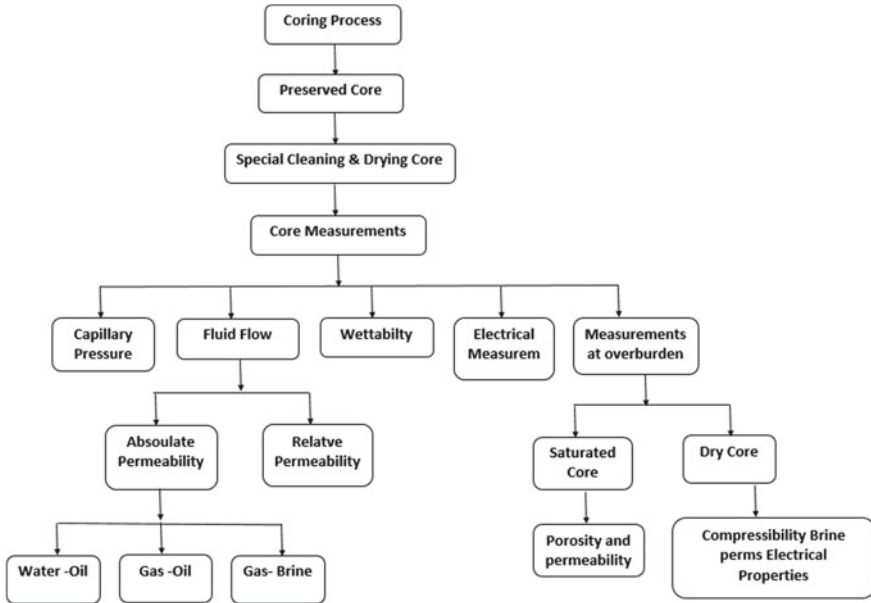
**Fig. 1.3**  A schematic diagram of common SCAL measurement

## 1.3  Nuclear Magnetic Resonance (NMR) Core Analysis

A more robust method preferred by reservoir engineers is the use of (NMR) to define critical pore and fluid properties of the reservoir core samples. NMR is well logging measurements and also used to calibrate the core analysis studies NMR has added a new horizon to determine porosity and pore-size distributions simply and rapidly. Furthermore, NMR measures the fluid mobility, permeability, capillary pressure, and gas/water or oil/water contents. Currently, NMR technology helps to measure pore structure and wettability properties optimize logging parameters. NMR core sample analysis and evaluation tests are:

1. Effective Porosity
2. Permeability Models
3. Pore Size Distribution
4. Pore Size Geometry
5. Fluid Saturation
6. Wetting Characteristics
7. Oil Viscosity
8. Diffusion Coefficient
9. BVI and Free-Fluid Index

Until recent years, a high level of skill and knowledge of the principles and practice of NMR were aquired to make NMR reservoir rock core analysis.

# Chapter 2
# Porosity

Porosity is a measure of void spaces in the rock. This void fraction can be either between particles or inside cavities or cracks of the soil or rock. Porosity defined as a unit fraction between 0 and 1 or as a percentage between 0 and 100%. For most rocks, porosity is normally varying from less than 1 to 40%.

Permeable rock is the key element of oil and gas reservoirs. Porous rocks are able to hold fluids. Normally, both oil and gas is generated from source rocks (kitchen), migrate upwards and trapped under sealing layers (impermeable) that will not permit oil and gas to escape to the surface. Reservoir rock was classified into clastics and carbonates hydrocarbon reservoirs. Clastics reservoirs for example sandstone are comprised of small particles usually buried and compacted in riverbeds for a long time. Carbonates reservoirs are normally generated by biological processes then buried and compacted for a long time. Approximately 60% of hydrocarbons are exists in clastics reservoir rocks and 40% in carbonates reservoir rocks refer to Fig. 2.1. Porosity is a key parameter as it is measuring the storage capacity for hydrocarbons. Typically, carbonate porosity varying from 1 to 35%, average porosity in dolomite formations is 10% and in limestone formations is 12% (Schmoker et al. 1985). Porosity is known simply as pore volume over by bulk volume.

It is difficult to visualize the pore space and pore-throat without using scanning electron microscopy (SEM) as seen in Fig. 2.2. In general, there might be fine paths termed as pore throats detached by wide passages known as pore bodies.

The critical concentration is the point where small grains completely fill the pore space of the large grain pack while the large grains are still in contact with each other (as shown in middle figure). This point indicates the separation between two structural domains. The domain on the left is where an external load is supported by the large grain framework, hence it is shaly sand. In the domain on the right the large grains are suspended in the small particle framework which is load bearing; e.g. sandy shale.
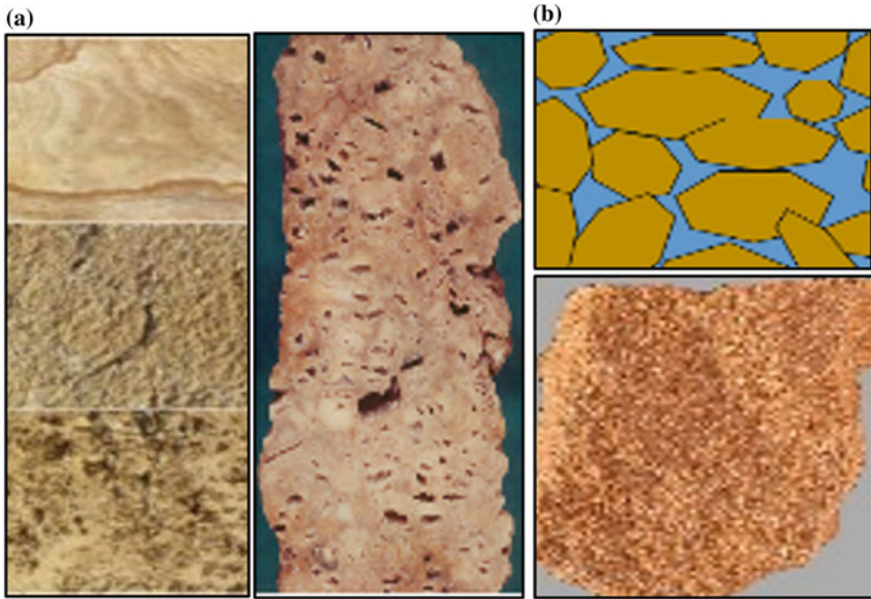
**Fig. 2.1** Pores and throat model. **a** Carbonate rock. **b** Clastic rock
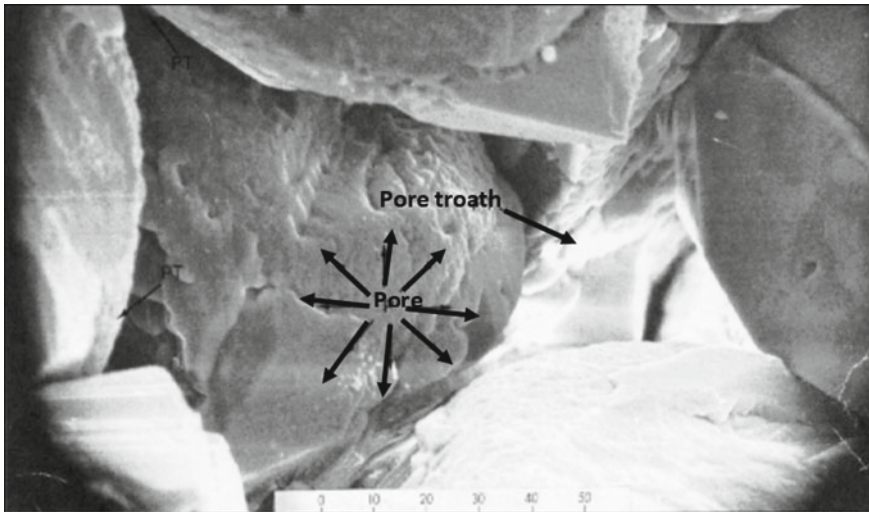


**Fig. 2.2** Microphotograph of bore and pore throat (*Source* Jorden and Campbell 1984)

## 2.1 Types of Geologic Properties

1. **Primary porosity**

It's the main porosity accompanying with the initial depositional structure of the sediment. The primary porosity is the aperture space between the particles. This form of porosity is identified as primary intergranular porosity. While the void space in mineral particles that was occurred former to deposition is known as a primary intragranular porosity. Figure 2.3 illustrates the primary porosity of the rock causing after its original depositional environment.

2. **Secondary porosity**

It's porosity that often enhancing overall voidage of a rock in the sedimentary basin. This porosity results from dissolving of particles, depositional environment, or cement which originally bounded the particles together at the initial place. Secondary intragranular porosity is so easily identifiable porosity. Secondary intergranular porosity is in some environments hard to recognize and measure.

Tectonic movement and degradation diagenetic processes may cause fracture and vug porosities. This type of porosity, which created after a long time of rock deposition, is known as secondary porosity as depicted in Fig. 2.4.

3. **Fracture porosity**

This porosity accompanying a tectonic fracturing system that can generate secondary porosity in rocks see Fig. 2.5.

In extremely unusual cases, non-reservoir rocks as granite can turn into reservoir rocks if adequate fracturing occurs. The orientation of the fracture can be everyplace from vertical to horizontal.
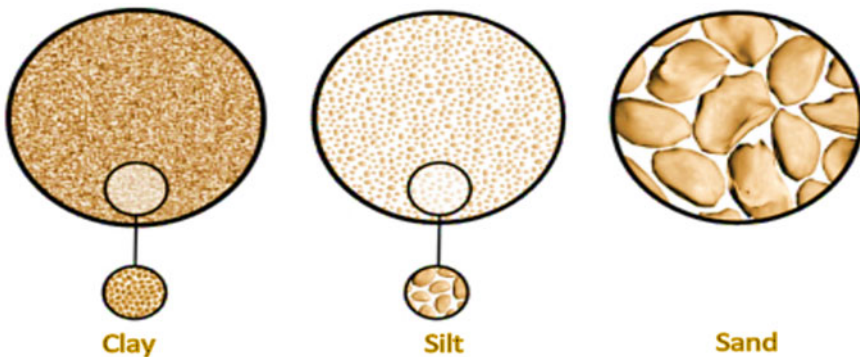


**Fig. 2.3** Diagram display primary porosity at different particle sizes
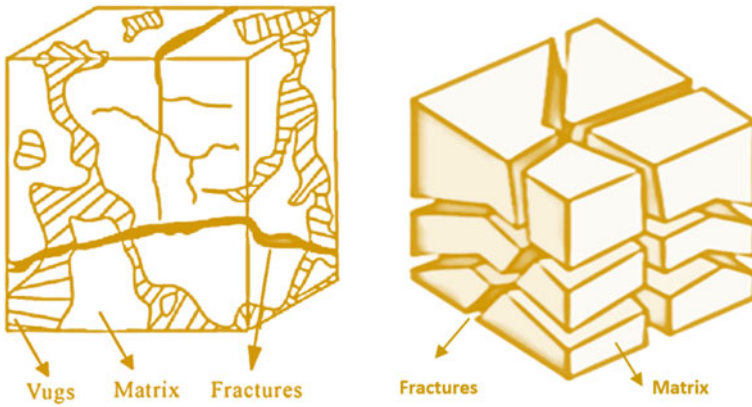
**Fig. 2.4**  Diagram shows type of secondary porosity existing in reservoir rock
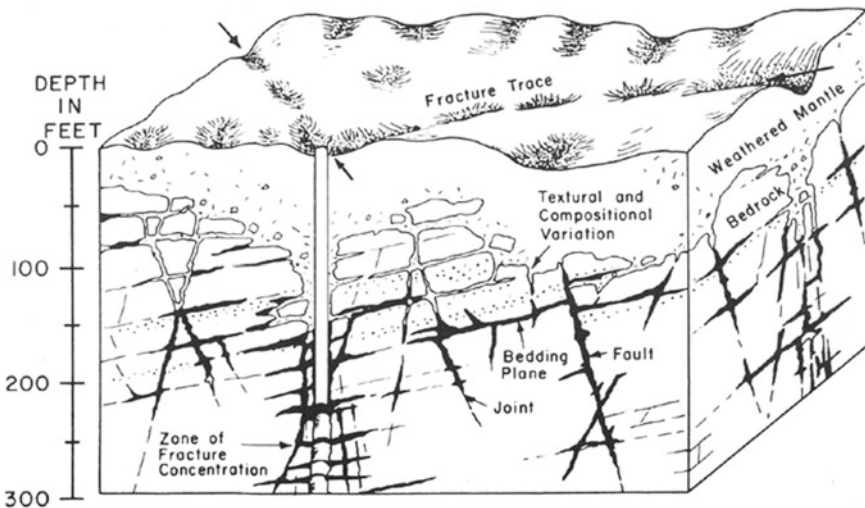


**Fig. 2.5**  Schematic showing cross-sections of fractures in carbonate rock (*Source* Parizek et al. 1971)

4. **Vuggy porosity**

It's a form of secondary porosity in which the pore spaces are formed by solution vugs, leaving large holes, caves, or vugs in a rock that are normally lined with mineral precipitates. Vugs generally exist as dissolved grains shown in Fig. 2.6.

Fig. 2.6 Showing carbonate vuggy porosity (*Source* Etminan and Abbas 2008)
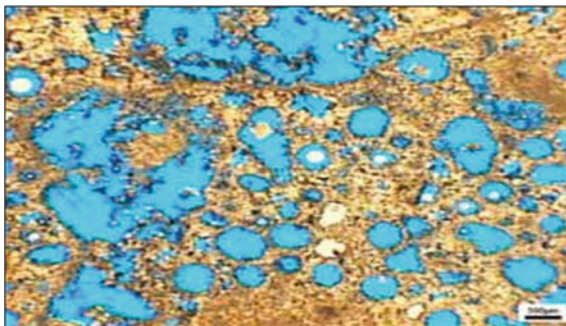
5. **Effective porosity**

It's known also as open porosity, and can be determined by subtracting the total porosity from the part of the void space filled by clay or shale. Typically, the total reservoir porosity in clean reservoir sands is identical to effective porosity.

Another description of effective porosity, it's known as interconnected pore space. Refer to Fig. 2.7 shows the clean pore space and the effective porosity.

Figure 2.8 shows the several types of clay distributions existing in reservoir rocks and their effect on reservoir porosity.



Fig. 2.7 Illustrates the interconnected porosity

CLEAN          LAMINAR         STRUCTURAL      DISPERSED
SAND           SHALE           SHALE           SHALE
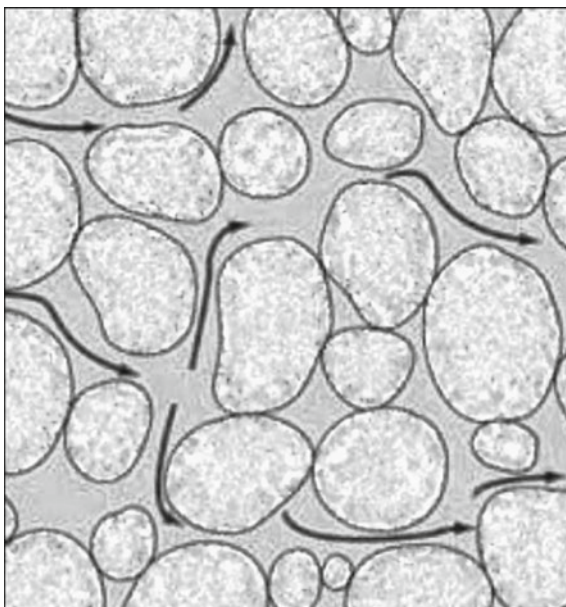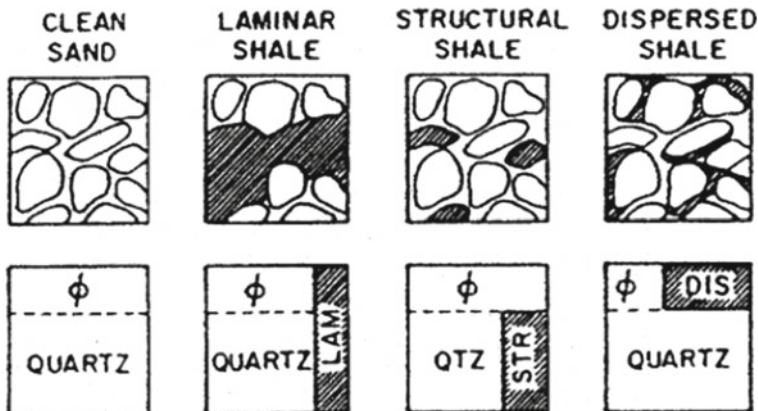


**Fig. 2.8** Show the effective porosity at different shale distributions (*Source* Dewan 1983)

6. **Ineffective porosity (also called closed porosity)**

This porosity also called closed porosity, where the pores are isolated and not inter-connected. Also, it's known as the part of the total volume where liquids or gases are exists but in which fluid flow can't efficiently occur includes the closed apertures see Fig. 2.9.

7. **Dual porosity**

Known as dual porosity reservoirs because the fractured reservoirs have two dis-similar porosities, call matrix porosity, and fractures porosity. However, naturally fractured reservoirs comprise of asymmetrical fractures, they might be character-ized by same homogeneous dual porosity systems. Dual porosity is defined also as a combination of primary, fracture and or vuggy mix where fluid flows are not simple shown Fig. 2.10.
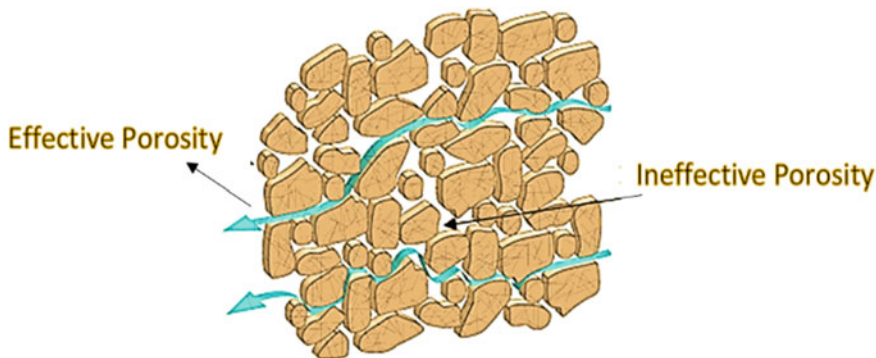


**Fig. 2.9** Diagram showing effective and ineffective porosity inside reservoir rock

**Fig. 2.10** Diagram represent dual porosity model
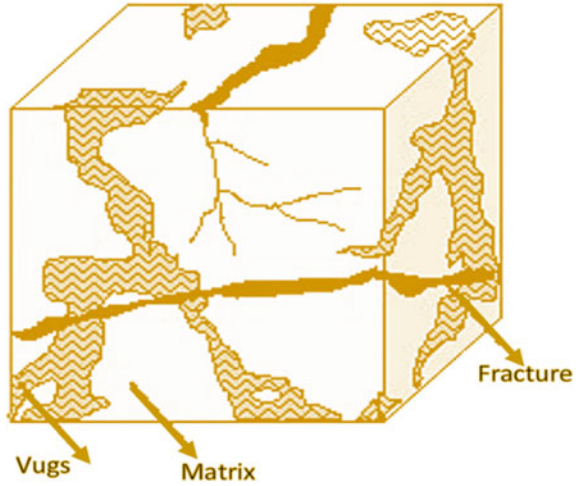
8. **Macroporosity**

The term 'macroporosity' point out to apertures bigger than 50 nm in diameter. Macroporosity is commonly used in the estimation of soil compaction. If the macroporosity decreased this may be lead to small drainage, and soil degradation. Figure 2.11 shows the interconnected porosity in the reservoir rock.

9. **Mesoporosity**

The term 'mesoporosity' point out to apertures bigger than 2 nm and less than 50 nm in diameter. It's defined as the rock which has its pore size in between microporous and macroporous. This porosity may contain a great amount of hydrocarbons in the pores above the free water level.
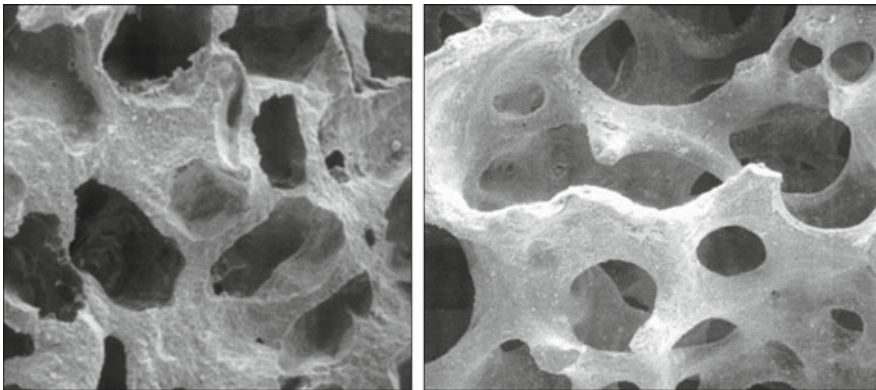


**Fig. 2.11** Showing interconnected macroporosity in the formations (*Source* Le Geros et al. 2003)

**Fig. 2.12** Microporosity matrix
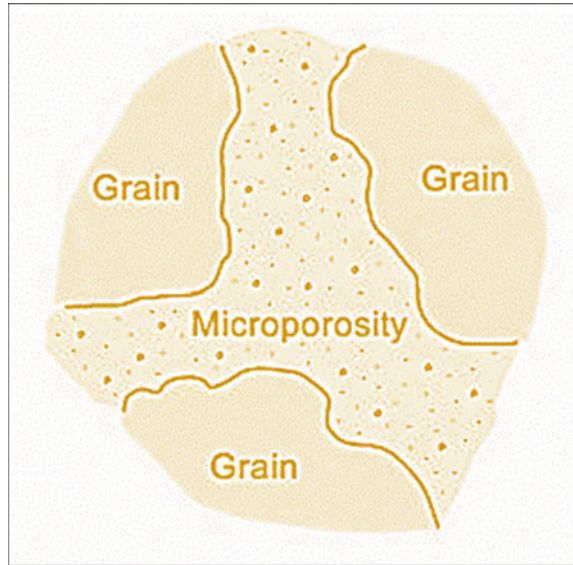
10. **Microporosity**

The term 'microporosity' point out to apertures lesser than 2 nm in diameter. Microporosity exists in siliciclastic rock and in carbonate rock shown in Fig. 2.12. Hence it's directly affect the existing fluid flow properties (i.e. output) and as well as the log response. Normally, it's existing in very fine grain mixture formed at rapid solidification.

Mostly dominant in carbonate rock, the presence of micropores raises the capillary pull to the wetting phase caused in rich bound water in the micropores. Consequently, the conventional logs reading may interpret high water saturation which resulting wrong hydrocarbon determination (Pittman 1983). Therefore, microporosity must be taken into account in any formation evaluation, to avoid erroneous calculation of hydrocarbon in place.

## 2.2 Porosity of Packing

The porosity of identical rock particle size is independent of the particles size. Figure 2.3a shows the maximum theoretical porosity of 47.6% is attained with cubic packing of spherical particles. While Fig. 2.3b shows 39.5% porosity of Hexagonal packing. Figure 2.3c shows Tetragonal packing. Figure 2.3d shows rhombohedral packing, which is more representative of reservoir environments. Figure 2.3e shows the second lesser size of spherical particles is hosted into cubic packing. This will reduce the porosity from 47.6 to 13%. Therefore, porosity is dependent on the amount
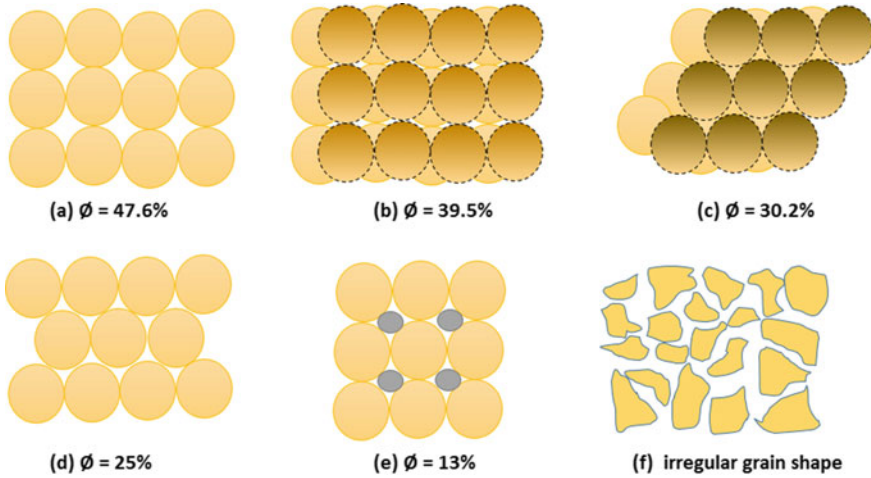
Fig. 2.13 Cubic packing (**a**), hexagonal (**b**), tetragonal (**c**), rhombohedral (**d**), cubic packing with two particle sizes (**e**), and sand with irregular particle shape (**f**)

of cementing materials, the arrangement of the particles, and particle size distribution. A classic reservoir sand shape is illustrated in Fig. 2.13f.

## 2.3 Particle Shape

Particle shape provides a remarkable amount of evidence about the geologic history environment of the sediment. Whether particles in the sediment are angular or rounded is determined by the amount of erosion the particles have undergone. This erosion somewhat wears down the edges of the sediment. Consequently, as a material transported from the origin place, further erosion takes place results in more rounded material. Generally, the primary porosity of the formations depends on the shape, sorting, and packing form of sediment grains. Where the sharpness of sediment may decrease or increase porosity of the rocks, subject if the grains connection openings or are packed together.

## 2.4 Factors Affecting Porosity

The best manifestation is in the rock type. Metamorphic and crystalline igneous rocks have no significant porosity. Table 2.1 shows the main factors affecting the porosity value of the deposited rocks.

Limestone porosity can be developed as secondary porosity through the presence of joints and faults. The outer stress of the rock formation can make compaction

**Table 2.1** Factors affecting the porosity value of the sedimentary rocks

| Factor | Description |
| --- | --- |
| Particle size | Particle size is not a factor in porosity. If all particles are the same size, there is more porosity than if the particles are of mixed sizes |
| Sorting | Good sorted sediments mostly have greater porosities than poorly sorted sediments |
| Particle shape | The more well-rounded the particles within a rock sample are, the more porosity the sample has |
| Packing | If the packing of the particles turns into tighter the porosity becomes small |

of the pores space which is being influenced by on the depth. Krumbein and Sloss (1951) presented that porosity decrease as a result of compaction increase by depth see Fig. 2.14. While the packing and rearrangement after compaction leading to porosity reduction.

The graphic shown in Fig. 2.15 denotes to the compaction process. Compaction is the irreversible volume reduction because of effective pressure caused by overburden sediments, drainage of pore fluids, and grain packing.

Rowan et al. (2003) used log data from 19 offshore wells, and derived a relationship between porosity versus depth for sand, silt, and shale sediments. They used the shale content ($V_{sh}$) from a Gamma log as a parameter for classification. The following are the three derived equations (Eqs. 2.1–2.3):

$$\text{For} \quad \text{sand} \ (V_{sh} < 0.01) \quad \emptyset = 0.5 \cdot (-0.29 \cdot z) \tag{2.1}$$

$$\text{For} \quad \text{silt} \ (0.495 < V_{sh} < 0.01) \quad \emptyset = 0.44 \cdot (-0.38 \cdot z) \tag{2.2}$$

$$\text{For} \quad \text{shale} \ (V_{sh} > 0.9) \quad \emptyset = 0.4 \cdot (-0.42 \cdot z) \tag{2.3}$$

## 2.5   The Range of Porosity Values in Environment

Table 2.2 shows the total porosity ranges in nature for many geologic materials. In general, the total porosity in rocks is not a fixed magnitude since the rock mainly clayey soil, alternately swells, compacts, cracks, and shrinks. In recent deposited sediments, for example, those may exist on the surface of a lagoon; porosity may be very excessive (more than 80%). For instance, the porosity of the loose sands can reach 45%. These sands can be very stabilized or unbalanced by cement. In the formation rocks, the secondary porosity can be created due to dissolution typically in carbonate rocks. Normally, in carbonate rocks, the porosity can be either too small or too high depending on the depositional environment.
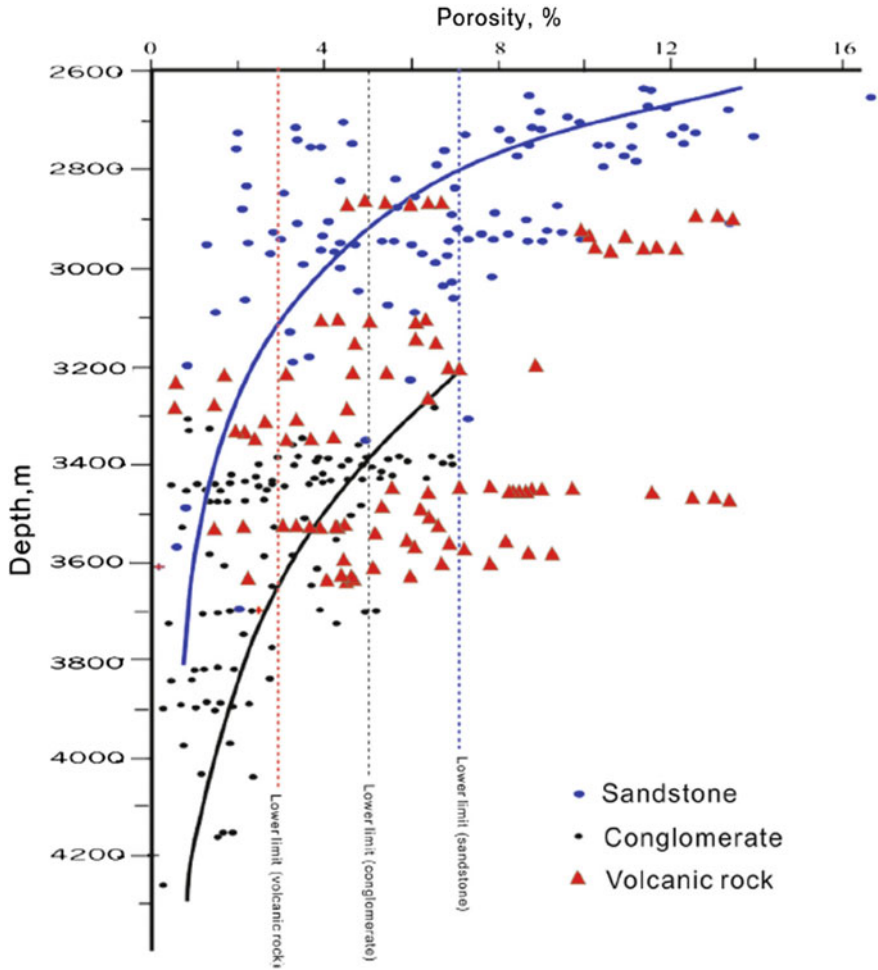
**Fig. 2.14** Porosity versus depth diagram of different lithologic reservoirs

The grouping and assessment of hydrocarbon reservoirs are depending on the rock parameter. Table 2.3 shows the gradations of rocks porosity giving by the industry standard of China. However, carbonate and clastic rocks have different gradation because of different classifications, size, and the measure of apertures in both rocks types.
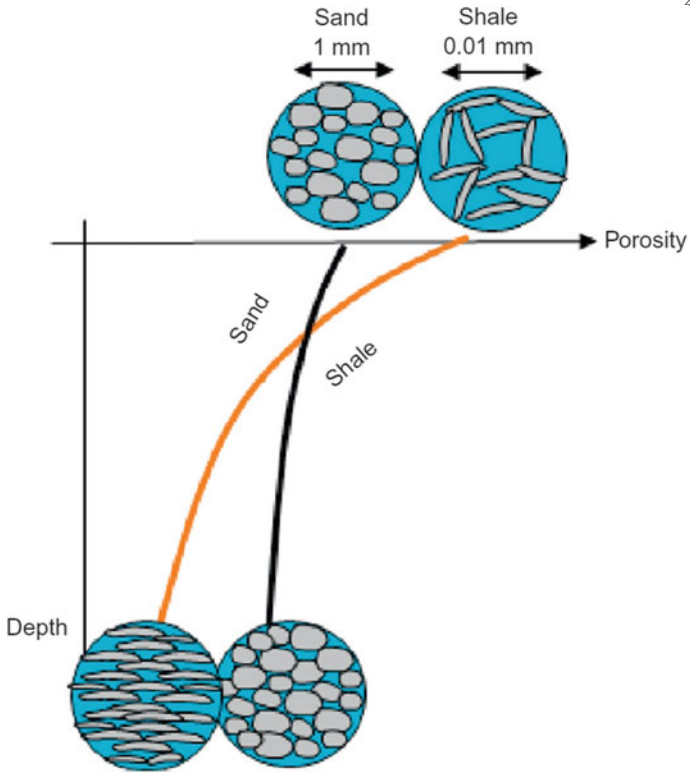
**Fig. 2.15** Compaction process for sand and shale

**Table 2.2** Rocks porosity range (after Paul 2001)

| Lithology | Porosity range (%) |
| --- | --- |
| Unconsolidated sands | 35–45 |
| Reservoir sandstones | 15–35 |
| Compact sandstones | 1–15 |
| Compact carbonate rocks | <1–5 |
| Shales | 0–45 |
| Clays | 0–45 |
| Massive limestones | 5–10 |
| Vuggy limestones | 10–40 |
| Dolomite | 10–30 |
| Chalk | 5–40 |
| Granite | <1 |
| Basalt | <0.5 |
| Gneiss | <2 |
| Conglomerate | 1–15 |

**Table 2.3** Reservoir porosity gradation [SY/T 6285-2011 (2011)]

| Clastic rock | | Carbonate rock | |
|---|---|---|---|
| Type of porosity | Porosity (%) | Type of porosity | Porosity (%) |
| Very high porosity | $\emptyset \geq 30$ | | |
| High porosity | $25 \leq \emptyset < 30$ | High porosity | $\emptyset \geq 20$ |
| Moderate porosity | $15 \leq \emptyset < 25$ | Moderate porosity | $12 \leq \emptyset < 20$ |
| Low porosity | $10 \leq \emptyset < 15$ | Low porosity | $4 \leq \emptyset < 12$ |
| Extremely low porosity | $5 \leq \emptyset < 10$ | Extremely low porosity | $\emptyset < 4$ |
| Ultra-low porosity | $\emptyset < 5$ | | |

## 2.6 Measurement of Porosity

Porosity measurement on core sample in a laboratory normally needs to measure pore volume and bulk volume of the core sample. The total porosity (Absolute Porosity) can be obtained either from core samples or from well logs refer to Fig. 2.16, that could involve effective porosities. Generally, the obtained porosity values using direct methods are more accurate. Therefore, it's used to rectify and calibrate with indirect methods such as log-derived porosity data.

The following Porosity, given the symbol $\emptyset$ can be calculated using Eq. 2.4

$$Porosity = \frac{Pore\ Volume}{Bulk\ Volume} = \frac{Bulk\ Volume - Matrix\ Volume}{(\text{Grain} + \text{Pore volume})}$$

$$\emptyset = \frac{V_p}{V_b} = (V_b - V_m)/V_b \tag{2.4}$$

where:

$V_p$    pore space volume,
$V_m$    matrix (solid rock) volume, and
$V_b$    bulk volume ($V_p + V_m$).

Bulk volume ($V_b$) can be calculated using Eq. 2.5, cylindrical core, or by fluid displacement methods, or directly by volume displacement.

$$V_b = \pi r^2 l \tag{2.5}$$

Porosity will rely on the average form of the particles and the packed method. This sequentially will reliant on deposition method for a long time period such as solid particles of sand dumped progressively on riverbeds (clastics), or evolution and degeneration of biological materials (carbonates). Reservoir engineers are usually concerned in connected porosity (Effective Porosity), which is defined as the total volume of connected pores to total bulk rock volume. Where the hydrocarbon pore volume is defined as the total rock volume that occupied with hydrocarbon. It is
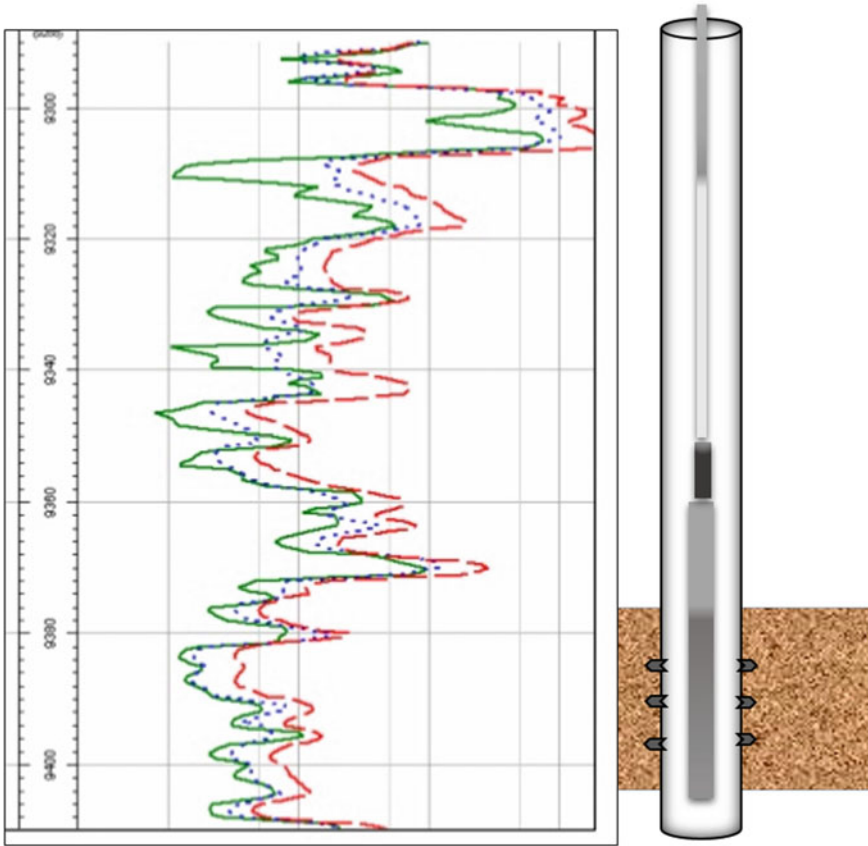
**Fig. 2.16**  Schematic of wireline well logging

known by the equation (Eq. 2.6):

$$HCPV = V_b \cdot \emptyset \cdot (1 - S_{WC}) \tag{2.6}$$

where:

$S_{wc}$ is the connate water saturation.

The following are the general conventional range and view of Porosity: 0–5% Negligible, 5–10% Poor, 10–15% Fair, 15–20% Good and 20–25% Very Good. Once more, the effective porosity can be defined as the total porosity minus the fraction of the aperture filled by shale or clay. In pure clean sands, total porosity is equivalent to effective porosity (Interconnected Pores) shown in Fig. 2.17. As seen in Fig. 2.18, effective porosity can be defined also as the aperture that contains hydrocarbon and non-clay water (Al-Ruwaili and Al-Waheed 2004). Therefore, the description of effective porosity is the total porosity less volume of clay-bound water.
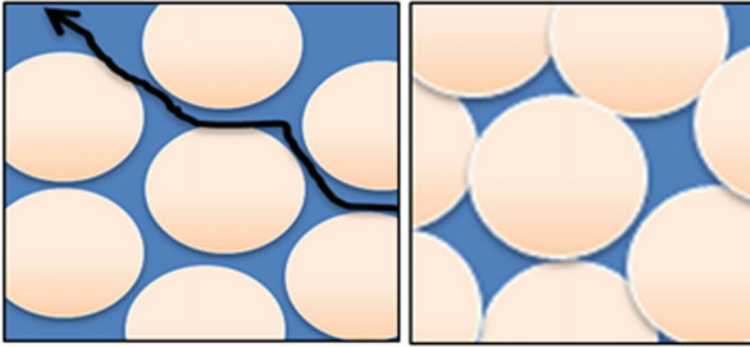
Fig. 2.17  Effective porosity
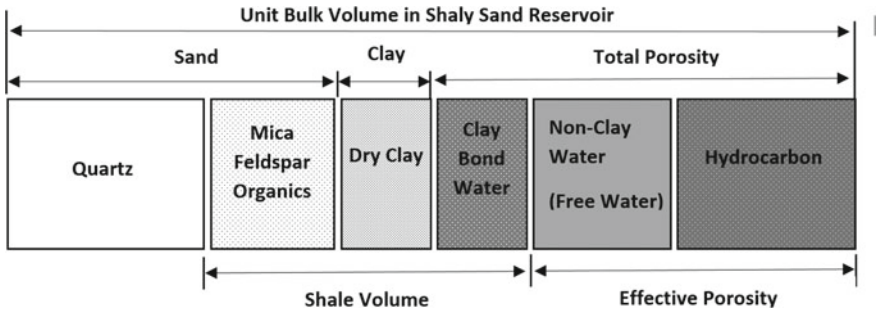


Fig. 2.18  Porosity model for a shaly sand reservoir

The following Eq. 2.7 shows the total porosity as a function of effective porosity for a shaly sand model:

$$\emptyset_t = \emptyset_e + V_{sh} x \emptyset_{sh} \tag{2.7}$$

In Eq. (2.7), $\emptyset_t$ = total porosity, fraction; $\emptyset_e$ = effective porosity, fraction; $V_{sh}$ = volume of shale, fraction; and $\emptyset_{sh}$ = shale porosity, fraction. It's difficult to determine the shale porosity from well logs because the selection of the 100% shale unit can be incorrect (Al-Ruwaili and Al-Waheed 2004). Hence, the estimated form of Eq. (2.8) is attained by changing shale porosity $\emptyset_{sh}$ with total porosity $\emptyset_t$:

$$\emptyset_t = \emptyset_e + V_{sh} x \emptyset_t \tag{2.8}$$

**Example 2.1**

10.10 cm Core sample long with 3.80 cm was carefully cleaned and dried. The core was saturated with 100% brine that has a specific gravity of 1.03. The saturated core

weight is 385 g and tried sample weight is 355 g. Determine the porosity of the core sample.

**Solution**
The bulk volume Eq. (2.2):

$$V_b = \pi r^2 l$$

$$V_b = \pi \left(\frac{3.80}{2}\right)^2 \times 10.10 = 114.591 \text{ cm}^3$$

The pore volume is known as:

$$V_p = \frac{wt.\,of\,saturated\,core - wt.\,of\,dried\,core}{specific\,gravity\,of\,brine}$$

$$V_p = \frac{385.0 - 355.0}{1.03} = 29.126 \text{ cm}^3$$

Using Eq. (2.1), porosity of the core sample is:

$$\varnothing = \frac{V_p}{V_b}$$

$$\varnothing = \frac{29.126}{114.591} = 0.2542 \quad \text{or} \quad 25.42\%$$

**Example 2.2**
An oil reservoir has initial pressure is the same to its bubble point pressure of 1000 psia, and the gas oil ratio is 500 SCF/STB at reservoir temperature of 150 °F and the gravity is 35° API with gas specific gravity is 0.63. The following are additional reservoir data available:

- Effective porosity = 18%
- Reservoir area = 550 acres
- Connate water saturation = 20%
- Average thickness = 15 ft
- Formation volume factor = 1.49 bbl/STB

Determine the initial oil in place in STB.

**Solution**
First, estimate the specific gravity of the oil ($\gamma_o$) using the API gravity.

$$API = \frac{141.5}{\gamma_0} - 131.5$$

Therefore,

$$\gamma_0 = \frac{141.5}{35 + 131.5} = 0.849$$

Determine the pore volume from Equation:

$$PV = 7758 \ Ah\emptyset \ \text{bbl}$$

$$PV = 7758 * 550 * 15 * 0.18 = 11{,}520{,}630 \ \text{bbl}$$

$$OIIP = 7758 \ Ah\emptyset(1 - S_w)/B_0$$

$$OIIP = 11{,}520{,}630 \frac{(1 - 0.20)}{1.49} = 6{,}185{,}573 \ \text{STB}$$

The reservoir rock could display enormous variants in porosity. The following are the mathematical techniques used for calculating the averaging porosity:

(1)  If there are vertically variants in porosity but does not show big deviations in porosity parallel to the bedding planes;

$$Arithmetic \ average \ \emptyset = \Sigma\emptyset_i/\text{n}$$

Or

$$Thickness \ weighted \ average \ \emptyset = \Sigma\emptyset_i h_i/\Sigma h_i$$

(2)  If there is any alteration in the depositional environment, that can create significantly different porosities over the reservoir area;

$$Areal \ weighted \ average \ \emptyset = \Sigma\emptyset_i A_i/\Sigma A_i$$

Or

$$Volumetric \ weighted \ average \ \emptyset = \Sigma\emptyset_i A_i\text{h}/\Sigma A_i h_i$$

Where, n is total number of core samples, A is reservoir area, $\emptyset$ is porosity, and h is thickness of core sample.

**Example 2.3**

Calculate the Areal weighted average for the below reservoir data measurements:

$\emptyset_a = 20\%, \emptyset_b = 11\%, \emptyset_c = 29\%,$

$L_1 = 0.35\ L + 0.24,$

$h_a = h_b = 0.5\ h_c$
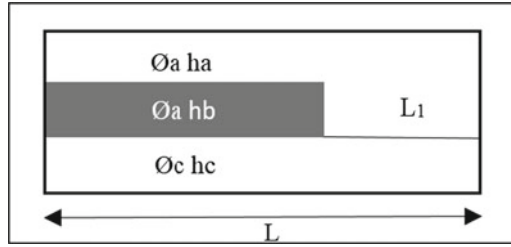


**Solution**

$$Areal\ weighted\ average\ \emptyset = \Sigma\emptyset_i A_i / \Sigma A_i$$

$$\Sigma\emptyset_i A_i = \emptyset a(ha * L) + \emptyset a(hb * 0.35\ L) + \emptyset b(hb * 0.65 * L) + \emptyset c(hc * L)$$

$$\Sigma\emptyset_i A_i = \emptyset a(0.5 * hc * L) + \emptyset a(0.5 * hc * 0.35\ L)$$
$$+ \emptyset b(0.5 * hc * 0.65 * L) + \emptyset c(hc * L)$$

$$\Sigma\emptyset_i A_i = hc * L(0.675\emptyset a + 0.325\emptyset b + \emptyset c)$$

$$\Sigma\emptyset_i A_i = 0.46075\ hc * L$$

$$\Sigma A_i = (1.35 * ha) + (0.65 * hb) + (hc * L)$$

If:

ha = hb = 0.5hc

$$\Sigma A_i = (1.35 * 0.5hc * L) + (0.65 * 0.5hc * L) + (hc * L)$$

$$\Sigma A_i = hc * L[(1.35 * 0.5) + (0.65 * 0.5) + 1]$$

$$\Sigma A_i = hc * L[(0.675) + (0.325) + 1]$$

$$\Sigma A_i = hc * L[(0.675) + (0.325) + 1]$$

$$\Sigma A_i = 2hc * L$$

$$\emptyset = \frac{0.46075 hc * L}{2hc * L}$$

$$\emptyset = 23\%$$

**Example 2.4**

The reservoir has porosity variation along the three reservoir sections. The average reservoir porosity and the area for each section as follows.

   Calculate the Areal weighted average porosity?

| Section | Avg. Porosity (%) | Area (ft²) |
|---------|-------------------|------------|
| 1 | 13 | 160,422,211 |
| 2 | 20 | 302,140,285 |
| 3 | 27 | 10,550,111 |
| Total | | 473,112,607 |

$$\emptyset = \frac{\Sigma \emptyset_i A_i}{\Sigma A_i} = ((0.13 * 160{,}422{,}211) + (0.20 * 302{,}140{,}285)$$
$$+ (0.27 * 10{,}550{,}111))/473{,}112{,}607$$

$$\emptyset = 18\%$$

**Example 2.5**

Determine the arithmetic average porosity and thickness weighted average porosity for the below reservoir data measurements?

| Core No. | Porosity (%) | Thickness (ft) |
|----------|--------------|----------------|
| 1 | 8 | 1.3 |
| 2 | 10 | 1 |
| 3 | 15 | 1.1 |
| 4 | 9 | 2 |

(continued)

| Core No. | Porosity (%) | Thickness (ft) |
|----------|--------------|----------------|
| 5        | 11           | 2.1            |
| 6        | 13           | 1.5            |

$$Arithmetic\ average\ \emptyset = \Sigma\emptyset_i/\text{n}$$

$$Arithmetic\ average\ \emptyset = \Sigma(8+10+15+9+11+13)/6$$
$$\emptyset = 11\%$$

$$Thickness\ weighted\ average\ \emptyset = \Sigma\emptyset_i h_i/\Sigma h_i$$

$$Thickness\ weighted\ average\ \emptyset = \Sigma(8*1.3)+(10*1)+15*1.1)$$
$$+(9*2)+11*2.1)+(13*1.5)/\Sigma(1.3+1+1.1+2+2.1+1.5)$$
$$\emptyset = 11.5\%$$

# References

Al-Ruwaili S, Al-Waheed H (2004) Improved petrophysical methods and techniques for shaly sands evaluation. Paper presented at the 2004 SPE International Petroleum Conference in Puebla, Mexico, November 8–9, 2004

Dewan J (1983) Modern open hole log interpretation. Pennwell Publ. Co., Tulsa Oklahoma, p 361

Etminan A, Abbas S (2008) An improved model for geostatistical simulation of fracture parameters and their effect on static and dynamic models. https://doi.org/10.2174/1874834100801010047

Jorden J, Campbell F (1984) Well logging I—rock properties, borehole environment, mud and temperature logging. Henry L. Doherty Memorial Fund of AIME, SPE: New York, Dallas

Krumbein WC, Sloss LL (1951) Stratigraphy and sedimentation, 2nd edn. W. H. Freeman, San Francisco and London, p 497 (1963, p 660)

LeGeros R, Lin S, Ramin R, Dindo M, John P (2003) Biphasic calcium phosphate bioceramics: preparation, properties and applications. https://doi.org/10.1023/a:1022872421333

Parizek R, White W, Langmuir D (1971) Hydrogeology and geochemistry of folded and faulted carbonate rocks of the Central Appalachian type and related land use problems, p 29. Prepared for the Annual Meeting of The Geological Society of America and Associated Societies

Paul G (2001) Petrophysics M.Sc. Course Notes.http://www2.ggl.ulaval.ca/personnel/paglover/CD%20Contents/GGL-66565%20Petrophysics%20English/Chapter%202.PDF; http://www2.ggl.ulaval.ca/personnel/paglover/CD%20Contents/GGL-66565%20Petrophysics%20English/Chapter%203.PDF

Pittman R (1983) Multilateral productivity comparisons with undesirable outputs. Econ J 93:883–891

Rowan E, Hayba D, Nelson P, Burns W, Houseknecht D (2003) Sandstone and Shale compaction curves derived from sonic and gamma ray logs in offshore wells, North Slope, Alaska—parameters for basin modeling. U.S. Geological Survey, Open-File Report 03–329

Schmoker JW, Krystinic KB, Halley RB (1985) Selected characteristics of limestone and dolomite reservoirs in the United States. AAPG Bull 69(5):733–741

SY/T 6285-2011 (2011) Evaluating methods of oil and gas reservoirs (China)

# Chapter 3
# Permeability

Flow of the hydrocarbon will only be premited if there is sufficient permeability in the reservoir rocks, which is an essential parameter in reservoir engineering. Permeability defined as the capability of fluids to flow in the porous media. It is quantifying the ability of the fluid to flow from the pourse media through the reservoir rock to the wellbore of the produced well; the higher the permeability, the faster the fluid flows.

Permeability is a significant parameter because it is the factor that relies on the rate at which oil and gas can be recovered. It's the most important parameter that the reservoir engineer tries to establish. Normally, permeability range varying lower than 0.01 millidarcy (mD) to more than 1 Darcy. Where permeability value of 0.1 mD is usually considered small for oil reservoir but for gas reservoir still viable. The permeability of very productive reservoir quality is generally measured in the Darcy range. Naturally, we can find a reservoir has low porosity would be impermeable to a fluid, in the same time a reservoir with high porosity to be impermeable as well, (i.e. zero permeability) shown in Fig. 3.1. Such a reservoir rock, will not produce hydrocarbons when drilled.

In 1856, Darcy developed an empirical formula based on experimental work carried out on packs of sand. This formula still applied in the petroleum industry to estimate the main permeability of the rock. Figure 3.2 shows Darcy apparatus
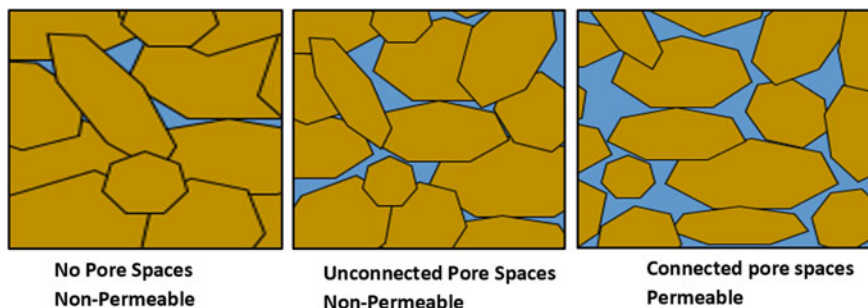


**No Pore Spaces**
**Non-Permeable**

**Unconnected Pore Spaces**
**Non-Permeable**

**Connected pore spaces**
**Permeable**

**Fig. 3.1** Porosity and permeability
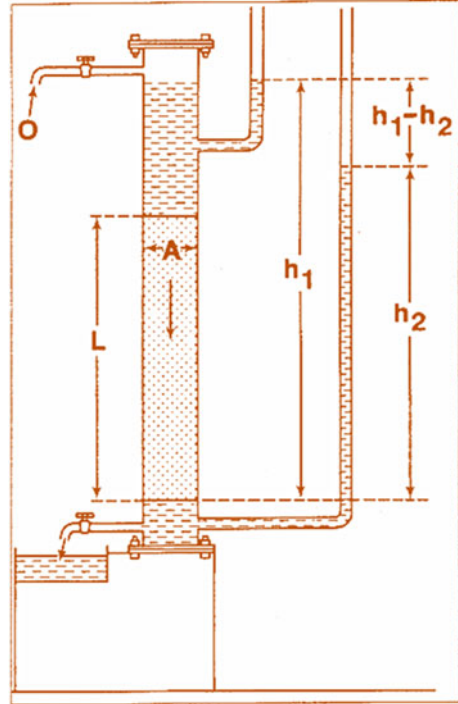
where he used a vertical sand pack through which water flowed under the influence
of gravity while measuring the fluid pressures at the top and bottom of the pack using
manometers.

The following is the Darcy's equation Eq. 3.1:

$$Q = \frac{KA(h2 - h1)}{\mu L} \tag{3.1}$$

where q is the volumetric flow rate, A is a cross-sectional area, $h_1$ and $h_2$ is the
hydraulic head above the standard datum of the water in the manometer positioned
at the input and output ports respectively, L is the height, and K is a constant of
proportionality found to be characteristic of the rock media.

Darcy's law, experiment was carried out on unconsolidated sand packs, assumes
unreactive aqueous fluids with constant properties. Therefore, the permeability
requires correction for the different viscosity of different fluids. Two main important
parameters control the fluid flow movement are the fluid pressure and gravity. It is
feasible to describe the relationship between hydraulic head and pressure, to estimate
pressure at any flow point. By rewriting the $\Delta h$ term in terms of absolute pressures,
Darcy's formula for single phase liquid permeabilities in the hydrocarbon can be
expressed as (Eq. 3.2):

$$Q = \frac{KA(p_i - p_o)}{\mu L} \tag{3.2}$$

where:

K   the permeability (Darcy)
Q   the flow rate ($cm^3$)
$P_o$   the outlet fluid pressure (dynes)
$P_i$   the inlet fluid pressure (dynes)
$\mu$   the fluid viscosity (cP)
L   the tube length (cm)
A   the area of the sample ($cm^2$).

For single phase liquid and gas, the following rearranged equations are applied in the industry to estimate the permeabilities:

For liquids (Eq. 3.3),

$$Q = 1000 \frac{L}{A} \mu \, Q \frac{1}{(p_i - p_o)} \tag{3.3}$$

For gasses (Eq. 3.4),

$$Q = 2000 \frac{L}{A} \mu \, Q \frac{P_{atm}}{(p_o^2 - p_i^2)} \tag{3.4}$$

## 1. **Averaging Absolute Permeabilities**

Absolute Permeability is simply referred to as permeability; it is used to assess the reservoir rock. The productivity of the formations can be determined by the combination of permeability data with porosity, and pore pressure other parameters. The absolute permeability is the most challenging reservoir properties to determine or predict. Typically, there is a variety of allocation of the absolute permeability all over the reservoir rock. To date still missing a suitable understanding of permeability scattering, also it is essential to the estimate of reservoir depletion at any field development plan method. It is not often to find out homogeneous reservoirs with single permeability. Practically the reservoir has different layers, with varying permeabilities. Moreover, since lesser scale heterogeneities constantly exist in the reservoir, core permeabilities need be averaged to describe the flow features of the whole reservoir structure or for each reservoir stratum. The right method of averaging the reservoir permeability is depending on the scattered reservoir permeability at the environmental deposition time period. Consequently, there are three techniques were being normally used to simple estimate average permeability to characterize a corresponding homogeneous system:

1. Weighted average permeability.
2. Harmonic average permeability.
3. Geometric average permeability.
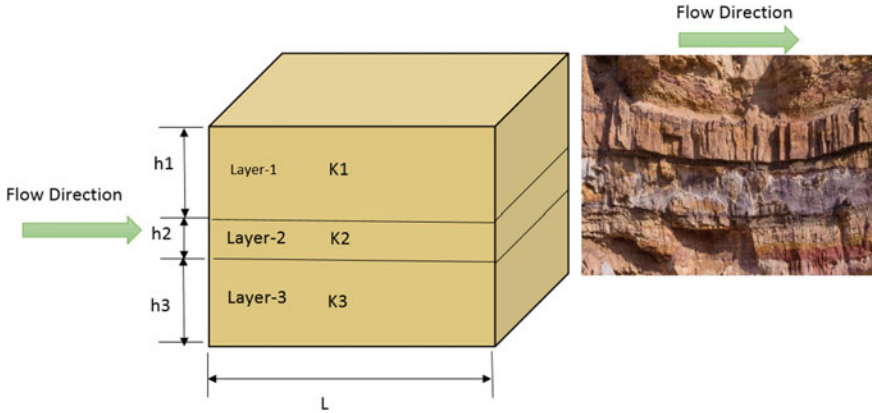
**Fig. 3.3** Linear flows through layered-parallel beds

**Fig. 3.4** Linear flows via layered-parallel stratums with a different area
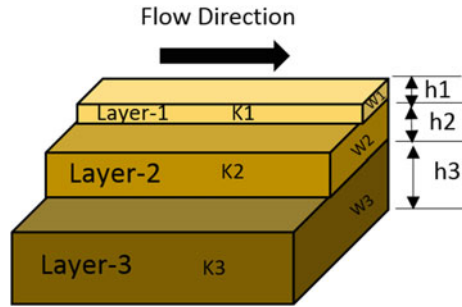


1. **Weighted Average Permeability**

This technique utilized to calculate the average permeability of layered-parallel zones with permeabilities. Assume the flow system contains parallel layers which are separated by thin sealed layers, as displayed in Fig. 3.3. Assuming all the zones has the same area of (A) with a width (w). The weighted average permeability for a parallel-layered scheme is identified in the formula Eq. 3.5:

$$K_{avg} = \frac{\sum_{i=1}^{n} k_i h_i}{\sum_{i=1}^{n} h_i} \tag{3.5}$$

where:

$k_{avg}$  Average permeability
$h_i$  Layer thickness.

Figure 3.4 displays layers with different width. Considering no cross-flow between the beds, the average permeability is expressed by the Eq. 3.6:
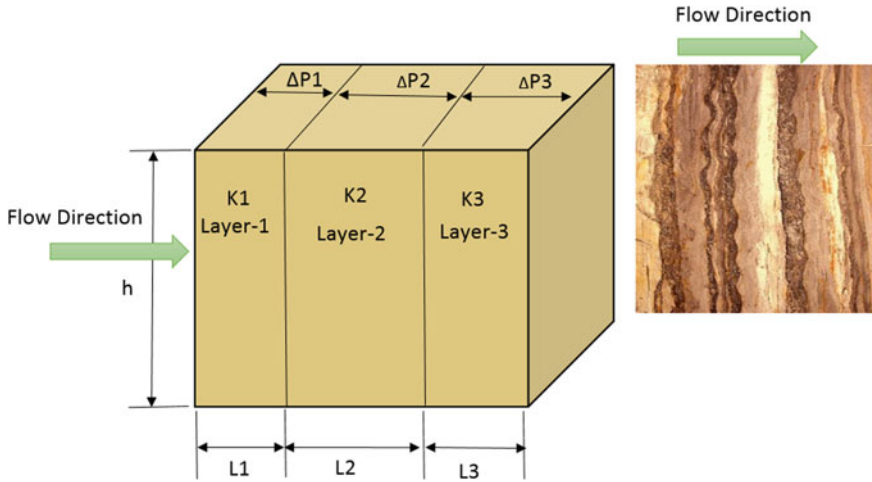
**Fig. 3.5** Beds in series-harmonic average

$$K_{avg} = \frac{\sum_{i=1}^{n} k_i A_i}{\sum_{i=1}^{n} A_i} \tag{3.6}$$

With:

$$A = h_i W_i \tag{3.7}$$

where:

$A_i$    Cross-sectional area of layer i
$W_i$    Width of layer i.

2. **Harmonic Average Permeability**

Average permeability of a linear, series model, grouping of layers with different permeabilities, is the harmonic mean of the permeability of each layer. Normally, harmonic average permeability is smaller than the arithmetic average permeability (Eq. 3.8). Figure 3.5, shows a sketch of fluid flow via a sequence grouping of layers with different permeabilities.

$$K_{avg} = \frac{\sum_{i=1}^{n} L_i}{\sum_{i=1}^{n} (L/K)_i} \tag{3.8}$$

In the radial system with series layers as seen in Fig. 3.6, the below general formula can be applied for average Harmonic permeability (Eq. 3.9):

**Fig. 3.6** Beds in
series-harmonic average
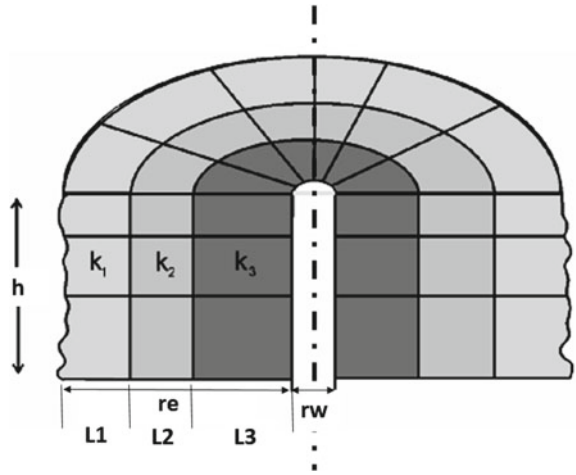




**Fig. 3.7** Beds randomly distributed

$$K_{avg} = \frac{ln\left(\frac{r_e}{r_w}\right)}{\sum_{i=1}^{n}\left[\frac{ln\left(\frac{r_j}{r_j}-1\right)}{K_j}\right]} \tag{3.9}$$

3. **Geometric Average Permeability**

In 1961, Warren and Price explained the performance of a heterogeneous formation method that of the same structure having a permeability that is the same to the geometric average. For instance, dolomites and limestones show arbitrary and rapid lithological and textural variations, therefore, they exhibit a generally different range in permeability. Figure 3.7 show averaging beds distribution based on a random isotropic or geometric basis. If the effective permeability attained from a well test

analysis is obtainable, it must be compared with the calculated averages using the core data. The following is the geometric average permeability equation (Eq. 3.10):

The following is the geometric average permeability equation:

$$K_{avg} = \text{esp}\left[\frac{\sum_{i=1}^{n}(h_i \ln(k_i))}{\sum_{i=1}^{n} h_i}\right] \tag{3.10}$$

where:

$k_i$   permeability of core sample i
$h_i$   thickness of core sample i
n   total number of samples.

Equation 3.11, can be used if all core samples have the same thickness ($h_i$),

$$K_{avg} = (K_1\, K_2\, K_3 \ldots K_n)^{\frac{1}{n}} \tag{3.11}$$

## 3.1 Methodology to Measure Permeability

Using permeability-porosity trend and arithmetic averaging of permeabilities has delivered a meaningfully better correlation between smaller-scale permeabilities and DST. In the existing methodology for quantifying the relative roles of the matrix, fracture flow and, vug, the range of conditional inputs and analyses can be approximately characterized with a simple Boolean model as seen in Fig. 3.8.

## 3.2 Measurement of Permeability

### 1. Laboratory Determination of Permeability

Darcy presented an experimental equation (Eq. 3.8) which is describing the fluid flow in porous media as a function of pressure gradient and gravitation (Lock et al. 2012). Absolute permeability of Single-phase flow is measured on core sample inside a steel cylinder depicted in Fig. 3.9.

Darcy's Law (Eq. 3.12):

$$Q = A\left(\frac{K}{\mu}\right)\left(\frac{\Delta P}{L}\right) \tag{3.12}$$

where:

Q        Rate of flow
K        Permeability
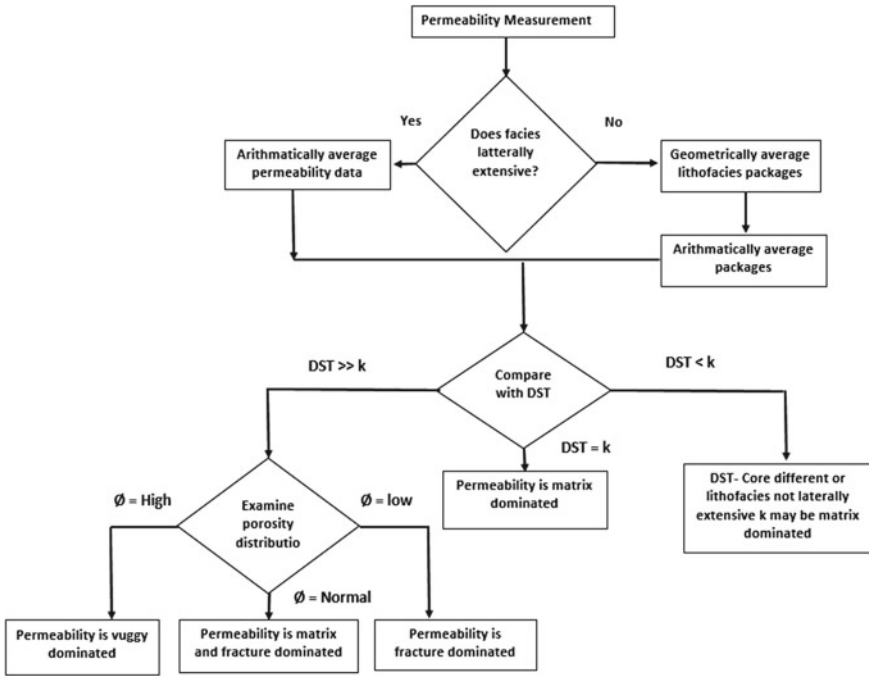
**Fig. 3.8** Schematic diagrams for the concepts and methodology to measure permeability

**Fig. 3.9** Darcy experimental method of determining rock permeability
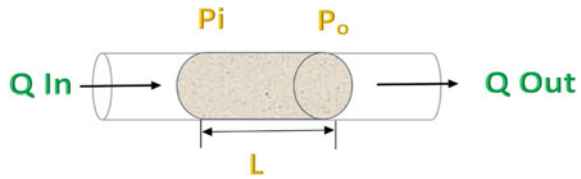


μ              Fluid viscosity
(ΔP)/L   Pressure drop across a horizontal sample
A              Cross-sectional area of the sample.

In 1941 Klinkenberg noticed that the permeability of the core sample is not constant by using gases as a test fluid. Klinkenberg effect is very important at laboratory scale only, because the permeability is normally determined at low pressures (Baehr and Hult 1991). The following formula is defining the gas permeability ($k_g$) at the mean pressure ($P_m$) and liquid permeability ($k_L$) (Eq. 3.13):

$$K_g = K_L\left(1 + \frac{b}{P}\right) \tag{3.13}$$

where the coefficient b is obtained experimentally and relies on both, rock aperture size and the type of gas used. Equation 3.13 proposes that a scheme of gas permeability versus mean pressure $(1/P_m)$ is a straight line. As seen in Fig. 3.10, once the mean pressure raises, the permeability comes close to the liquid permeability. Therefore, regardless of the type of gas used, the same permeability to liquid is obtained for a given rock sample (Amyx et al. 1960).

2. **Permeability from Well-Test Analysis**

The permeability can be determined from well-tests using pressure buildup test analyses. During the production test, the reservoir pressure drops, the well is closed, and the increases of the pressure rate are recorded using pressure gauges, which is a function of the reservoir effective permeability (Babadagli et al. 2001). The average effective permeability of the tested zone can be calculated using equation (Eq. 3.14):

$$\text{Slope} = \left(\frac{\text{psi}}{\log \text{cycle}}\right) = 162.6\frac{(q\mu B_o)}{kh} \tag{3.14}$$

where:

q    Flow rate, stb/day
μ    Viscosity, cP
$B_o$    Oil formation volume factor, bbl/stb
K    Permeability, mD
H    Net reservoir interval, ft.
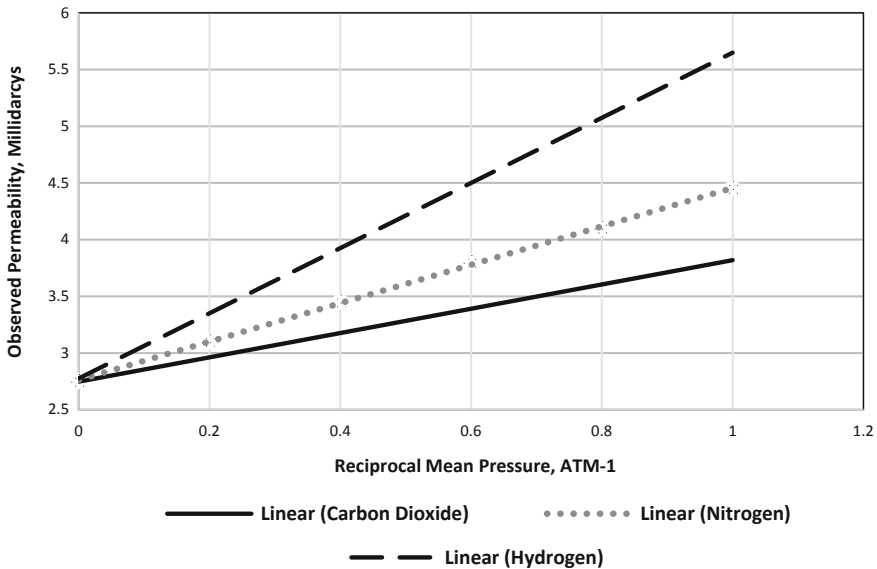


**Fig. 3.10** Klinkenberg effect (*Source* Amyx et al. 1960)
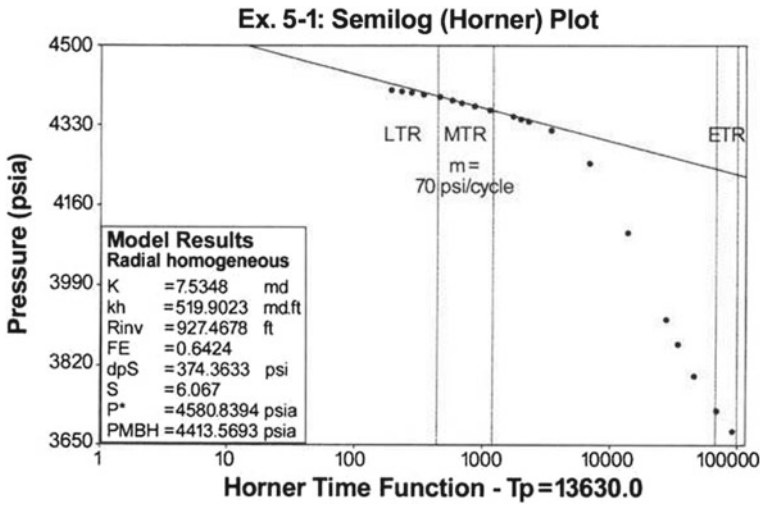
**Fig. 3.11**  Horner pressure buildup plot (*Source* Dake 1978)

Buildup test is used to determine reservoir pressure, skin effect, and average effective permeability as seen in Fig. 3.11.

The permeability is expressed as flow capacity (kh), and effective permeability is determined by dividing flow capacity on the thickness of the tested reservoir zone.

## 3.3  Absolute Permeability Correlations

The capillary pressure measurement used to estimate the connate water saturation of varying permeability from a core sample deliver a good accuracy. Therefore, it's achievable to correlate connate water content with the core sample permeability in a particular reservoir to a certain distance. The complication of the relationship between pore geometry and permeability has determined in many studies. No relationship connecting the two parameters has been proved yet. As an alternative, there are overabundance correlations for calculating permeability. The following are the two empirical approaches are widely used to determine the permeability using connate water saturation and porosity parameter.

1.  **The Timur Equation**

Timur (1968) suggested the below equation to estimate the permeability as a function of connate water saturation and porosity, and the equation can only be applied in hydrocarbon-bearing zones (Eq. 3.15):

$$K = 8.58102 \left( \frac{\emptyset^{4.4}}{Swc^2} \right) \tag{3.15}$$

The following a logarithmic-linear Equation, are functional mainly in sandstones (Eq. 3.16):

$$log\,10^k = C log\,10^{\emptyset e} + D \tag{3.16}$$

2. **The Morris-Biggs Equation**

Morris and Biggs (1967) proposed the below two equations to estimate the permeability of both oil and gas reservoirs.

For oil reservoir (Eq. 3.17),

$$K = 62.5 \left( \frac{\emptyset^3}{Swc} \right)^2 \tag{3.17}$$

For gas reservoir (Eq. 3.18),

$$K = 2.5 \left( \frac{\emptyset^3}{Swc} \right)^2 \tag{3.18}$$

Where $\phi_e$ is effective porosity as a bulk volume fraction, k is absolute permeability in millidarcies, and $S_w$ is effective water saturation above the transition zone as a part of PV. Parameters C and D are very approximate Figures (equal to about 7).

## 3.4  Vertical and Horizontal Permeability

The horizontal permeability is considered the same in all direction (but not constant). However, vertical permeability is considerably lesser than horizontal permeability once sediments are poorly sorted, angular, and irregular, particularly in clastics. Vertical/horizontal ($k_v/k_h$) values are generally in the range 0.01–0.1.

## 3.5  Factors Affecting the Permeability Value

Various factors influence the value and/or direction of permeability.

- Textural properties

    a.  Pore size/particle size
    b.  Particle size distribution
    c.  Geometry of particles
    d.  The particle Sorting

- Cementation
- Void ratio of particles
- The lithology of the formation type
- Porosity of the formation
- Fracturing and solution
- Overburden pressure
- High velocity flow effects
- type of fluid in formation
- Gas slippage
- Degree of saturation
- Temperature and viscosity of water (Impurities in water)
- Entrapped air and organic matter.

## 3.6   PoroPerm Relationships

Permeability is of paramount importance to the hydrocarbon industry because it defines the viability of the fluids that can be extracted from reservoir rock. The most effective parameter on permeability is porosity. Naturally, higher porosities mean there are many fairways for fluid to flow. One of the important practices that are used to permeability data is to plot it on a logarithmic scale poroperm cross-plot diagram refer to Fig. 3.12.

To obtain better results, poroperm cross-plots need to be plotted for clearly defined reservoir zones. In the same time, Poroperm plot for different reservoir rocks can be constructed together on the same plot, and form a map of poroperm relationships, as shown in Fig. 3.11. This plot would be time consumed to identify all reservoir rock units, but the interpretation can be made. Normally, there is a sort of relationship within a specific rock unit and the variations between rock units which might be
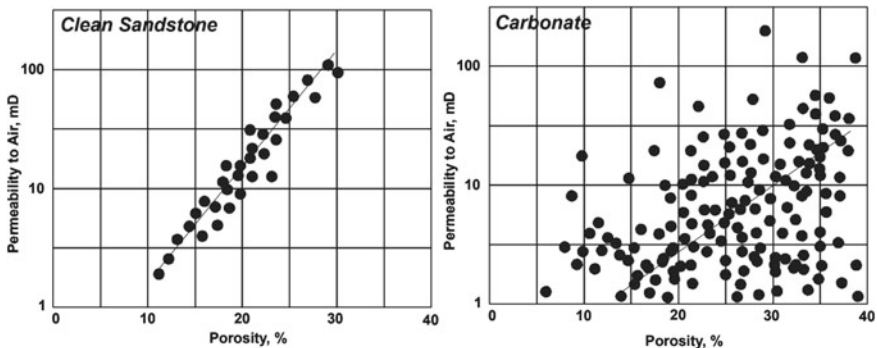


**Fig. 3.12**   Poroperm cross-plots (*Source* Glover, formation evaluation M.Sc. course notes)

**Fig. 3.13** Poroperm relationships for different lithologies (*Source* Glover, formation evaluation M.Sc. course notes)
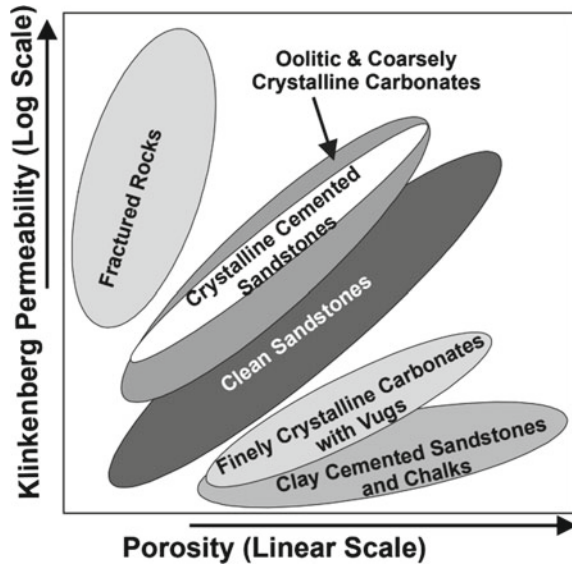


important in the reservoir rock analysis. The main purposes of the poroperm cross-plot are to predict the permeability when the porosity data is available only and to create a porosity cut-off.

The plotted data on Fig. 3.13, as an example, shows the permeability of the sandstone is very well controlled by the porosity, while the carbonate plot displays more scattering data showing that the porosity has an effect, but there are other main factors governing the permeability. Commonly, some carbonates reservoirs have high porosities and low permeabilities; this is because there is no interconnecting between the effective porosity (vugs or cavity) of the reservoir.

## 3.7 Microbialite Poro-Perm

The exploration of widespread hydrocarbon accumulations in carbonate formations defined as "Microbialites" in the palaeo-lacustrine deposition in a pre-salt carbonate formation. Currently, proto-Atlantic sag and rift formations offshore of Brazil (Fig. 3.14) (Beasley et al. 2010), and Angola (Wasson et al. 2012) are the most discussed pre-salt carbonate reservoirs.

These greatly potential Cretaceous basins made during the separation of Africa and South America continentals (Reston 2009). Many explorations activities proved that these unique pre-salt carbonate reservoirs, holding giant accumulations of oil. At the end of 2007, a giant oil and gas reserve was discovered in the pre-salt reservoir covering more than 800,000 m offshore which is located between the Brazilian states of Espirito Santo and Santa Catarina, which is the highest accumulation of pre-salt
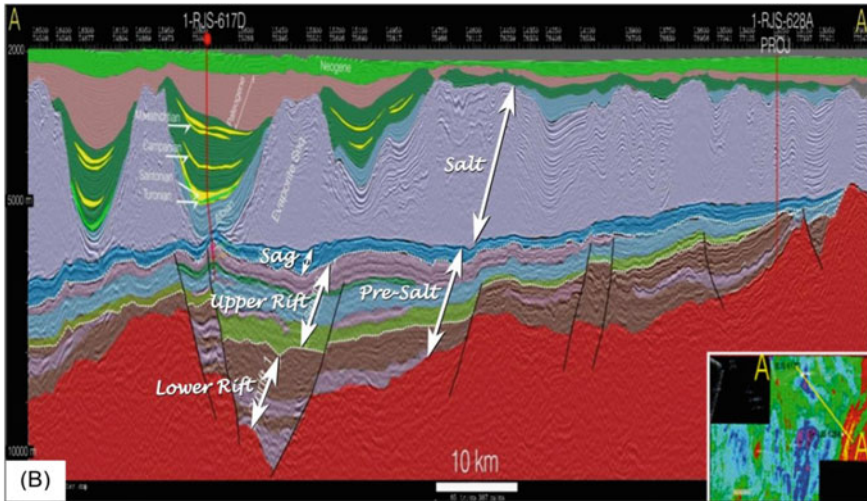
**Fig. 3.14** A Pre-Salt location map of Santos, Campos and Espírito Santo basins, offshore Brazil. B Pre-Salt seismic map from Santos basin (*Source* Bueno et al. 2009)

oil are discovered from the Northeast to South of Brazil, in the Gulf of Mexico and in Africa's West coast (Izundu 2009).

Pre-salt refers to any phenomenon occurring before the deposition of the salt layer (e.g. oil generation and migration, fold generation, sedimentary deposition). Sub-salt refers to any phenomenon or thing occurring below an existing layer of the mass of salt (e.g. oil trapping, a seismic reflector, a layer of rock). The Pre-Salt play has been successfully drilled in the Brazilian and Angolan Aptian and in other basins where the stratigraphy and salt age is older.

Figure 3.15 display one of the reservoir characteristics of the Pre-Salt section. Terra et al. (2010) characterized the different external morphologies and textural rock types from the Pre-Salt reservoirs.

For pre-salt carbonate formations that may comprise vugs and fractures, there is no identifiable relationship. Generally, reservoir rock properties are governed by Interparticle pore networks, and vuggy pore network. Typically reservoir properties are highly affected by vugs interconnection either separate vugs or direct vug-vug contact (Lucia 1999, 2007).

Petrographic researches at microscopic scales proved that pre-salt carbonates exhibit a wide range of textures that can differ within sub-centimeter space see Fig. 3.16 and that none of the textural rock types keeps special pore space characteristics refer to Fig. 6 (Chitale et al. 2014).

Figure 3.17 clearly shows the highest obvious effects of diagenesis on the pre-salt carbonate pore space. Some of the diagenetic methods increase the original porosity and permeability but others may yield the opposite result. Generally, the diagenesis process may increase porosity with simultaneous reduction in permeability and
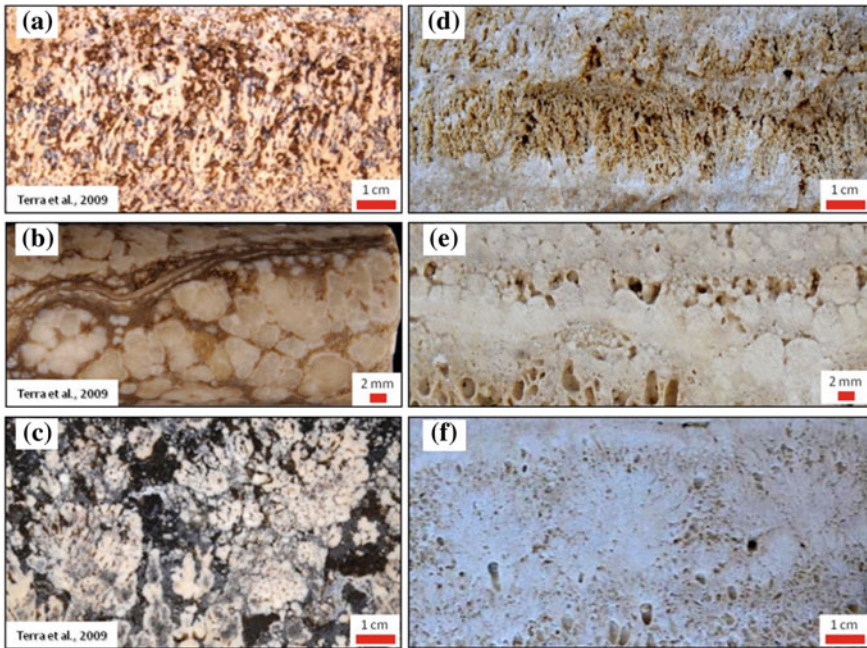
**Fig. 3.15** Images from (**a**) to (**f**) show Pre-Salt textural rock type (Exhibit different porosity and pore size distribution) (*Source* Terra et al. 2010)

vice versa. Accordingly, fluid saturations in these pre-salt rocks are affected as well depicted in Fig. 3.18 (Source: Chitale et al. 2014).

In general, the new applied technologies are proved to be as a good tool to improve the formation evaluation accuracy of the pre-salt carbonate formation which is required for exploration and appraisal assessments. Also, the advanced logs such as elemental spectroscopy, NMR, borehole imaging along with advanced core analysis methods can help to characterize the heterogeneities the pre-salt carbonates.

## 3.8  Estimating Permeability Based on Kozeny-Carman Equation

The Carman-Kozeny equation has been used to calculate permeability (k). The equation derived from the combination of Darcy's and Poiseuille's laws. Whereas Darcy's formula macroscopically measures fluid flow, Poiseuille's formula defines the parabolic movement of a viscous fluid in a straight-circular tube.

The Kozeny-Carman equation is proposed as a permeability function of porosity, grain size, and tortuosity (Kozeny 1927). The equation is normally applied to determine fluid pressure drop in pores media that includes consolidated sand grains. This
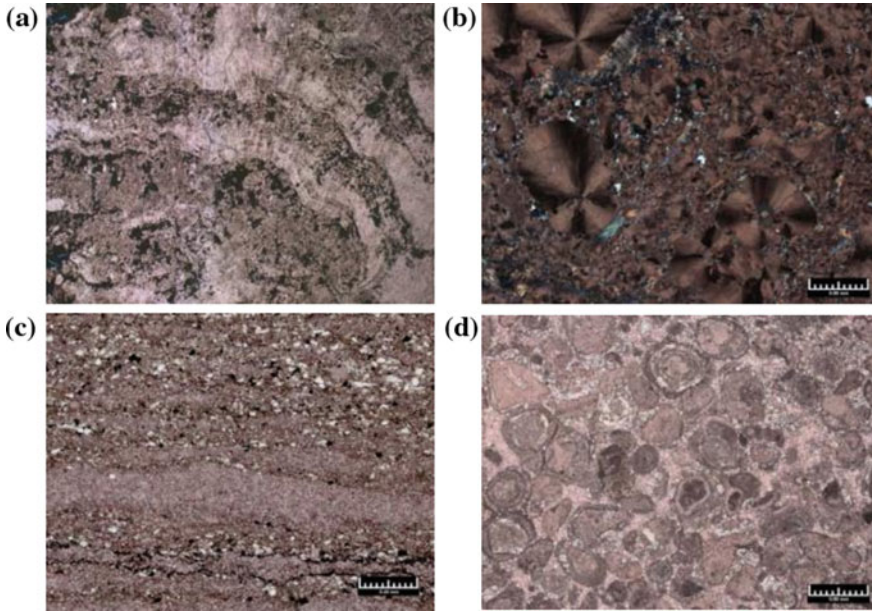
**Fig. 3.16** Pre-salt carbonates core structure. **a** Darker microbe rich layers with lighter silica rich bands; **b** Spherules, **c** Dolo-mudstone and silica, **d** Oolites (*Source* Chitale et al. 2014)
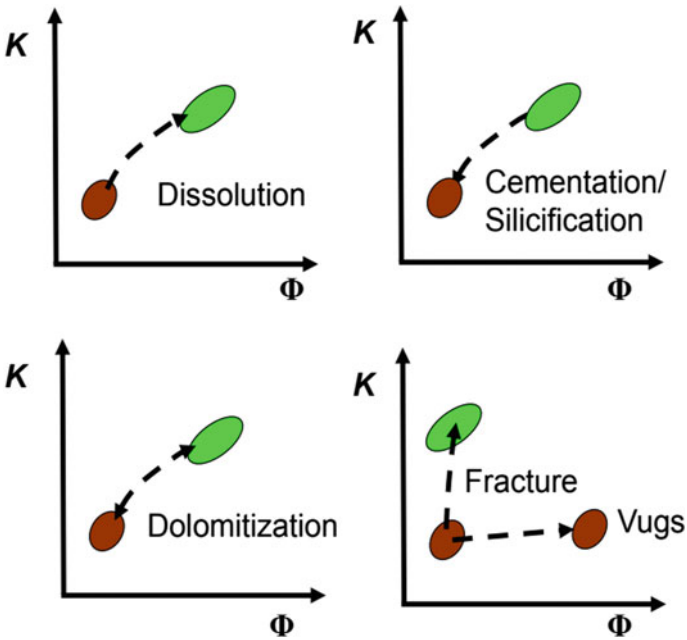


**Fig. 3.17** Common pre-salt carbonate diagenetic processes against possible variations in porosity and permeability (*Source* Chitale et al. 2014)
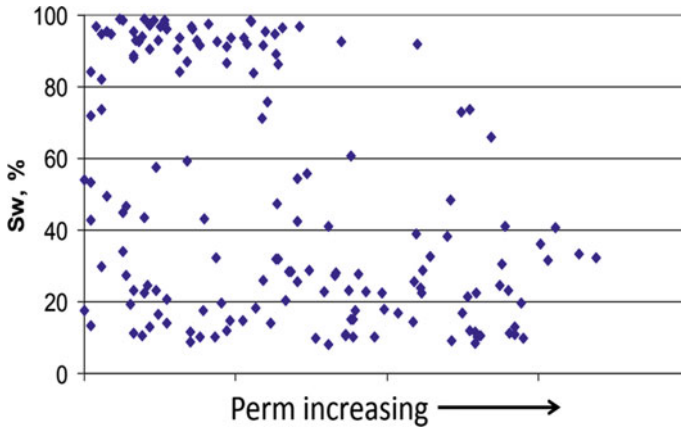
**Fig. 3.18** Example of pre-salt carbonates showing the large variation in permeability versus fluid saturation (*Source* Chitale et al. 2014)

equation is applicable to calculate permeability models for a particular single-phase flow. As the Kozeny equation is applied to estimate permeability development versus porosity, the particle size and tortuosity are kept constant. Usually, the Kozeny equation relates the absolute permeability $k_A$ (mD) to porosity Ø (fraction) and grain size *d* (mm) as (Eq. 3.19):

$$kA \sim d2\,\text{Ø}3 \tag{3.19}$$

This relation is often applied to simulate permeability versus porosity development in datasets. Therefore, in the calculations, the grain size d is usually held constant. The following is the single-phase Kozeny equation (Mc Cabe et al. 2005) (Eq. 3.20):

$$K = a\frac{\text{Ø}^3 D_p^2}{(1 - \text{Ø})^2} \tag{3.20}$$

where a is the proportionality and unity factor [mD/mm$^2$]. The combined proportionality and unity factor a has normally average value of $0.8 \times E^6/1.0135$ fluctuating from high to low clay content, however, for clean sand, it might reach a value of $3.2 \times E^6/1.0135$.

## 3.9 Directional Permeability

Typically, in very homogeneous reservoirs the permeability is considered to be identical in all directions. Conversely, in heterogeneous reservoirs, the permeabilities in all directions are considerably different. Such variations in the permeabilities in all
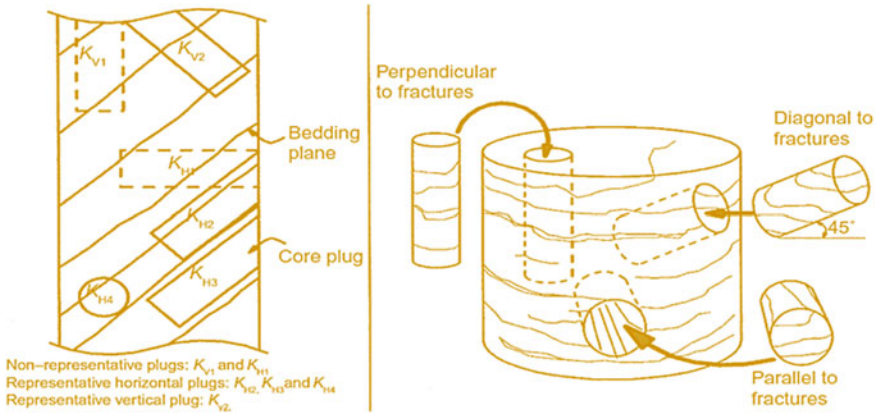
**Fig. 3.19**  Orientation core plugs for determine directional permeabilities

directions have a significant impact on the efficiency of the natural recovery and on the waterflood process. Directional permeabilities can be obtained by using core plugs in the lab and by horizontal well test analysis using selective zonal well testing techniques. Normally, core plugs are cut perpendicularly from the main wellbore core. Also, the vertical permeability is cut perpendicular to the bedding plane, as seen in Fig. 3.19. The latest technological developments in well logging also provide the estimates of directional permeability.

Directional permeability is often used to describe the amount of heterogeneity in the reservoir rock. The main effect of anisotropy is either the loss or gain in effective permeability of a reservoir rock. This can occur because the permeability increased in one direction and decreased in another direction. This effect, causing average permeability is less than the highest permeability in any direction. To illustrate these phenomena when a vertical fractured reservoir has higher permeability in the vertical direction and low matrix permeability in the horizontal direction. These differences in reservoir rock permeability known as anisotropy.

## 3.10  Lorenz Coefficient

In 1950, Schmalz and Rahme (1950) presented a single factor that defines the degree of reservoir rock heterogeneity within a pay zone section. The term is named Lorenz coefficient and varies between zeros, for a totally homogeneous reservoir rock, to one for a totally heterogeneous reservoir rock.

The main steps for calculating the Lorenz coefficient are as follows:

(1)  Put all the permeability values in descending order.
(2)  Determine both, the cumulative permeability capacity $\sum kh$ and cumulative volume capacity $\sum \phi h$.

(3)  Normalize both cumulative capacities from 0 to 1.
(4)  Plot the normalized cumulative permeability capacity against the normalized cumulative volume capacity on a Cartesian scale.

Figure 3.20 shows the normalized flow capacity. The totally identical system which has all permeabilities are equal, and a plot of the normalized $\sum kh$ against $\sum \phi h$ would be a straight line. Figure 3.20 displayed that as the difference between high and low permeability values increases the plot displays greater concavity toward the upper left corner. As seen in the plot, the deviation from a straight line is a sign of the degree of heterogeneity. The plot can be applied to define the reservoir heterogeneity quantitatively by computing the Lorenz coefficient. The coefficient is defined by the following expression (Eq. 3.21):

$$L = \frac{Area\ ABCD}{Area\ ADCA} \tag{3.21}$$

where the Lorenz coefficient L can vary between 0 and 1.

0  Totally homogeneous
1  Totally heterogeneous.
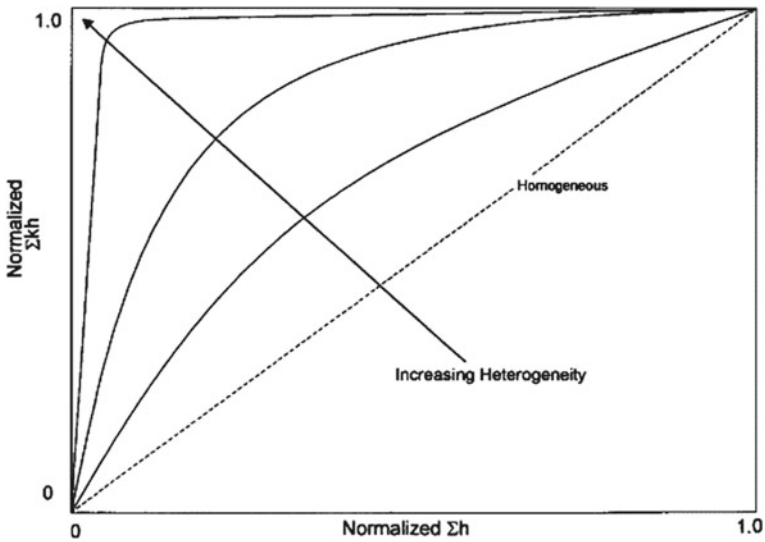


**Fig. 3.20**  Normalized flow capacity (*Source* Craig 1971)

## 3.11   Dykstra-Parsons Coefficient

The Dykstra-Parsons coefficient ($V_K$), is an alternative measure of heterogeneity. It is unitless method of sample diffusion (Jensen et al. 1997). It is identified as the ratio of the sample standard deviation(s) to the mean. $V_K$ is frequently used in oil and gas industry studies as evaluation of permeability heterogeneity in the reservoir rock (Saner and Sahin 1999). For data from many sources, the mean and standard deviation will differ together such that $V_K$ stays relatively constant. Any big variations in $V_K$ between two plug samples confirm a dramatic difference in the sources related to those plugs (Jensen et al. 1997). Besides, the coefficient of variation is applied to have a relative measure of data diffusion compared to the mean for the normal distribution. The coefficient of variation may be described either as a simple decimal value, or percentage value ($0 < V_K < 1$). When the coefficient value is near 0, the data scatter compared to the mean is small. Consequently, when the $V_K$ is near 1 the data scatter compared to the mean is large. Generally, Dykstra and Parsons applied the log-normal distribution of permeability to describe the coefficient of permeability changes (Dykstra and Parsons 1950) (Eq. 3.22).

$$V_k = \frac{s}{\overline{k}} \tag{3.22}$$

where s is the standard deviation, $\overline{k}$ is the mean value of $k$. For the group of data, the standard deviation is (Eq. 3.23):

$$s = \sqrt{\sum_{i=1}^{n} (k_i - \overline{k})^2)/n - 1} \tag{3.23}$$

Or Eq. 3.24:

$$s = \sqrt{\sum_{i=1}^{n} (k_i^2 - n\overline{k}^2)/n - 1} \tag{3.24}$$

where $\overline{k}$ is the arithmetic average of permeability, $n$ is the total number of data, and $k_i$ the permeability of each single core samples. In a normal distribution, the $k$ value is such that 84.1% of the permeability values are less than $\overline{k} + s$ and 15.9% of the $k$ values are less than $\overline{k} - s$.

The Dykstra-Parsons coefficient of permeability variation, $V_K$, can be obtained graphically by plotting permeability values on log-probability paper, as shown in Fig. 3.21, and then using the following Eq. 3.25:

$$V_k = \frac{k_{50} - k_{84.1}}{k_{50}} \tag{3.25}$$

**Fig. 3.21** Log-normal permeability distribution (*Source* Dykstra and Parsons 1950)
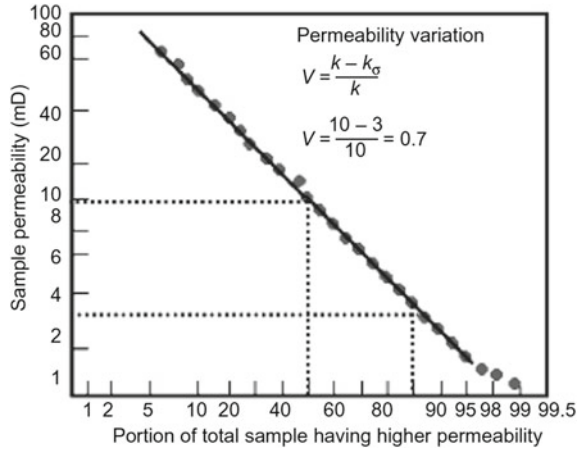


where $k_{50}$ is the value of the permeability with 50% probability and $k_{84.1}$ is the value of the permeability at 84.1% of the cumulative sample.

For a log-normal permeability distribution, the Dykstra-Parsons coefficient can be estimated from the following (Eq. 3.26):

$$V_k = 1 - \exp\left[-\sqrt{ln\left(-\frac{k_a}{k_h}\right)}\right] \qquad (3.26)$$

where $k_a$ is the arithmetic average permeability, $k_h$ is the harmonic average permeability. The $V_K$ is also referred to as the Reservoir Heterogeneity Index. The range of this index is $0 < V_K < 1$. When $V_K = 0$, ideal homogeneous reservoir; $0 < V_K < 0.25$, slightly heterogeneous reservoir; $0.25 < V_K < 0.50$, heterogeneous reservoir; $0.50 < V_K < 0.75$, the reservoir is very heterogeneous; $0.75 < V_K < 1$, the reservoir is extremely heterogeneous; $V_K = 1$, perfectly heterogeneous reservoir.

**Example 3.1**
Brine water with viscosity 1.1 cP was flowing in the core sample at a constant rate of 0.35 cm$^3$/s with 1.5 atm pressure differential. The core sample long is 3.5 cm and the cross section area is 4 cm$^2$.

Calculate the absolute permeability.

**Solution**
Darcy Law:

$$q = \frac{kA}{\mu L}(P_1 - P_2)$$

$$k = \frac{q\mu L}{A}(P_1 - P_2)$$

$$k = \frac{(0.35)(1.1)(3.5)(1.5)}{4}$$

$$k = 0.505 \ D$$

## Example 3.2

Use the same data in Example 1 assuming that an oil viscosity used this time is 3 cP to determine the absolute permeability at same deferential pressure with 0.2 cm³/s flow rate?

**Solution**

$$k = \frac{(0.2)(3)(3.5)(1.5)}{4}$$

$$k = 0.788 \ D$$

## Example 3.3

Determine the average permeability of the reservoir rock has the following permeability core data analysis:

| Bed | Interval depth (ft) | Permeability value (md) |
|-----|---------------------|-------------------------|
| 1   | 2500–2504           | 150                     |
| 2   | 2504–2508           | 120                     |
| 3   | 2508–2015           | 180                     |
| 4   | 2515–2520           | 130                     |
| 5   | 2520–2525           | 110                     |
| 6   | 2525–2531           | 200                     |

**Solution**

| Bed | Thickness ($h_i$) (ft) | Permeability ($K_i$) (md) | $h_i \ k_i$ (ft. md) |
|-----|------------------------|---------------------------|----------------------|
| 1   | 4                      | 150                       | 600                  |
| 2   | 4                      | 120                       | 480                  |
| 3   | 7                      | 180                       | 1260                 |
| 4   | 5                      | 130                       | 650                  |
| 5   | 5                      | 110                       | 550                  |

(continued)

| Bed | Thickness ($h_i$) (ft) | Permeability ($K_i$) (md) | $h_i$ $k_i$ (ft. md) |
|-----|-----|-----|-----|
| 6 | 6 | 200 | 1200 |
| | $\Sigma h_i = 31$ | | $\Sigma h_i k_i = 4740$ |

$$k = \Sigma h_i k_i / \Sigma h_i$$

$$k = \frac{4740}{31} = 153 \, \text{md}$$

## Example 3.4

Calculate an average reservoir permeability for a series reservoir beds have average permeability of 10, 50 and 1000 md, which are 6, 18 and 40 ft respectively in length but of equal cross-section when placed in series as shown in the below Figure.
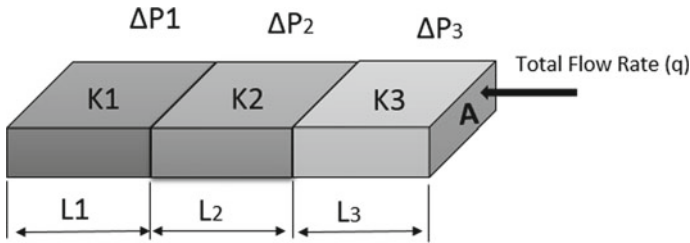


$$Q_t = Q_1 = Q_2 = Q_3$$
$$\Delta P_t = \Delta P_1 + \Delta P_2 + \Delta P_3$$
$$L_t = L_1 + L_2 + L_3$$

$$Q_t = \frac{K_{avg} A \Delta P_t}{\mu L}, \, Q_1 = \frac{K_{avg} A \Delta P_1}{\mu L}, \, Q_2 = \frac{K_{avg} A \Delta P_2}{\mu L} \quad \text{and} \quad Q_3 = \frac{K_{avg} A \Delta P_3}{\mu L}$$

Solving for pressure and substituting for $\Delta p$.

$$\frac{Q_t \mu L}{K_{avg} A} = \frac{Q_t \mu L}{K_1 A} + \frac{Q_t \mu L}{K_2 A} + \frac{Q_t \mu L}{K_3 A}$$

$$\frac{L}{K_{avg}} = \frac{L}{K_1} + \frac{L}{K_2} + \frac{L}{K_3}$$

$$K_{avg} = \frac{L}{\sum_{i=1}^{n} K_I L_i}$$

$$K_{avg} = \frac{6 + 18 + 40}{\frac{6}{10} + \frac{18}{50} + \frac{40}{1000}} = 64md$$

## Example 3.5

There are six reservoir stratums were stacked in series. All stratums have equal thickness. The length and permeability for each stratum are given in the below table. Estimate the average reservoir permeability of linear flow system.

| Bed | Length (ft) | Permeability (md) |
|-----|-------------|-------------------|
| 1 | 100 | 90 |
| 2 | 200 | 70 |
| 3 | 150 | 60 |
| 4 | 300 | 45 |
| 5 | 150 | 30 |
| 6 | 200 | 15 |

**Solution**

| Bed | $L_i$ (ft) | $k_i$ (md) | $L_i k_i$ |
|-----|-----------|-----------|-----------|
| 1 | 100 | 90 | 9000 |
| 2 | 200 | 70 | 14,000 |
| 3 | 150 | 60 | 9000 |
| 4 | 300 | 45 | 13,500 |
| 5 | 150 | 30 | 4500 |
| 6 | 200 | 15 | 3000 |
| | $\Sigma L_i = 1100$ | | $\Sigma L_i k_i = 53,000$ |

$$k = \Sigma h_i k_i / \Sigma h_i$$

$$k = \frac{53,000}{1100} = 48 \, md$$

## Example 3.6

There are six reservoir segments were stacked in series. All stratums have equal thickness. The length and permeability for each stratum are given in the below table.

By assuming wellbore radius is 0.24 ft, Estimate the average reservoir permeability of redial flow system.

| Bed | $r_i$ (ft) | $k_i$ (md) | $\ln(r_i/r_{iB1})$ |
|-----|-----------|-----------|-------------------|
| 1 | 150 | 80 | 6.397 |
| 2 | 350 | 50 | 0.847 |
| 3 | 650 | 30 | 0.619 |
| 4 | 1150 | 25 | 0.571 |
| 5 | 1350 | 10 | 0.160 |

| Bed | $r_i$ (ft) | $k_i$ (md) | $\ln(r_i/r_{iB1})$ | $[\ln(r_i/r_{iB1})]/k_i$ |
|-----|-----------|-----------|-------------------|--------------------------|
| 1 | 150 | 80 | 6.397 | 0.080 |
| 2 | 350 | 50 | 0.847 | 0.017 |
| 3 | 650 | 30 | 0.619 | 0.021 |
| 4 | 1150 | 25 | 0.571 | 0.029 |
| 5 | 1350 | 10 | 0.160 | 0.016 |

$$\Sigma[\ln(r_i/r_iB_i)]/k_i = 0.163$$

Then,

$$k_{avg} = \frac{LN\left(\frac{1350}{0.25}\right)}{0.163} = 53 \, \text{md}$$

## Example 3.7
Using Timur equation, calculate the absolute of an oil-bearing zone has the average porosity of 20% and water saturation 25%.

## Solution
Timur equation:

$$K = 8.58102\left(\frac{\emptyset^{4.4}}{Swc^2}\right)$$

$$K = 8.58102\left(\frac{0.2^{4.4}}{0.25^2}\right) = 0.115 \, \text{Darcy}$$

**Example 3.8**

Using Morris and Biggs equation, calculate the absolute of an oil-bearing zone has the average porosity of 20% and water saturation 25%.

**Solution**

Morris and Biggs equation:

$$K = 62.5 \left( \frac{\emptyset^3}{Swc} \right)^2$$

$$K = 62.5 \left( \frac{0.2^3}{0.25} \right)^2 = 0.064 \, \text{Darcy}$$

**Example 3.9**

A gas flow test is performed at two pressures:

**Test 1**; applied P = 12 atm
**Test 2**; applied P = 3 atm.

The test used a rock has absolute permeability of 2.0 md, and the gas viscosity of 0.01 cP, can be considered as constant value for both tests. Klinkenberg's b-factor approximately equal to 1.0 for rock has a permeability of 2.0 mD.

Calculate the apparent gas permeability for the two tests?

**Solution**

Therefore, for test 1, the apparent gas permeability is estimated to be:

$$K_g = K_L \left( 1 + \frac{b}{P} \right)$$

$$K_g = 2 \left( 1 + \frac{1}{12} \right) = 2.2 \, \text{md}$$

For Case 2,

$$K_g = 2 \left( 1 + \frac{1}{3} \right) = 2.7 \, \text{md}$$

This difference of 50% will generate a major error in calculated permeability value if Klinkenberg's effect was ignored. The Klinkenberg effect is also reliant on gas composition as seen in Fig. 3.10.

**Example 3.10**

Typically, the permeability of the damaged layer next to the wellbore affects the average reservoir permeability more than undamaged zone permeability. Calculate the average permeability using the following data:

$k_1 = 15$ mD $r_1 = 1.5$ ft
$k_2 = 250$ mD $r_2 = 200$ ft
$r_w = 0.24$ ft



**Solution**

$$K_{avg} = \frac{ln\left(\frac{r_e}{r_w}\right)}{\sum_{i=1}^{n}\left[\frac{ln\left(\frac{r_j}{r_j}-1\right)}{K_j}\right]}$$
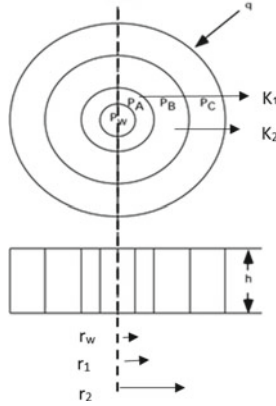
$$K_{avg} = \frac{ln\left(\frac{200}{0.24}\right)}{\sum_{i=1}^{n}\left[\frac{ln\left(\frac{1.5}{0.24}\right)}{15} + \frac{ln\left(\frac{200}{1.5}\right)}{250}\right]} = 47.4\,\text{md}$$

**Example 3.11**
Using Poiseuille's and Darcy's Equations for high viscosity flow through capillary tubes (consider the flow through channels and fractures), estimate the permeability of a rock composed of strongly packed capillaries 0.0002 inch in diameter.
   Poiseuille's equation used for high viscosity flow through capillary tubes;

$$q = \frac{\pi r^2}{8\mu L}(P_1 - P_2)$$

where

$$A = \pi r^2$$

$$q = \frac{A}{8\mu L}(P_1 - P_2)$$

Darcy Equation for linear flow of liquids;

$$q = \frac{kA}{\mu L}(P_1 - P_2)$$

Considering the equations have consistent units

$$\frac{A}{8\mu L}(P_1 - P_2) = \frac{A}{\mu L}(P_1 - P_2)$$

Thus

$$K = \frac{r^2}{8} = \frac{d^2}{32}$$

where:

d = inches, k = $20 \times 10^9$ d$^2$ mD
k = $20 \times 10^9$ d$^2$
k = $20 \times 10^9$ (0.0002 in)$^2$
k = 800 mD

**Example 3.12**
Use the Figure to calculate the Lorenz (LK).
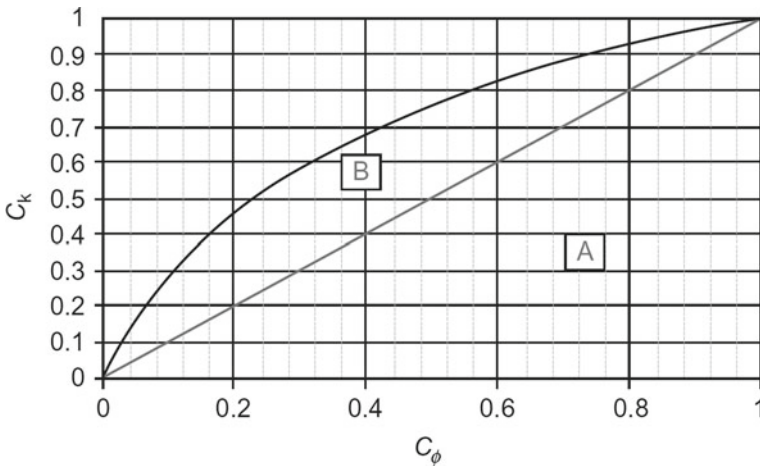
**Solution**

The areal summation method yields 0.5 for the area A and 0.21 for area B, then applying Lorenz coefficient Eq. 3.4.

$$L = \frac{Area\ ABCD}{Area\ ADCA}$$

L = 0.21/0.5 = 0.42.

# References

Amyx J, Bass D, Whiting R (1960) Petroleum reservoir engineering physical properties. ISBN:9780070016002, 0070016003

Babadagli A, Al-Bemani K, Al-Shammakhi (2001) Assessment of permeability distribution through well test analysis. https://doi.org/10.2118/68707-ms, SPE-68707-MS, SPE Asia Pacific Oil and Gas Conference and Exhibition, 17–19 April, Jakarta, Indonesia

Baehr A, Hult M (1991) Evaluation of unsaturated zone air permeability through pneumatic tests. Water Resour Res 27(10):2605–2617

Beasley C, Fiduk J, Bize E, Boyd A, Frydman M, Zerilli A, Dribus J, Moreira J, Capeliero A (2010) Brazil's subsalt play. Oilfield Rev 22(3):28–37

Bueno R, Lavín MF, Marinone SG, Raimondi PT, Shaw WW (2009) Rapid effects of marine reserves via larval dispersal. PLoS ONE 4(1):e4140. https://doi.org/10.1371/journal.pone.0004140

Chitale V, Gbenga A, Rob K, Alistair T, Paul (2014) Learning from deployment of a variety of modern petrophysical formation evaluation technologies and techniques for characterization of a pre-salt carbonate reservoir: case study from campos basin, Brazil. Presented at the SPEWLA 55th Annual Logging Symposium Abu Dhabi, 18–22 May. SPWLA-2014-G

Craig Jr (1971) The reservoir engineering aspects of Waterflooding. In: SPE of A.I.M.E., Dallas, 1971, pp 64–66

Dake L (1978) Fundamentals of reservoir engineering. Elsevier, Amsterdam

Dykstra H, Parsons R (1950) The prediction of oil recovery in waterflood. Secondary recovery of oil in the United States, 2nd edn. American Petroleum Institute (API), Washington, DC, pp 160–174

Folk R (1959) Practical petrographic classification of limestones. AAPG Bulletin 43:1–38

Izundu U (2009) Soco spuds Liyeke Marine-1 oil well off Congo. Oil Gas J, 24 Aug

Jensen J, Lake L, Corbett P, Goggin D (1997) Statistics for petroleum engineers and geoscientists. Prentice Hall, Upper Saddle River, NJ, pp 144–166

Kozeny J (1927) ber kapillare Leitung des Wassers im Boden (Aufstieg Versikerung und Anwendung auf die Bemasserung), Sitzungsber Akad., Wiss, Wein, Math. Naturwiss. Kl 136 (Ila), pp 271–306

Lock M, Ghasemi M, Mostofi V, Rasouli (2012) An experimental study of permeability determination in the lab. WIT Trans. Eng. Sci. 81. Department of Petroleum Engineering, Curtin University, Australia. http://dx.doi.org/10.2495/PMR120201

Lucia FJ (1999) Characterization of petrophysical flow units in carbonate reservoirs: discussion. AAPG Bull 83(7):1161–1163

Lucia FJ (2007) Predicting petrophysical properties based on conformance between diagenetic products and depositional textures (abs.). American Association of Petroleum Geologists Annual Convention 16:85

McCabe W, Smith J, Harriot P (2005) Unit operations of chemical engineering (7th ed.). McGraw-Hill, New York, pp 163–165, ISBN 0-07-284823-5

Morris RL, Biggs WP (1967) Using log-derived values of water saturation and porosity. In: Transactions of the SPWLA 8th annual logging symposium, Paper X, p 26

Reston T (2009) The extension discrepancy and syn-rift subsidence deficit at rifted margins. Petrol Geosci 15(3):217–237

Saner S, Sahin A (1999) Lithological and Zonal porosity-permeability distributions in the Arab D Reservoir, Uthmaniyah Field, Saudi Arabia. Am Assoc Petrol Geol Bull 83(2):230–243

Schmalz J, Rahme H (1950) The variation in waterflood performance with variation in permeability profile. Producer's Mon, 9–12

Terra G et al (2010) Carbonate rock classification applied to Brazilian sedimentary basins. Boletin Geociencias Petrobras 18(1):9–29

Timur A (1968) An investigation of permeability, porosity and residual water saturation relationships for sandstone reservoirs. Log Anal 9(4)

Wasson M, Saller A, Andres M, Self D, Lomando A (2012) Lacustrine microbial carbonate facies in core from the lower Cretaceous Toca Formation, Block 0, offshore Angola. Abstract AAPG Hedberg Conference "Microbial Carbonate Reservoir Characterization" June 4–8, 2012—Houston TX, p 4

# Chapter 4
# Wettability

Check for
updates

If two immiscible fluids get in touch with a solid surface, one phase will have more a tendency to adhere to the solid surface than the other phase. This due to the balance of intermolecular forces and surface energies between immiscible fluids and the solid. As displayed in Fig. 4.1, vector forces are balanced at the contact point of oil-water-solid, which is defined by Eq. (4.1):

$$\sigma_{OS} - \sigma_{WS} = \sigma_{OW} \cos \theta_c \tag{4.1}$$

where:

$\sigma_{OS}$   Interfacial tension between oil and solid
$\sigma_{WS}$   Interfacial tension between water and solid
$\sigma_{OW}$   Interfacial tension between oil and water
$\theta_c$   Contact angle between water and oil at the measured contact point through the water

Contact angles, when $\theta < 90°$, the system is identified as "water wet" and water will extend on the solid surface; and when $\theta > 90°$, the system is identified as "oil-wet" and oil will extend on the solid surface.
Adhesion Tension (Eq. 4.2),

$$\sigma_{WS} - \sigma_{oS} = \sigma_{oW} \cos \theta \tag{4.2}$$

Adhesion Tension = When the solid is "water-wet"

**Fig. 4.1** Interfacial interactions of water-oil-solid



$\theta > 90°$

$\theta < 90°$

Non-wetting     Wetting

$$\sigma_{WS} \geq \sigma_{oS}$$

Adhesion Tension $= +$

$$\cos \theta = +$$
$$0° \leq \theta \leq 90°$$
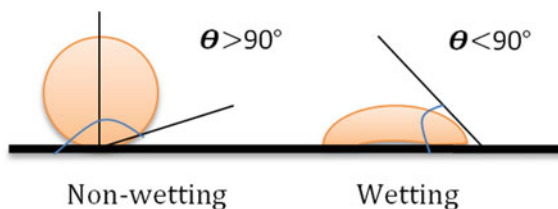
When $\theta = 0°$—strongly water-wet
When the solid is "oil-wet"

$$\sigma_{WS} \geq \sigma_{oS}$$

Adhesion Tension $= -$

$$\cos \theta = -$$
$$90° \leq q \leq 180°$$

When $\theta = 180°$—strongly oil-wet.

## 4.1   Surface Tension and Contact Angle

Characteristically, the form of a liquid droplet is designed by the surface tension of the liquid. Where in a very clean liquid, every molecule is dragged similarly in all directions by adjacent liquid molecules, causing an equilibrium net force of zero. However, the molecules located at the surface of droplet do not have adjacent molecules at any directions to make a stable net force. Instead, they are dragged internally by the adjacent molecules see Fig. 4.2, generating an internal pressure. Consequently, the liquid freely bonds its surface area to keep the lowest surface free-energy.

Therefore, the intermolecular energy to bond the surface area is termed the surface tension, and it controls the form of liquid droplets. In fact, the gravity forces can reshape the droplet; accordingly, both gravity force and surface tension can designate

**Fig. 4.2** Surface tension is generated by equilibrium forces of liquid molecules at the solid surface

the contact angle. Ideally, the contact angle is anticipated to be characteristic for a specified solid-liquid system in an ascertain environment (Jacco and Bruno 2008).

As proposed by Young (1805), the mechanical equilibrium of the liquid droplet is designed the contact angle on a solid surface under the effect of the liquid-vapor, solid-vapor, and solid-liquid interfacial tensions (Eq. 4.3).

$$\gamma_{lv}\cos\theta_Y = \gamma_{sv} - \gamma_{sl} \tag{4.3}$$

where: $\gamma_{lv}$, $\gamma_{sv}$, and $\gamma_{sl}$ denote the liquid-vapor, solid-vapor, and solid-liquid interfacial tensions, respectively, and $\theta_Y$ is referred to Young's contact angle.

Typically, the determination of a single static contact angle to describe wetting phase performance is no longer satisfactory. Once there is three-phase flow, the contact line is in physical motion, which in this case referred to dynamic contact angle. Especially, the contact angles shaped by extending and bonding the liquid are denoted to as the advancing contact angle, $\theta_a$, and the receding contact angle, $\theta_r$ shown in Fig. 4.3.

The advancing angles approaching a maximum range value, and the receding angles approaching a minimum range value. By using different flow rates, the dynamic contact angles can be determined. At a low flow rate, the dynamic contact angle might be close or equal to the static contact angle value. The difference between the advancing angle and the receding angle is known as the hysteresis (H) (Eq. 4.4):

$$H = \theta_a - \theta_r \tag{4.4}$$

The determination of the contact angle hysteresis is very significant to evaluate the quality of the material surface. An inclined plate approach was presented by Mc Dougall and Ockrent (1942), who improved the sessile drop technique and determined to advance and receding contact angles by inclining the solid surface till the droplet just starts to move (Fig. 4.4). This approach was applied by other researches to investigate the contact angle hysteresis of liquids on a diversity of polymer surfaces.



**Fig. 4.3**  Diagram showing advancing and receding contact angles

**Fig. 4.4** Diagram showing the inclined plate approach, once the droplet begins to move
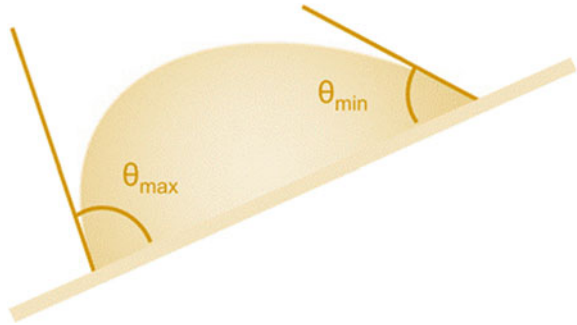
However, this particular relationship between both advancing and receding angles contact angles must be applied carefully because sometimes they can be to a certain degree different.

Lately, Jung and Bhushan (2008) presented an environmental scanning electron microscopy (ESEM) study of the dynamic wetting of super hydrophobic surfaces. Static contact angles were determined when a dynamic equilibrium between condensation and evaporation was reached. By cooling the substrate, the advancing contact angles were determined. On the contrary, receding angles were obtained by heating the substrate. Therefore, the hysteresis was determined, which revealed no clear difference compared to macroscopic drops. The investigators concluded that the hysteresis reliant on the geometric physical characteristics of the patterned surface seen in Fig. 4.5.

ESEM has many advantages for describing micro and nanofibers. Wettability studies at the micro- and nanoscale have open the way for the improvement of wetting configurations.

Generally, the simple and advanced methods applied to characterize the wettability at different scales, such as macro, micro, and nanoscale have been obtained. However, there are several complications with regards wetting mechanisms and for controlling the wetting behavior at both micro- and nanoscales need to be investigated. Atomic force microscopy (AFM) and ESEM are currently the best applicable techniques for imaging ultra-small drops on surfaces. AFM delivers great resolution at the nanometer scale and ESEM provides high resolution at micrometer scale only.

## 4.2 Hysteresis

Hysteresis the history of the permeable rock (Account of water, oil or gas that has flooded the aperture of the rock) will have a physically powerful impact on its wettability; this is identified as "hysteresis" Wettability is very significant in estimating relative permeability and capillary pressure.

Both capillary pressure and the relative permeabilities reliant on the trend of saturation change, as the example displayed in Fig. 4.6. The example shows the gas-oil
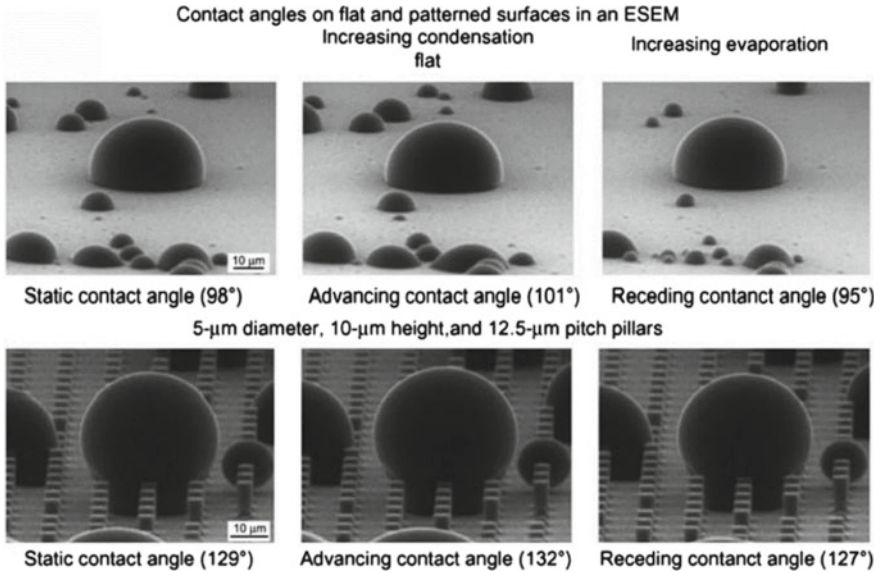
**Fig. 4.5** ESEM images of static, advancing, and receding contact angles of microscopic droplets. *Sources* Jung and Bhushan (2008)
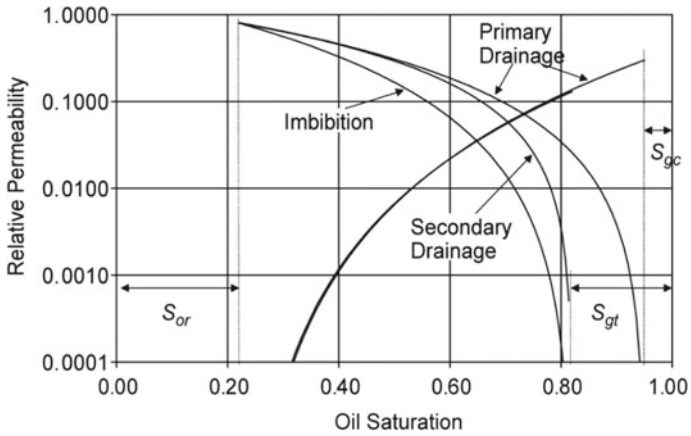


**Fig. 4.6** Hysteresis performances of relative permeabilities. *Source* Geffen et al. (1950)
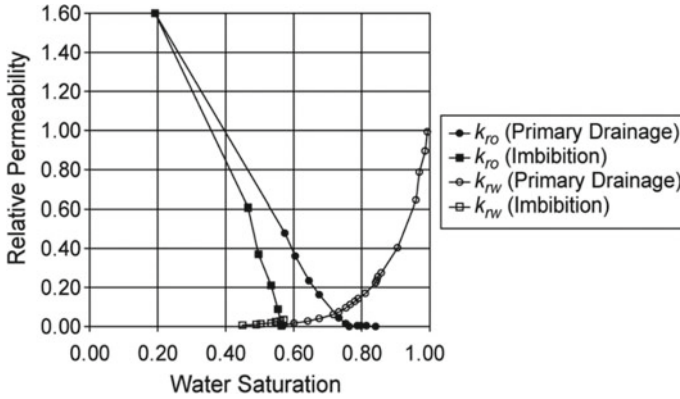
**Fig. 4.7** Hysteresis for sandstone. *Source* Geffen et al. (1950)

system hysteresis is greater for the gas relative permeability. Typically, the hysteresis of the oil wetting phase in the Fig. 4.6 is very small. Where the irreducible gas saturation $S_{gt}$ that residues after imbibition process is a crucial feature of hysteresis.

The actual explanations of hysteresis for water-oil systems are displayed in Fig. 4.7 (Geffen et al. 1950), for instance, one phase illustrates large hysteresis, and the other phase illustrates lesser hysteresis.

## 4.3  Wettability Alteration Using Nanoparticles

Numerous investigators presented results on the wettability alteration applying Nanoparticles (NPs) either alone or as a mixture with the surfactant shown in Fig. 4.8. There are many factors affect the wettability alteration by using NPs such as the con-
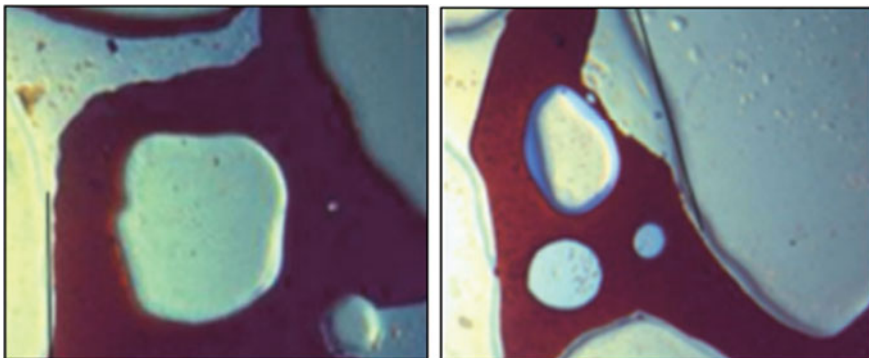


**Fig. 4.8** Pore-scale investigation of wettability (NPs injection). *Source* Maghzi et al. (2012)

centration of NPs, and nature of reservoir condition, nature of oil, concentrations, and kind of NPs. For example, Lipophilic polysilicon NPs can alter the rock wettability from oil-wet to water-wet. Also, NPs can reinforce the wettability of water-wet rock to strong water-wet rock this will delay oil production which effects oil recovery (Onyekonwu and Ogolo 2010). Similarly, Hydrophobic polysilicon NPs can alter the rock wettability from water-wet to oil-wet to more oil-wet rock. Polysilicon NPs can alter the rock wettability to an intermediate wet rock because of the existence of hydrophobic and hydrophilic moieties.

Some other researchers investigated the influence of modified silicon oxide ($SiO_2$) NPs on both light and heavy oil recovery. They concluded that $SiO_2$ NPs can alter the rock wettability of light oil reservoir more than heavy oil reservoir (Roustaei et al. 2012). The optimal concentration of NPs is needed to reach the preferred wettability. There are many wettability alteration studies on Sandston rocks available are available in the literature; however, there are very few researches available on carbonate rocks.

## 4.4 Imbibition and Drainage

Imbibition is the fact of rising wetting-phase in the apertures, while drainage is the reduction in the wetting phase (Fig. 4.9).

Imbibition describes the flow process where the saturation of the wetting phase increases and the non-wetting phase saturation decreases. It is also known as spontaneous imbibition if the capillary pressure is positive and the force is negative. This phenomenon represents water-flood process of an oil reservoir that is water-wet rock. Commonly, it happens when saturated oil placed in water-wet rock, it will absorb water into the smallest apertures, moving oil. Similarly, when the saturated water placed in an oil-wet rock, it will imbibe oil into the smallest apertures, moving water.
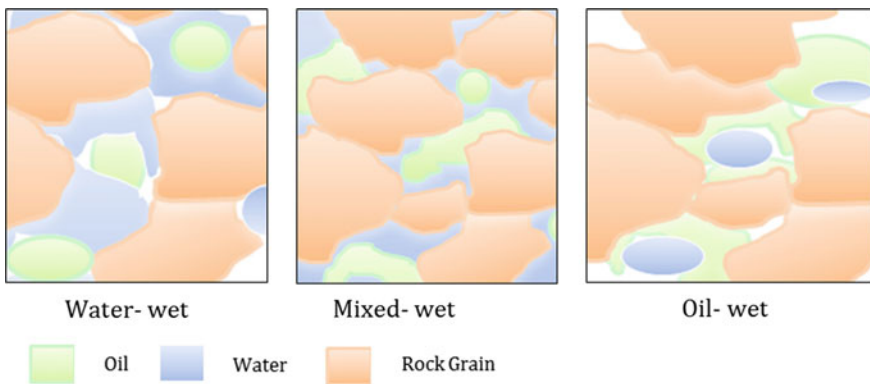


**Fig. 4.9** Types of wettability
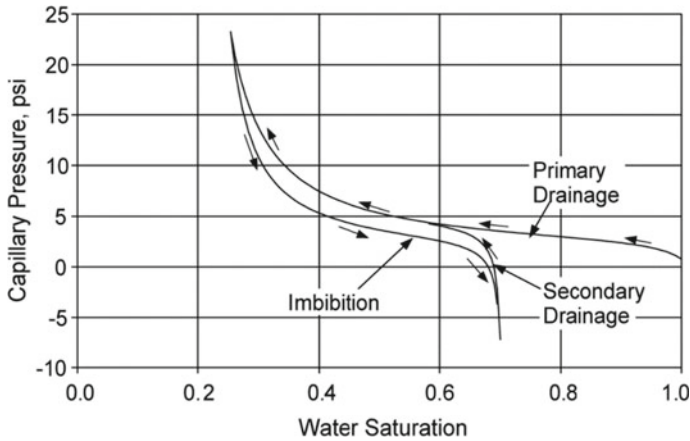
**Fig. 4.10** Primary drainage, imbibition, and secondary drainage for a gas-water system in which the water wets the solid surface. *Source* Morrow and Melrose (1991)

Drainage is defined as the flow process where the water saturation is decreasing. It is also known as spontaneous drainage when the capillary pressure is negative and it is termed forced drainage when it is positive. This phenomenon happens for water-flood process of an oil reservoir that is oil wet (Morrow and Melrose 1991).

The imbibition curves for the "as received" condition are curved and go to zero oil saturation. This is an indication of film drainage where the oil remains connected and goes to low residual oil saturation. With each step of cleaning, the imbibition curves become more vertical and have larger residual oil saturation. This is an indication that oil is trapped as a discontinuous phase. After determination capillary pressure for primary drainage, the path of saturation change can be reversed, where one more saturation and capillary pressure relationship can be obtained. This phenomenon is called an imbibition relationship. Both primary drainage and imbibition relationships vary considerably, as seen in Fig. 4.10 for a gas-water system. (Source Morrow and Melrose 1991).

Generally, the values of capillary pressure reliant on the saturation value and the trend of saturation change. For instance, for imbibition of a strongly-wetting phase, the capillary pressure does not reach zero till the wetting-phase saturation is high, as shown in Fig. 4.10. Also for a less strongly-wetting phase, the capillary pressure reaches zero at a small saturation, as shown in Fig. 4.11. The secondary drainage also is shown in Figs. 4.10 and 4.11.

## 4.5  Measuring Wettability

Some of the approaches are accessible to calculate a reservoir's wetting preference. Core measurements consist of imbibition and centrifuge capillary pressure. There
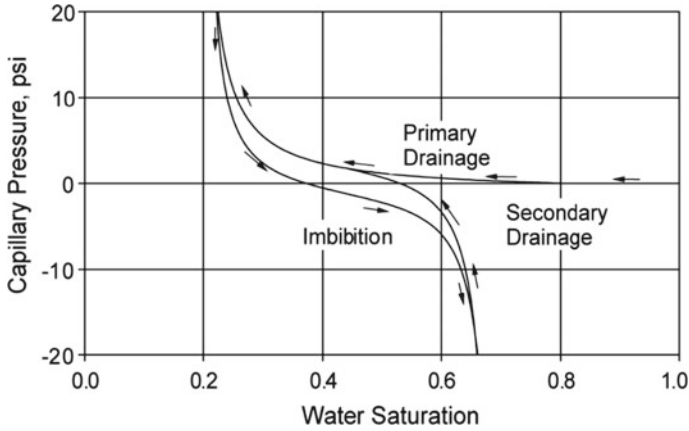
**Fig. 4.11** Primary drainage, imbibition, and secondary drainage for an oil-water system in which the oil and water wet the solid surface equally. *Source* Morrow and Melrose (1991)

are few Laboratory techniques to determine the rock wettability to several fluids. The following are the main Techniques:

1. Microscopic observation

This method includes the direct observation and measurement of wetting angles on core samples. This can be done by using a petrographic microscope or Scanning Electron Microscope (SEM). The measurements are very difficult, and obtaining good results depend on luck than judgement (Abeysinghe et al. 2012).

2. Amott wettability measurements

This is method is mainly a macroscopic wettability measurement. It includes the measurement of the amount of fluids spontaneously and powerfully imbibed in the core sample. This method provides an absolute measurement without validity, but is it valid to use in the industry to compare the wettability for different core samples (Abeysinghe et al. 2012).

The Amott method shown in Fig. 4.12 includes four simple measurements. Figure 4.13 displays the data obtained from the water wetting index specified by AB/AC and the oil wetting index by CD/CA.

where:

(1) The amount of water spontaneously imbibed denoted by AB,
(2) The amount of water forcibly imbibed denoted by BC,
(3) The amount of oil spontaneously imbibed denoted by CD,
(4) The amount of oil forcibly imbibed denoted by DA.

The spontaneous measurements are performed by setting the sample in a flask containing an identified volume of the fluid to be imbibed such that it is completely immersed (steps 1 and 3 shown in Fig. 4.12), and measuring the volume of the fluid
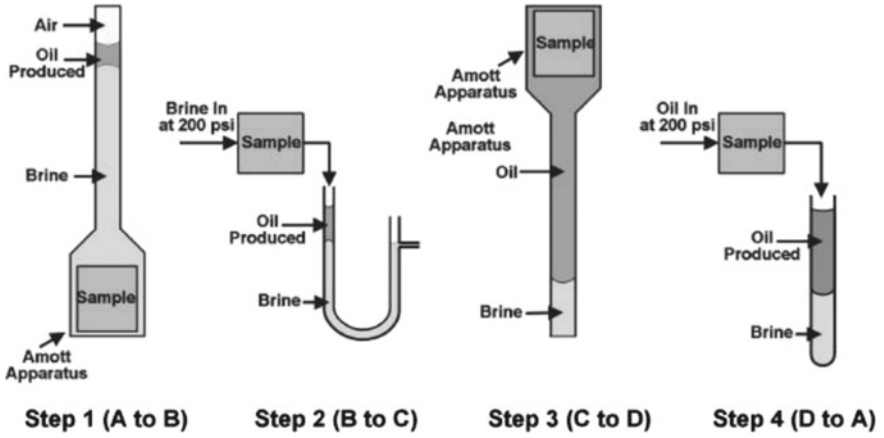
**Fig. 4.12** Displays the initial settings of the sample to be oil saturated at $S_{wi}$. *Source* (Glover, formation evaluation M.Sc. course notes)

**Fig. 4.13** Wettability test data
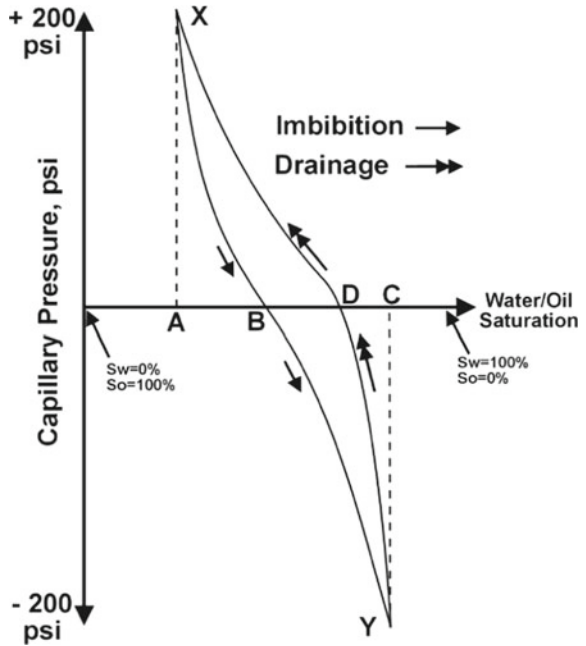
displaced by the imbibing fluid (e.g. oil in step 1 shown in Fig. 4.12). The forced measurements are made by flowing the imbibing fluid inside the core sample and calculating the volume of the displaced fluid (steps 2 and 4 shown in Fig. 4.12), or by using a centrifuge.

The oil wettability ratios (AB/AC) or water wettability ratios (CD/CA) are the ratios of the spontaneous imbibition to the total imbibition of each fluid.

Generally, the core samples need to centrifuged or flooded with brine, and then flooding or centrifuging in oil to determine $S_{wi}$. Then, the Amott method can be carried out. The Amott-Harvey wettability index is calculated as following (Eq. 4.5):

$$Index = \frac{Spontaneous\ Water\ Imbibition}{Total\ Water\ Imbibition}\ \frac{Spontaneous\ Oil\ Imbibition}{Total\ Oil\ Imbibition}$$

$$Index = \frac{AB}{AC}\frac{CD}{CA} \tag{4.5}$$

Wettability indices are commonly cited to the nearest 0.1 and are more decreased to weakly, moderately or strongly wetting; the closer to unity the stronger the tendency.

3. USBM (U.S. Bureau of Mines) method.

This is method is mainly a macroscopic wettability measurement. It is mostly alike to the Amott method, but measures the work needed to do a forced fluid displacement. Also, it has no validity as an absolute measurement. It is typically done using a centrifuge and the wettability index W is calculated from the areas under the capillary pressure curves $A_w$ and $A_o$ (Eq. 4.6):

$$W = \log\frac{A_w}{A_0} \tag{4.6}$$

where:
$A_w$ and $A_o$ are identified in Fig. 4.14.

## 4.6 Comparison of the Amott and USBM Wettability Methods

Amott and USBM methods are used in the oil industry. Both methods display significant differences especially close the neutral wettability area. Commonly, the Amott method is possibly the most accurate method mainly in the neutral wettability area. Table 4.1 shows the comparison of the Amott and USBM, wettability methods.
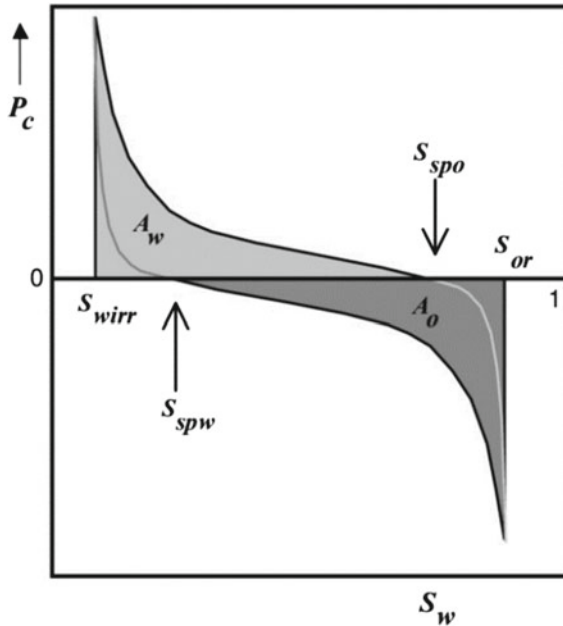
**Fig. 4.14** Wettability index parameters applied for Amott-Harvey and USBM. *Source* Jules et al. (2014)

**Table 4.1** Comparison of the Amott and USBM wettability methods

|                                        | Oil wet      | Neutral wet | Water wet   |
| -------------------------------------- | ------------ | ----------- | ----------- |
| Amott wettability index water ratio    | 0            | 0           | 0           |
| Amott wettability index oil ratio      | > 0          | 0           | 0           |
| Amott-Harvey wettability index         | −1 to 0.3    | −0.3 to 0.3 | 0.3–1.0     |
| USBM wettability index                 | About 1      | About 0     | About 1     |
| Minimum contact angle                  | 105°–120°    | 60°–75°     | 0°          |
| Maximum contact angle                  | 180°         | 105°–120°   | 60°–75°     |

# References

Abeysinghe K, Fjelde I, Lohne A (2012) Dependency of remaining oil saturtaion on wettability and capillary number. Paper SPE 160883 presented at the SPE Saudi Arabia Section technical Symposium and Exhibition, Al-Khobar, 8–11 April

Geffen T, Owens W, Parrish D et al (1950) Experimental investigation of factors affecting laboratory relative permeability measurements. J Pet Technol 3(4):99–110. SPE-951099-G. http://dx.doi.org/10.2118/951099-G

Glover P Chapter 7: wettability formation evaluation M.Sc. course notes, date unknown, pp 84–94

Jacco HS, Bruno A (2008) A microscopic view on contact angle selection. Phys Fluids 20:057101. https://doi.org/10.1063/1.2913675

Jules R, Kristoffer B, Fred B, James JH, Jos M, Niels S (2014) Advanced core measurements "best practices" for low reservoir quality chalk

Jung Y, Bhushan B (2008) Wetting behaviour during evaporation and condensation of water micro-droplets on superhydrophobic patterned surfaces. J Microsc–Oxford 229:127–140. https://doi.org/10.1111/j.1365-2818.2007.01875.x

Maghzi A, Mohammadi S, Ghazanfari M, Kharrat R, Masihi M (2012) Monitoring wettability alteration by silica nanoparticles during water flooding to heavy oils in five-spot systems: a pore-level investigation. Exp Thermal Fluid Sci 40:168–176

MacDougall G, Ockrent C (1942) Surface energy relations in liquid/solid systems I. The adhesion of liquids to solids and a new method of determining the surface tension of liquids. Proc R Soc 180A, 151. https://doi.org/10.1098/rspa.1942.0031

Morrow N, Melrose J (1991) Application of capillary pressure measurements to the determination of connate water saturation. In: Morrow NR (ed) Interfacial phenomena in petroleum recovery. Marcel Dekker Inc., New York City, pp 257–287

Onyekonwu MO, Ogolo NA (2010) Investigating the use of nanoparticles in enhancing oil recovery. In: 34th annual SPE international conference and exhibition, Tinapa-Calabar, Nigeria: Society of Petroleum Engineers

Roustaei A, Moghadasi J, Bagherzadeh H, Shahrabadi A (2012) An experimental investigation of polysilicon nanoparticles' recovery efficiencies through changes in interfacial tension and wettability alteration. SPE, Society of Petroleum Engineers, Noordwijk

Young T (1805) An essay on the cohesion of fluids. Philos Trans R Soc Lond 95:65–87

# Chapter 5
# Saturation and Capillary Pressure

## 5.1 Saturation

Saturation is defined as the ratio of the fluid volume in the porous medium to the pore volume of the rock. That means, saturation is the proportion of interrelated aperture full by a specified phase. For a gas-oil-water system. Therefore, the following formulas show the saturation ratio for every single phase in the porous medium (Eqs. 5.1–5.4):

$$S_w = \frac{V_w}{V_p} \tag{5.1}$$

$$S_o = \frac{V_o}{V_p} \tag{5.2}$$

$$S_w = \frac{V_g}{V_p} \tag{5.3}$$

$$S_w + S_o + S_g = 1 \tag{5.4}$$

where:

$S_w$ = water saturation
$S_o$ = oil saturation
$S_g$ = gas saturation

## 5.2   Determination of Fluid Saturation from Rock Sample

There are two available techniques used to determine rock saturation. The first method applied is by evaporating the fluids in the rock and the second method is by extracting the fluids out of the rock using solvent. The following are the applied techniques:

1. **Retort method**

In this method placed the core sample at high temperature to vaporize all the fluids in the core plug (water and oil). Then, collect these condensed fluids in a vessel and measure the saturation for every single liquid. There are a few disadvantages to using this method. For instance, the method needs high temperature to vaporize all the oil in the core plug (1100 °F), this will drive the water as well causing water recovery values more than just interstitial water. Also, at high temperature the oil tends to cock and crack. Consequently, the test results need to be corrected before use.

2. **ASTM method**

This approach is relying on the extracting the liquids from the core sample by using solvent. The core sample is sited and vapor of either toluene, gasoline, or naphtha goes through the core plug and is condensed to inflow back over the core plug. This procedure leaks out liquids in the sample see Fig. 5.1. The experiment continues until no additional water is collected in the graduated tube. After complete the experiment, water saturation can be measured directly, while for oil saturation can be measured by deducting the core plug weight before the test, the dried core weight after the test, and the extracted water weight.

**Fig. 5.1**   Dean-Stark apparatus

## 5.3  Reservoir Saturation with Depth

The key significance of capillary pressure is its influence on the distribution of fluids in the reservoir along with the depth. For every phase ($k$), reservoir pressure rises with depth (z) dependent on phase density (Eqs. 5.5–5.10):

$$\frac{dp_k}{dz} = \rho_k g \tag{5.5}$$

and since,

$$P_o - P_w = P_{cow} \tag{5.6}$$

$$\frac{dp_{cow}}{dz} = -(\rho_o - \rho_w) \cdot g \tag{5.7}$$

Therefore

$$\frac{\Delta p_{cow}}{\Delta z} = -(\rho_o - \rho_w) \cdot g \tag{5.8}$$

if Dz = width of the transition zone, where

$$\Delta p_{cow} = P_{cow}(S_O - = 1 - S_{wc}) - P_{cow}(S_O = 0) \tag{5.9}$$

But

$$P_{cow}(S_O = 0) = 0$$

so that

$$\Delta z = -\frac{P_{cow}(S_O - = 1 - S_{wc})}{(\rho_o - \rho_w) \cdot g} \tag{5.10}$$

High permeability at about 90° contact angle systems results in small capillary pressures, resulting in smaller transition zone. However, low permeability with small contact angle systems will result large capillary pressures and wide transition zones. Figure 1.11 displays a diagram for an oil-water reservoir of oil and water pressures versus depth (right-hand plot) and of oil/water capillary pressure versus water saturation (left-hand plot). Initially, the reservoir has been saturated with water ($S_w$ = 100%). After that, oil migrated and displaced water from the reservoir shown in Fig. 5.2.
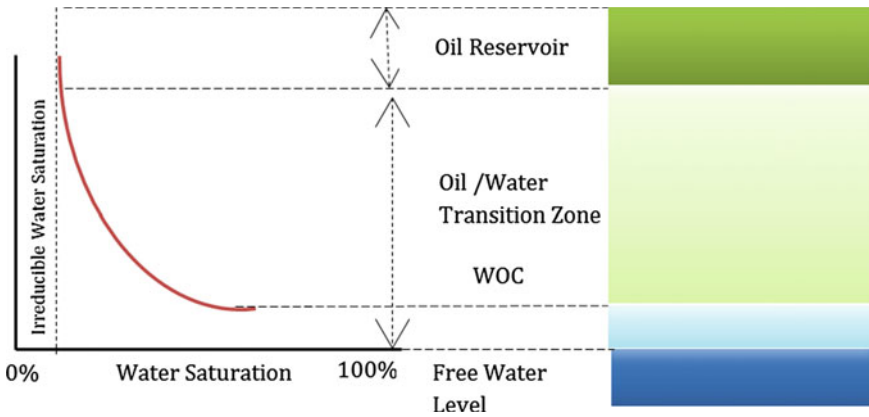
**Fig. 5.2** Water saturation versus capillary pressure with diagram of oil-water capillary transition zone

## 5.4 Capillary Pressure

The combination of the impact of the surface and interfacial tensions of the reservoir fluids, the aperture size and shape, and the wetting features of the system will generate capillary forces in hydrocarbon reservoir (two immiscible fluids available in the aperture of the reservoir rock). Usually, one phase defined as a wetting phase and the other phase defined as a non-wetting phase. When both fluids are in contact, a discontinuity in pressure present between the two immiscible fluids, which rely on the curvature of the interface splitting the fluids. This pressure difference identified as capillary pressure ($P_c$).

The aperture size can be determined using mercury capillary pressure curves, that are obtained by injecting mercury (non-wetting phase) into a core sample containing air (wetting phase). The mercury injected with increasing pressure and a plot of injection pressure versus the volume of mercury injected ($H_g$ saturation) see Fig. 5.3. The Hg saturation plotted versus bulk volume or pore volume. The curve is known as the drainage curve shown in Fig. 5.3a. If the injection pressure is decreased wetting phase, either air or water will flow inside the aperture and the non-wetting fluid will be expelled (Kolodizie 1980). This method is called imbibition, and a plot of pressure versus saturation is identified as the imbibition curve see Fig. 5.3b.

The capillary pressure data are needed for three key uses:

- The calculation of initial reservoir fluid saturations.
- Cap-rock seal capacity.
- As additional data for evaluation of relative permeability data.

Pore-throat size is known as the aperture size that connects the bigger apertures. It depends on the idea that the inter-particle aperture can be envisioned as spaces with connecting gates (Swanson 1981). The gates are the pore-throats that connect the larger apertures, or spaces.
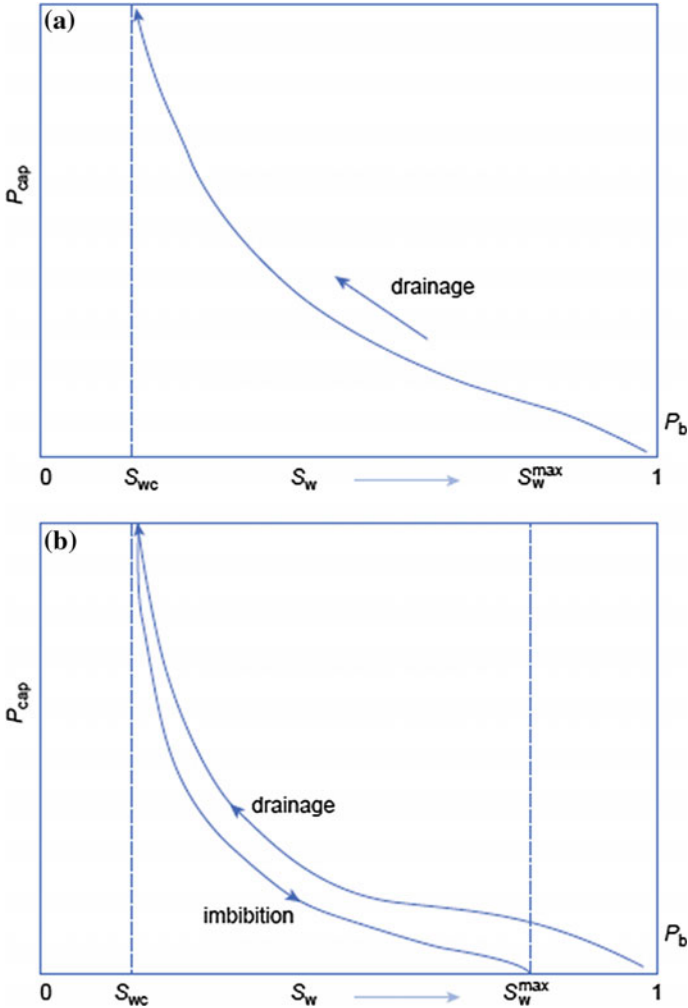
**Fig. 5.3** Capillary pressure versus water saturation. **a** Drainage capillary pressure curve. **b** Drainage and imbibition capillary pressure curves

The fundamental relationship depicted in Figs. 5.4 and 5.5 between capillary pressure, aperture radius, interfacial tension, and the contact angle is expressed by Eq. 5.11. Figure 5.4 showing a three-phase water-wet system (water-oil-rock) at equilibrium. The curvature of the interfacial boundary is deepening on of interstitial volume, grain size, fluid saturation, and surface tension. The contact angle ($\theta$) is a depend on the relative wetting characteristics of the two fluids with respect to the solid.

$$P_c = \frac{2\sigma \cos \theta}{r} \cdot A \qquad (5.11)$$
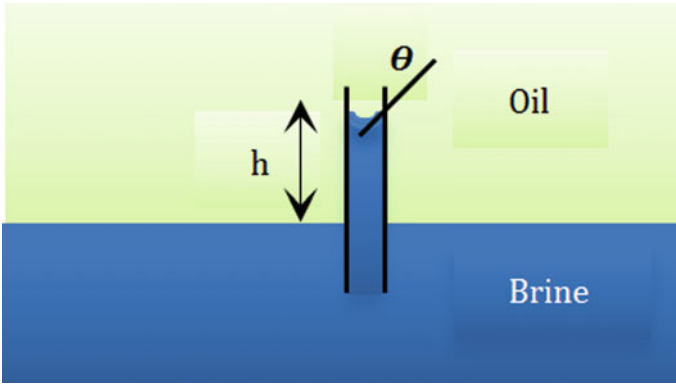
**Fig. 5.4** Capillary pressure definitions

**Fig. 5.5** Diagram showing
radii of interfacial curvature
at equilibrium for the
three-phase system
(oil-water-rock)
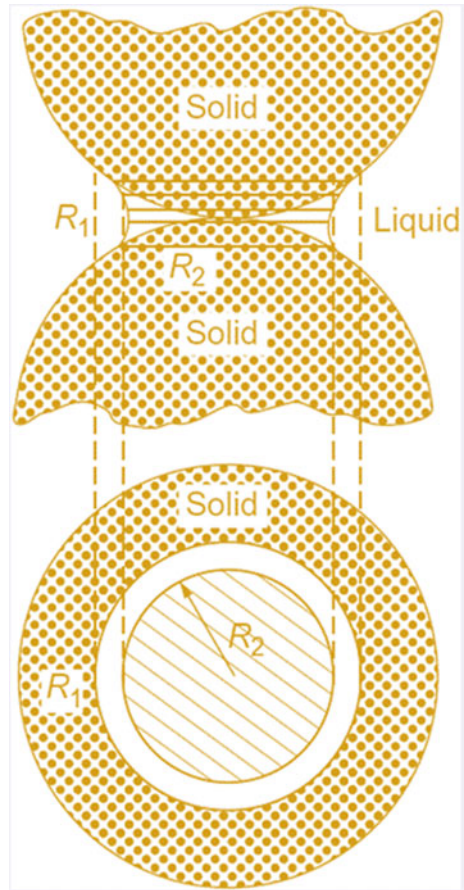
where:

$P_c$ = Capillary pressure (psi)
$\sigma$ = Interfacial tension (dynes/cm)
$\theta$ = Contact angle (degrees)
r = Radius of the pore throat (microns)
$A = 145 \times 10^{-3}$ (constant to convert to psi)

Identifying the wetting fluid pressure by $p_w$ and non-wetting fluid pressure by $p_{nw}$, the capillary pressure can be presented as Capillary pressure = (pressure of the non-wetting phase) − (pressure of the wetting phase). The Capillary pressure can be defined as (Eq. 5.12):

$$P_c = (\rho_{nw} - \rho_w)gh = \frac{2\sigma \cos \theta}{r} \cdot A \tag{5.12}$$

where:

$\rho_{nw}$ = Density of Non-wetting phase, (lb/ft$^3$)
$\rho_w$ = Density of wetting phase, (lb/ft$^3$)
g = Acceleration, (ft/sec$^2$)
h = Capillary rise, (ft)

Typical Values for changing mercury/air/oil/water capillary pressure curves to reservoir conditions of gas/oil/water are specified in Table 5.1.

Figure 5.6 illustrations some cases for sandstone formation that has almost the same porosity with different permeability.

Core A: porosity $\emptyset = 0.216$, permeability k = 430 mD
Core B: porosity $\emptyset = 0.220$, permeability k = 116 mD
Core C: porosity $\emptyset = 0.196$, permeability k = 13.4 mD

**Table 5.1** Capillary Pressure Properties at reservoir and laboratory conditions for Different types of Fluid

| System | $\theta$ | $\sigma$ | | $\sigma \cdot \cos \theta$ | |
|---|---|---|---|---|---|
| | | Dynes cm$^{-1}$ | N cm$^{-1}$ = $P_{am}$ | Dynes cm$^{-1}$ | N cm$^{-1}$ = $P_{am}$ |
| *Laboratory* | | | | | |
| Air-water | 0 | 72 | 0.072 | 72 | 0.072 |
| Oil-water | 30 | 48 | 0.048 | 42 | 0.042 |
| Air-mercury | 40 | 480 | 0.480 | 367 | 0.367 |
| Air-oil | 0 | 24 | 0.024 | 24 | 0.024 |
| *Reservoir* | | | | | |
| Water-oil | 30 | 30 | 0.030 | 26 | 0.026 |
| Water-gas | 0 | 50 | 0.050 | 50 | 0.050 |

*Source* Hartmann and Beaumont (1999) and Darling (2005)
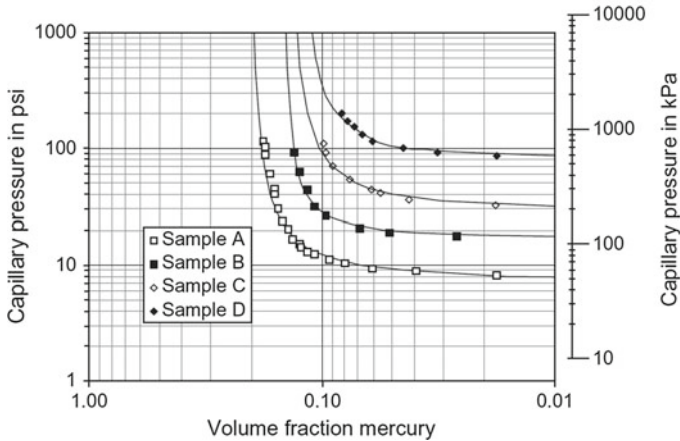
**Fig. 5.6** Capillary pressure curves from a sandstone reservoir. *Source* Archie (1950) and Jorden and Campbell (1984)

Core D: porosity Ø = 0.197, permeability k = 1.2 mD.

The figure exhibits the effect of pore radius on the permeability and capillary pressure. Where at large pore throat diameter, the results show high permeability and low capillary pressure. Conversely, at small pore throat diameter the results show low permeability and high capillary pressure. The conclusion of the capillary pressure curve functions is:

1. Defines the fluid saturation diffusion in a reservoir rock, which reliant on the pore size distribution and wettability of the fluid mechanisms.
2. Characterizes the fluid dispersion as a function of pressure.
3. Indicate the largest pores in the reservoir rock, from displacement pressure, which control the permeability.
4. Obtain both, irreducible water saturation and residual oil saturation;
5. Provide good indication for the distribution of the pore size in the reservoir rock.

Usually, the capillary pressure is a function of the height above the free water level (FWL). Therefore, when the capillary pressure curve and the FWL are known, then it becomes simple to determine the water saturation at any depth in the reservoir see Fig. 5.7. If water saturation value for a given well is matched with the estimated water saturations from wireline tools and core, the wireline water saturation value can be applied in the other reservoir section where no cores are available within the same field.
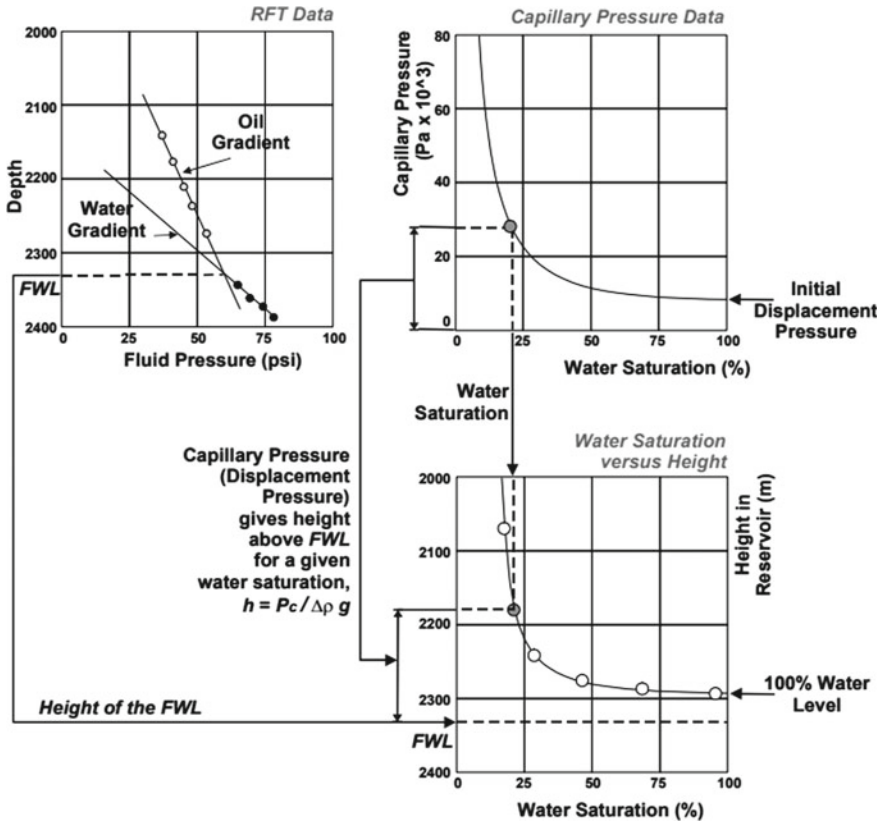
**Fig. 5.7** Determination of water saturation in a reservoir

## 5.5 Laboratory Methods of Measuring Capillary Pressure

There are three main approved techniques to measure capillary pressures in the laboratory are:

1. Mercury Injection Method
2. Porous plate Diaphragm (or restored state) Method
3. Centrifugal Method

Typically, these techniques carried out in the laboratory using core samples from reservoir. There are so many factors and process that affect or alter the initial condition of the core sample such as drilling and coring fluids, coring method, core handling, and transportation, packing and experimental procedures. Consequently, special cares are required to prevent changing the initial core condition. In case of altering the initial core conditions due to any of the upper mentioned reasons, the core must be restored to its initial condition before conducting capillary pressure test.
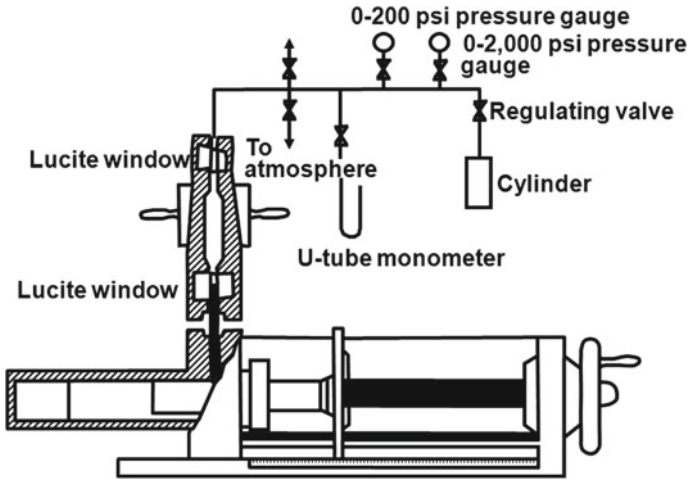
**Fig. 5.8** Mercury injection apparatus

1. **Mercury Injection Method**

Commonly, this method used cleaned and dried core samples. the Mercury Injection procedures are as following:

1.  Place the core in a chamber and immersing the core sample in Mercury at $<10^{-3}$ mm $H_g$ and evacuate the core within the mercury injection apparatus showing in Fig. 5.8.
2.  Inject the mercury in the core sample.
3.  The mercury volume that has filled the pores at each forced pressure can be measured from volumetric readings, and the Mercury entered the pore space can be calculated.
4.  Additional readings can be obtained as the pressure is dropped to provide data for the imbibition case from $S_{wi}$ to $P_c = 0$.
5.  Continue for several pressures and plot the pressure against the mercury saturation.

Usually, to convert to oil-brine or gas-brine data using suitable contact angles and interfacial tensions. General conversions are given below (Eqs. 5.13–5.16):

$$P_C(\text{gas-brine}) = P_C(\text{Air-Hg})\frac{72\cos 0°}{480\cos 130°} \tag{5.13}$$

$$P_C = 0.233\ P_C(\text{Air-Hg}) \tag{5.14}$$

$$P_C(\text{oil-brine}) = P_C(\text{Air-Hg})\frac{25\cos 0°}{480\cos 130°} \tag{5.15}$$

**Fig. 5.9** Porous plate apparatus
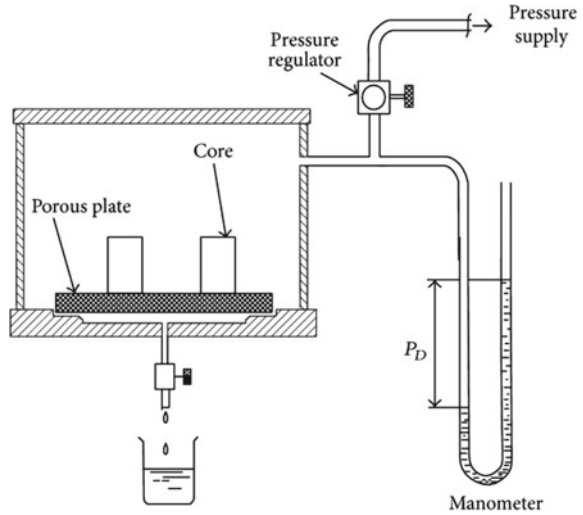
$$P_C = 0.070 \ P_C(\text{Air-Hg}) \tag{5.16}$$

The non-wetting phase saturation can be obtained by dividing the volume of mercury injected by the pore volume. In the experiment, the capillary pressure is injection pressure. This method can be conducted very fast, and there is no pressure limitation. The method can only be applied for shaped cores.

2. **Porous Diaphragm Method**

Porous plate method used a core sample saturated totally with a wetting fluid. The experimental procedures are stated as follows:

1. Saturate the core plug and the Porous plate with the fluid to be displaced.
2. Place the core on a porous plate as shown in Fig. 5.9).
3. Use a different level of pressure (e.g. 1, 2, 4, 8, 16, 32, 64 psi), wait for the core to reach static equilibrium. In the end, a capillary pressure curve can be plotted against water saturation in the sample shown in Fig. 5.10. To reach the equilibrium, it takes from 10 to 40 days.

**The capillary pressure = height of liquid column + applied pressure**

$$Saturation = \frac{Pore \ Voulme - Colume \ Produced}{Pore \ Voulme} \tag{5.17}$$

3. **Centrifugal Method**

This method uses a core sample of 100% saturated with a wetting fluid. The main centrifugal method procedures are as the following:

**Fig. 5.10** Capillary pressure measurements using porous plate
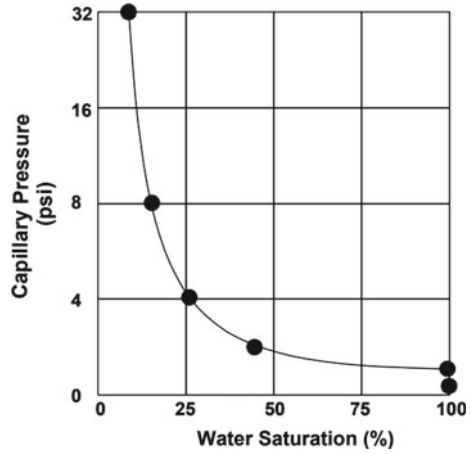
1. The core sample placed in the core holder in the centrifuge depicted in Fig. 5.11 and rotates at a fixed constant speed. The speed of rotation causes a centripetal force displaces some wetting fluid, which can be determined at the window using a stroboscope. Also, the saturation can be obtained. At low rotation speeds, the centripetal force is only displacing water from the biggest pores. However, at higher speeds, the centripetal force is capable to displace water from very smaller pores in the core plug.
2. The rotary motion of the centrifuge is converted to capillary pressure using appropriate equations.
3. Repeat for several speeds and plot capillary pressure with saturation refer to Fig. 5.12.
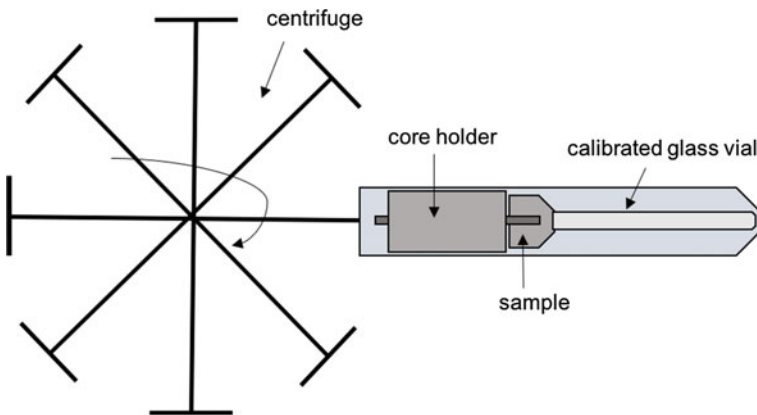


**Fig. 5.11** A schematic of a centrifuge set-up for determining capillary pressure

**Fig. 5.12** Capillary pressure measurements using centrifuge apparatus
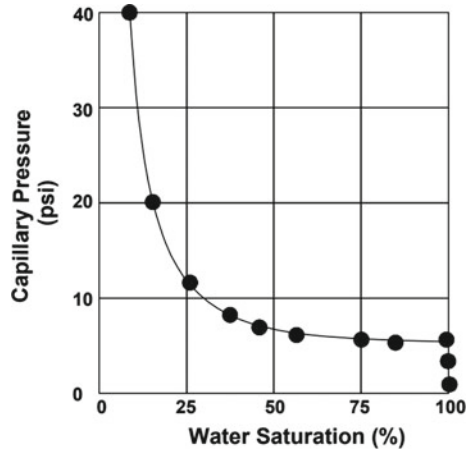


## 5.6 Capillary Hysteresis

Correct measurements of capillary pressure and relative permeability are very significant for assessing oil and gas recovery methods. Besides, resistivity index parameters are very significant in estimating fluid diffusion in reservoirs. The different in drainage and imbibition processes, generally known as hysteresis. Therefore, the hysteresis phenomenon is known as the equilibrium situations of the air-water interfaces in a system of pores are reliant on water content in the system is increasing or decreasing.

## 5.7 Averaging Capillary Pressure Data: Leverett J-Function

Normally, the capillary pressure measurements are obtained on small core samples that characterize small section of the reservoir. Consequently, it is required to use all obtained capillary pressure data to describe a given reservoir.

Typically, there are different capillary pressure-saturation curves for many reservoir rock types that have various features see Fig. 5.13. Therefore, a common equation to describing all such curves was developed by Leverett (1941). Initially, Leverett converted all capillary pressure data to a general curve. However, a general capillary pressure curve does not available as the rock properties have big variation with rock type.

Leverett noticed that capillary pressure is dependent on porosity, permeability, interfacial tension, and pore radius. Leverett presented his equation as dimensionless equation which called "J-function ($J(S_W)$)" and it is function of saturation (Eq. 5.18). Actually, J-function is away to extrapolating capillary pressure data for a particular
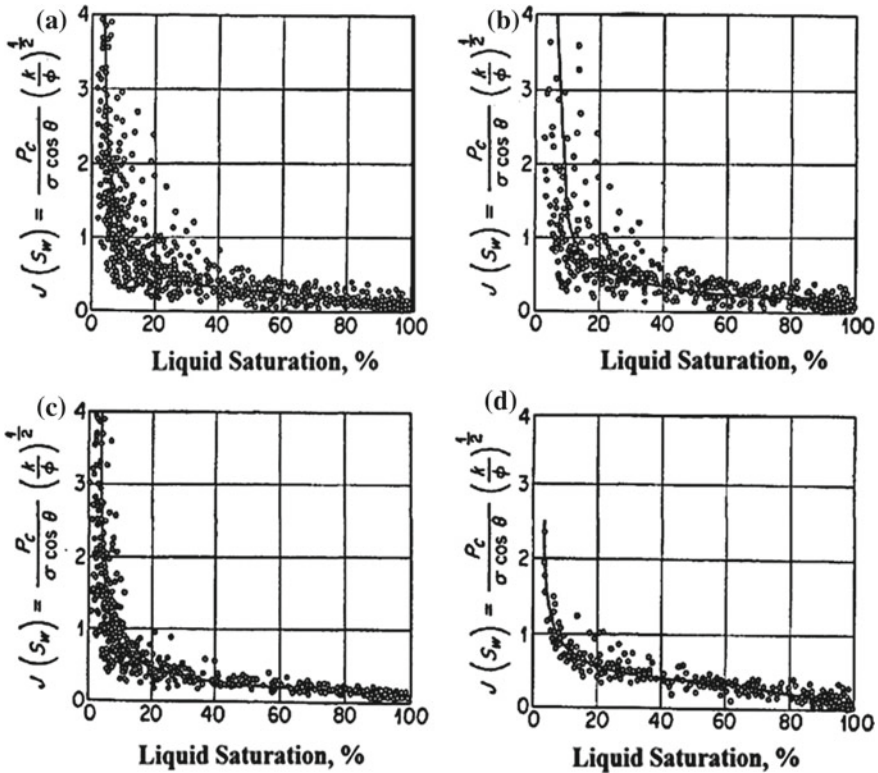
**Fig. 5.13** J-function curve for **a** all core samples; **b** limestone samples; **c** dolomite samples; **d** micro-granular limestone samples; **e** coarse-grained limestone samples. *Source* Amyx et al. (1960)

reservoir rock to other rocks that have similar rock type with differing permeability, porosity and wetting properties.

$$J(S_w) = C \cdot \frac{P_c}{\sigma} \sqrt{\frac{k}{\varnothing}} \qquad (5.18)$$

where:

C = is constant.

For the same reservoir rock, this dimensionless equation helps to remove discrepancies in the $P_c$ versus $S_w$ curves for many cases and decrease them to a common curve.

Some writers changed Eq. 5.19 by including cos θ:

$$J(S_w) = \frac{P_c}{\sigma \cos \theta} \sqrt{\frac{k}{\varnothing}} \qquad (5.19)$$

This equation is not unique, but it works better when the rocks are classified as to same rock types.

## Example 5.1
Match of mercury injection capillary pressure data with porous diaphragm data.
  A. Determine capillary pressure ratio?/

$$P_{cAH_g} / P_{cAw},$$

Giving the following data:

$$\sigma_{AH_g} = 480 \, \text{Dynes/cm}$$
$$\sigma_{AW} = 72 \, \text{Dynes/cm}$$
$$\theta_{AH_g} = 140°$$
$$\theta_{AW} = 0°$$

  B. Aperture shape is very difficult. The curvature of the interface and aperture radius is not essentially depends on contact angles. Determine the capillary pressure ratio by applying the following correlation?

$$\frac{P_{cAH_g}}{P_{cAw}} = \frac{\sigma_{AH_g}}{\sigma_{AW}}$$

## Solution
(A)

$$\frac{P_{cAH_g}}{P_{cAw}} = \frac{\sigma_{AH_g} \cos \theta_{AH_g}}{\sigma_{AW} \cos \theta_{AW}} = \frac{480 \cos 140°}{72 \cos 0°}$$
$$\frac{P_{cAH_g}}{P_{cAw}} = 5.1$$

(B)

$$\frac{P_{cAH_g}}{P_{cAw}} @ \frac{\sigma_{AH_g}}{\sigma_{AW}} = 480/72$$
$$\frac{P_{cAH_g}}{P_{cAw}} = 6.9$$

**Example 5.2**

Change laboratory scale data to reservoir conditions. State reservoir capillary pressure data by applying lab data.

Laboratory data:

$$\sigma_{AW} = 72 \text{ dynes}$$

$$\theta_{AW} = 0°$$

Reservoir data:

$$\sigma_{oW} = 24 \text{ dynes/cm}$$

$$\theta_{oW} = 20°$$

**Solution**

$$P_{cR} = \frac{(\cos\theta)_R}{(\cos\theta)_L} \cdot P_{cL}$$

$$P_{cR} = \frac{24(\cos 20)_R}{72(\cos 0)_L} \cdot P_{cL}$$

$$P_{cR} = 0.333 P_{cL}$$

**Example 5.3**

Using the laboratory capillary pressure curve capillary pressure curve given below, determining Water Saturation. Use $P_{cR} = 0.333\, P_{cL}$, and assume the height of water saturation is 40 ft. above oil-water contact level. $\rho_o = 0.85 \text{ gm/cm}^3$, $\rho_w = 1.0 \text{ gm/cm}^3$.
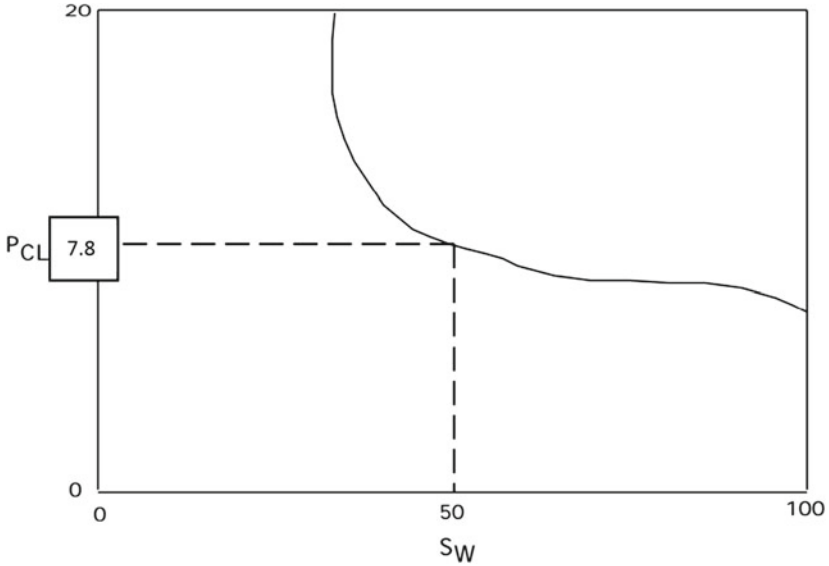
**Solution**

$$P_{cR} = \frac{(\rho_w - \rho_o)}{144} . h$$

$$P_{cR} = \frac{(1 - 0.85)\left(\frac{62.5id}{ft3}\right) * 40}{144}$$

$$P_{cR} = 2.6\,\text{psi}$$

$$P_{cR} = 0.333\,P_{cL}$$

$$P_{cL} = \frac{P_{cR}}{0.333}$$

$$P_{cL} = \frac{2.6}{0.333} = 7.8\,\text{psi}$$

From y-axis at $P_{cL} = 7.8$ psi move to the right horizontally to cross the capillary pressure curve and drop vertically to the x-axis, and read $S_w$ value. $S_w = 50\%$.

**Example 5.4**

1. A goblet tube is positioned upright in a cup of water. The air-water interfacial tension is 72 dynes/cm with the contact angle is equal to 0°?

   (a) Determine the capillary increase of water in the tube if the tube radius is 0.01 cm.

    (b)  Determine the difference in pressure across the interface of air-water in the tube.

2.  55 psi is the displacement pressure for a water saturated porcelain plate of air. What is the diameter of the biggest aperture in the porcelain plate? Use 72 dynes/cm with a contact angle is equal to 0 degrees?

**Solution**

(1)  $\sigma_{AW} = 72$ dynes
     $\rho_W = 1$ gm/cm$^3$
     $g = 980$ dynes/gm
     $\theta = 0°$

    (a)  Capillary increase of water if radius is 0.01 cm

$$h = 2\sigma_{AW} \cos\theta / r\rho g$$

$$h = \frac{2(72)\cos 0}{(0.01)(1)(980)} = 14.69\,\text{cm}$$

    (b)  Pressure drop across interface

$$Pc = p_a - p_w = r_w g\, h = (1.0)(980)(14.69)$$

$$Pc = 0.0142\,\text{atm}\left(14.696\frac{\text{psi}}{\text{atm}}\right)$$

$$Pc = 0.209\,\text{psi}$$

(2)  $Pc = 2\sigma_{AW}\cos\theta / r$

$$Pc = 55\,\text{psi}$$

$$Pc = 55\,\text{psi}\left(\frac{\text{atm}}{14.696\,\text{psi}}\right)\left(\frac{1.0133 \times 10^6\,\text{dynes/cm}^2}{\text{atm}}\right)$$

$$Pc = 3.792 \times 10^6\,\text{psi}$$

$$r = 2\sigma_{AW}\cos\theta / Pc$$

$$r = \frac{2(72)\cos 0}{3.792 \times 10^6} = 3.797 \times 10^{-5}\,\text{cm}\left(\frac{\text{in}}{2.54\,\text{cm}}\right)$$

$$r = 1.495 \times 10^{-5}\,\text{in}$$

$$d = 2.99 \times 10^{-5}\,\text{in}$$

# References

Amyx J, Bass D, Whiting R (1960) Petroleum reservoir engineering physical properties. McGraw-Hill, New York. ISBN: 9780070016002, 0070016003

Archie GE (1950) Introduction to petrophysics of reservoir rocks. AAPG Bull 34:943–961

Darling T (2005) Well logging and formation evaluation. Gulf Professional Publishing/Elsevier Inc.; de Lima OAL (1995) Water saturation and permeability from resistivity, dielectric, and porosity logs. Geophysics 60:1756–1764

Hartmann D, Beaumont E (1999) Predicting reservoir system quality and performance. In: Beaumont EA, Forster NH (eds) AAPG treatise of petroleum geology, exploration for oil and gas traps, Chap. 9 (9-1 to 9-154)

Jorden J, Campbell F (1984) Well logging I—rock properties, borehole environment, mud and temperature logging. Henry L. Doherty Memorial Fund of AIME, SPE: New York, Dallas

Kolodizie Jr (1980) Analysis of pore throat size and use of the Waxman-Smits equation to determine OOIP in Spindle Field, Colorado. SPE paper 9382 presented at the 1980 SPE annual technical conference and exhibition, Dallas, Texas

Leverett MC (1941) Capillary behavior in porous solids. Pet Trans AIME 27(3):152–169

Swanson BJ (1981) A simple correlation between permeability and mercury capillary pressures. J Pet Technol 2488–2504

# Chapter 6
# Relative Permeability

It was noted that Darcy's law for fluid flow in permeable media. Was predicated upon the condition that the porous media was entirely saturated with the flowing fluid such a circumstance does not often exist in nature, particularly in the hydrocarbon reservoir. Gas or oil is usually fauna coexistent with water and frequently gas, oil, and water may occupy together the pores of the reservoir.

Flowing reservoirs normally contains many fluids (multiphase flow), where the capability of one phase to flow is subjected to the existence of other phases in the reservoir rock. Sequentially, to improve the prediction of fluid performance in reservoirs, this phenomenon has to quantified somehow. The idea of recounting this multiphase flow in reservoirs is identified as relative permeability, which is known as the ratio of the effective permeability of a fluid to the absolute permeability of the rock (which is the permeability at 100% saturation of the flowing fluid) (Eqs. 6.1–6.3). Relative permeability is an indicator to explain the quantitatively the simultaneous move of two or more immiscible fluids via a porous medium. The basic assumptions are that every fluid stays continuous and that all flow is in one direction (John and Black 1983). The effective permeability is a relative quantifying of the conductance of the permeable medium for one phase in the attendance of other phases.

$$K_{ro} = \frac{K_o}{K} = \frac{\text{effective oil permeability}}{\text{absolute permeability}} \tag{6.1}$$

$$K_{rw} = \frac{K_w}{K} = \frac{\text{effective oil permeability}}{\text{absolute permeability}} \tag{6.2}$$

$$K_{rg} = \frac{K_g}{K} = \frac{\text{effective gas permeability}}{\text{absolute permeability}} \tag{6.3}$$

where:

$K_{ro}$   Oil relative permeability
$k_{rg}$   Gas relative permeability
$k_{rw}$   Water relative permeability
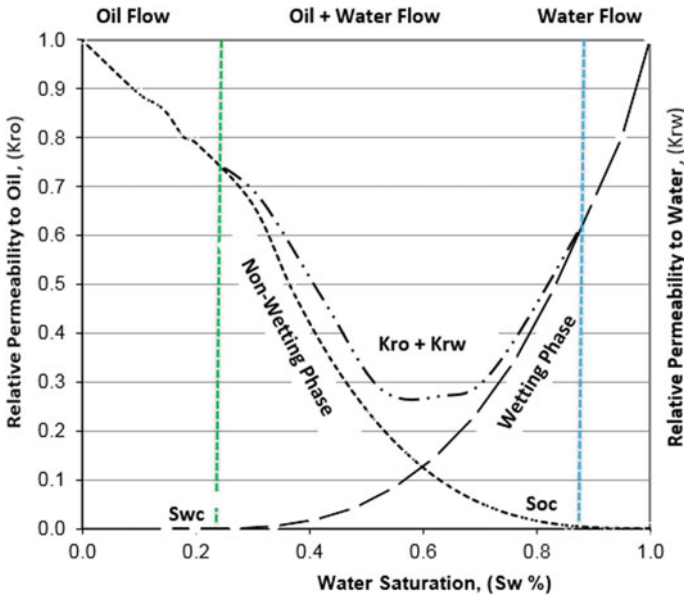
**Fig. 6.1** Common relative permeability curve

k     Absolute permeability
$k_o$   Oil effective permeability
$k_g$   Gas effective permeability
$k_w$   Water effective permeability

Bear in mind that in water-wet systems capillary forces help water to enter apertures, where in the oil wet systems they avoid water to move inside the apertures (Qingjie et al. 2010). Due to the capillary forces, the wetting phase resided in the lesser apertures at small saturations, and these apertures do not support the fluid flow. Conversely, as the non-wetting phase exists in the central or bigger apertures which considerably support the fluid flow throughout the reservoir, the relative permeability to the wetting phase is described by a fast drop in value for little reduces in the wetting phase saturation from initial saturation.

Usually, the relative permeability to wetting phase is come close to zero or disappears at high wetting phase saturation. This due to the wetting phase exists in the smaller apertures, where capillary forces are the maximum. At this point, the water saturation is known as the irreducible water saturation $S_{wir}$ or connate water saturation $S_{wi}$ shown in Fig. 6.1. Irreducible water saturation initially in consolidated formations is more than unconsolidated rocks. One more key phenomenon comes with fluid flow in the porous media is the idea of residual saturation. Because when one immiscible phase is displaced another, it's not possible to decrease the saturation of the displaced fluid to zero. At very small saturation at which the displaced phase stops to be continuous, the flow of the displaced phase will stop. This saturation

is known as residual saturation. This is very significant as it estimates the highest recovery from the reservoir rock. On the other hand, the fluid has to expand a certain least amount saturation before the phase will start to flow. The critical saturation it's known as the saturation at which a fluid will just start to flow. Supposedly, the residual and the critical saturation are the same for any fluid; however, they are not equal. Critical saturation is determined in the trend of rising saturation, while irreducible saturation is determined in the trend of decreasing saturation. Hence, the saturation histories for both of them are dissimilar (Tarek 2010).

Figure 6.1 is a representative relative permeability curve for a water-oil system in a water-wet system. The figure shows that the non-wetting phase starts to flow at the low saturation of the non-wetting phase. The oil saturation at this point is known as critical oil saturation Soc. Some researchers named as the "equilibrium saturation", which the non-wetting phase turns out to be mobile. This saturation can vary from zero to 15% non-wetting phase saturation. Figure 6.1 illustrates the attribution of the oil phase to flow reach 100% in saturation below 100% due to capillary pressure effect. The capillary pressure pushing the wetting phase to exist in the smallest apertures at low saturation that have a neglectable role to the flow.

The curve depicted in Fig. 6.1 is very common for wetting and non-wetting phases and from the plot easy to understand the performance of an oil-wet system. Also, the plot shows the total permeability of $k_{rw} + k_{ro}$, is smaller than 1, at the two-phase flow region.

## 6.1  Corey Relations

The Corey model has been used extensively as a technique to estimate relative permeability via capillary pressure data. During 1954, Corey combined estimates of a tube-bundle model with his experiential expression for capillary pressure to acquire expressions for oil and gas relative permeabilities (Corey 1954). The normalized drainage effective permeability equations (Eq. 6.4–6.7) developed by Burdine (1953), were extended by Corey relations.

$$K_{rW} = (S_{W*})^{\frac{2+3\lambda}{\lambda}} \tag{6.4}$$

$$K_{rn} = K_r^\circ (S_m - S_w/S_m - S_{iw})^2 \left(1 - (S_{W*})^{\frac{2+3\lambda}{\lambda}}\right) \tag{6.5}$$

$$S_{W*} = (S_w - S_m)/(1 - S_{iw}) \tag{6.6}$$

$$K_r^\circ = 1.31 - 2.6 S_{iw} + 1.1(S_{iw})^2 \tag{6.7}$$

where:

$k_{rn}$  Relative permeability of the non-wetting phase
$k_{rw}$  Relative permeability of the wetting phase

$k_r^o$     Non-wetting phase relative permeability at irreducible wetting phase saturation
$S_w$*    Normalized wetting phase saturation
$S_w$     water saturation
$S_m$     $1 - S_{or}$ (1—residual non-wetting phase saturation)
$S_{iw}$    Initial water saturation
$\lambda$      Pore size distribution index.

The non-wetting phase equation Eq. (6.5) shows the main difference with the Burdine solutions. The $k_{ro}$ term is added to consider the non-wetting phase have to be at irreducible wetting phase saturation. The critical saturation point, $S_m$ term, it's the further adjustment suggested by the Corey to be the point where the non-wetting phase initial begins to flow. So, for a stage at the start of the non-wetting phase curve, there is a stage where there is no connectivity existing. At the critical saturation, there are a little number of apertures are interconnected, at which point flow is feasible and the first relative permeability value can be predicted. The $S_m$ term pointing to the saturation at which flow is initial feasible, and is required to estimate realistic relative permeability values.

## 6.2  Estimating Aperture Size Distribution Index

The aperture size distribution index ($\lambda$) in Eqs. (6.4) and (6.5) is important in estimating relative permeability. The actual number notify how consistent is the aperture size in the reservoir rock. If $\lambda$ value (i.e. 2) is very small that is reflected a different range of aperture sizes. Also, if the $\lambda$ value is very high that is reflects more uniform aperture size distribution. By applying $\lambda = 2$ in Eqs. (6.4) and (6.5) results in the Corey equations. Where $\lambda = 2$ is assumed to represent an extensive range of aperture sizes. Normally, pore size distribution index ($\lambda = 2$) is used once no more information is identified about the reservoir. With $\lambda = 2.4$ results in Wyllie's equation for three rock categories (Standing 1974):

$\lambda = 2$ (oolotic, cemented sandstones and small-vug limestones)
$\lambda = 4$ (poorly sorted unconsolidated sandstones)
$\lambda = $ Infinity (well sorted unconsolidated sandstones).

Wyllie's equations can be applied, once there is general information about the reservoir geology. The Corey and Wyllie equations are adequate for estimate purposes, while to get a better aperture size distribution index, $\lambda$ can be determined experimentally from capillary pressure data. The following equation (Eq. 6.8) was proposed by Brooks and Corey (1964, 1966), relates capillary pressure to normalized wetting phase saturation:

$$lof\, P_c = \log P_e - \frac{1}{\lambda} \log S_{W^*} \tag{6.8}$$

where:

$P_c$  Capillary pressure,
$P_e$  Minimum threshold pressure,
$S_w^*$  Normalized water saturation.

The log-log plots of the normalized water saturation versus capillary pressure will show a straight line with a slope of $-1/\lambda$ and an intercept of $P_e$.

## 6.3 Laboratory Measurements of Relative Permeability

There are five techniques utilized to determine relative permeability data:

- Steady-state fluid flow process (Lab measurement).
- Unsteady state fluid flow process (Lab measurement).
- Using capillary pressure data.
- Using field performance data.
- Theoretical/empirical correlations.

Relative permeability data acquired from laboratory measurements are often reliable for engineering computations because it's directly measured and not estimated.

The steady-state process was considered as the most accurate technique, on the other hand, it's costly and time consuming because the process injecting oil and water at once till the output rates equal the input rates (Jerry 2007). The unsteady state process is less accurate than the steady state process but quicker because the core saturated with oil and afterward flooded with water see Fig. 6.2. A third technique is



**Fig. 6.2** Schematic of unsteady-state and steady-state techniques of determining oil and water relative permeability

faster and cheaper to determine the effective permeabilities at irreducible water and residual oil. This is known as the endpoint method.

The difficulty in determining relative permeability in the Lab is the restoration of the core samples to reservoir conditions. Pore surfaces, mainly in carbonate rocks, are reactive to alter in fluids, and these reactions can alter the wettability state. Very complicated techniques have been used to protect the initial wettability state of the core, and the precision of relative permeability data is reliant on the performance of these techniques.

Typically, the core sample is mounted in a cylindrical holder as can be seen in Fig. 6.3. All core sample surfaces are sealed to avoid flow. Also, to apply radial confining stress on the sample, the core was sealed with a rubber sleeve. Through the two ports of the core sample, the injected and the produced Fluids can flood. There are other ports are used for pressure measurement. Also, other types of equipment are used to:

- insert and gather fluids
- Determine pressures
- Make confining pressure
- Determine saturations.

All of these facilities are shown in Fig. 6.4 fluid saturations can be measured from:

- The alteration of rock sample mass
- The alteration of electrical conductivity
- The alteration of X-rays absorption (Oak et al. 1990) or other rays.

Acoustic techniques (Islam and Berntsen 1986) and CT scanning (MacAllister et al. 1993; DiCarlo et al. 2000) are also utilized. To determine the alteration in mass, the rock sample is rapidly disconnected and weighed, and then returned back to the assembly. This process may affect to change the saturation of the core sample.
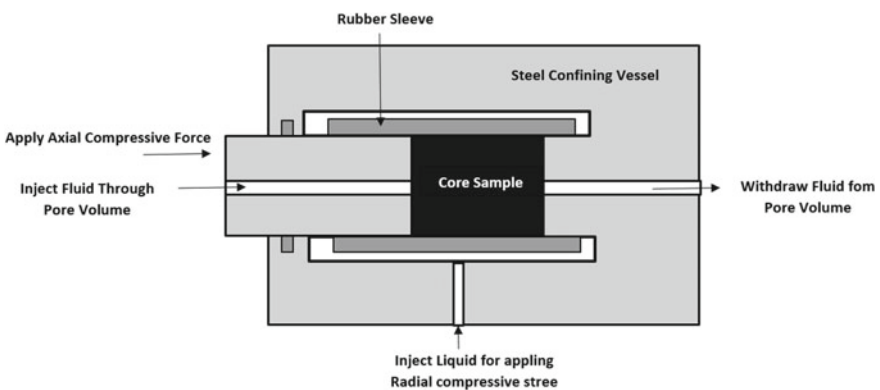


**Fig. 6.3**  Classic core sample assembly for relative permeability measurements
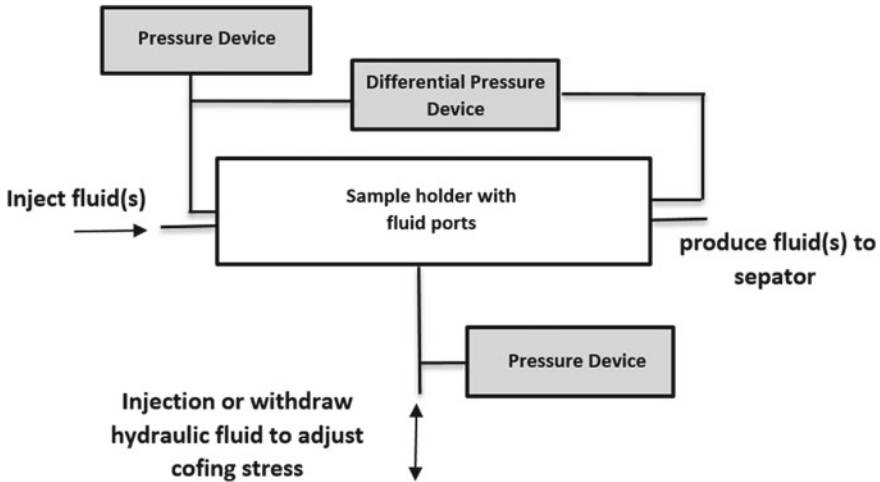
**Fig. 6.4** Core sample apparatus for control and monitoring the displacement process

## 6.4   Steady State Method

Steady-state techniques all consist of a sequence of experiments with time-independent pressure drop and fluid saturations. In each experiment of a sequence, fluids are injected at a constant rate (Richard and Susan 1995). Although pressure drops and fluid saturations change in the early part of the experiment, pressure drop and saturation are not recorded until they reach stable values. Once stable values are reached and recorded, flow conditions are then changed to obtain fluid saturations and the associated pressure drops for the next experiment in the sequence. Thus, steady-state methods require a sequence of experiments performed over a range of discrete, steady flow conditions.

Each step in the sequence may take a day to a week to complete, depending on the permeability and porosity of the rock sample and the corresponding time required to reach stable values of pressure drop and saturation. Within the category of steady-state methods, four sub-categories can be used to classify methods according to the experimental approach for minimizing the influence of capillary end effects:

(1)   The multiple-core method,
(2)   The high-rate method,
(3)   The stationary-liquid method, and
(4)   The uniform capillary-pressure method.

Although the names of the sub-categories of steady-state methods vary widely in the literature, the names used here describe of the approach used.

## 6.5  Unsteady-State Method

Unsteady-state methods consist of single experiments in which a fluid is injected into a rock sample and the transient behavior of pressure decay and fluid saturation is recorded. The time required to complete an experiment is significantly less than for steady-state experiments, taking an hour or less even for rocks with permeabilities of about 1 mD.

A larger number of variations on unsteady-state measurement methods are reported in the literature than for steady-state methods. Variations include injecting fluids at a constant flow rate, constant pressure, or in a pulsed manner. In centrifugal experiments, fluid is drained from a rock sample at an exponentially declining rate, whereas in other experiments a pressure difference between the injected fluid and the displaced fluid is applied and then allowed to decrease toward an equilibrium value which is determined by capillary pressure properties.

It is significant to note that relative permeability and capillary pressure must be determined separately using most unsteady-state methods. Unsteady-state methods are further divided under four sub-categories (Richard and Susan 1995):

(1)  High flow rate methods,
(2)  Low flow rate methods,
(3)  Centrifuge methods, and
(4)  Stationary-liquid methods.

## 6.6  The Relationship Between Relative Permeability, Capillary Pressure, and Fractional Flow

In the reservoir, both irreducible water saturation and critical water saturation take place at similar values of water saturation. The irreducible water saturation and critical water saturation in low-permeability reservoirs can be radically dissimilar. In the hydrocarbon reservoir, there is a large range of water saturation at which water and gas can flow refer to Fig. 6.5. In low permeability reservoirs, there is a large range of water saturation wherein none of gas or water can flow. In the same time in an extremely low permeability reservoir, there is almost no movable water even at extremely high water saturation.

Figure 6.6 illustrates the correlation between capillary pressure, relative permeability, fractional flow, the conceptual fluid distribution within the reservoir, and the expected initial production behavior. In the upper part of the picture, the relative permeability of Oil ($K_{ro}$) is presented as a green curve, the relative permeability of water ($K_{rw}$) is the blue curve, and the fractional flow ($f_w$) is the magenta curve. The lower part of the picture shows the capillary pressure curve in red.

At water saturations lower than the Critical ($S_{wc}$) or equal to the irreducible ($S_{wirr}$) the relative permeability of the water is zero (there is no free or mobile water)
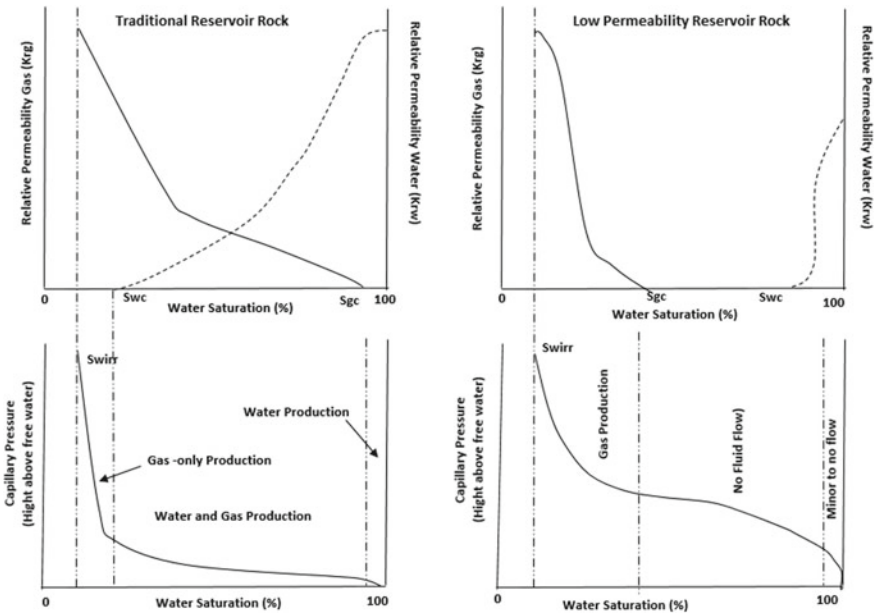
Fig. 6.5  Assessment of relative permeability curves and capillary pressure for gas (left) and tight gas (right)

and clean oil production is expected. As the water saturation increases, the relative permeability of oil gradually decreases and becomes zero at the residual oil saturation ($S_{or}$). At this point, only water is expected to be produced. In the reservoir, this corresponds to the water-oil contact (WOC). At water saturations higher than Swc and lower than $1 - S_{or}$, oil and water production is expected and in the reservoir, this corresponds to the transition zone. The fraction of water and oil flow is given by the fractional flow curve, and not only depends on the porous media properties but also on the properties of the fluids (Francisco 2017). The main fluid property affecting the flow is the viscosity. For example, if gas and oil have the same relative permeability, more gas than oil will flow because of the significant difference in viscosity.

**Example 6.1**
A steady-state flow method was applied to obtain the below data at a temperature of 70 °F.

1.  Calculate absolute permeability using 100% water saturated core sample.
2.  Calculate effective permeabilities to oil and water.
3.  Calculate relative permeabilities
4.  Calculate water saturations
5.  Draw the relative permeability curve.
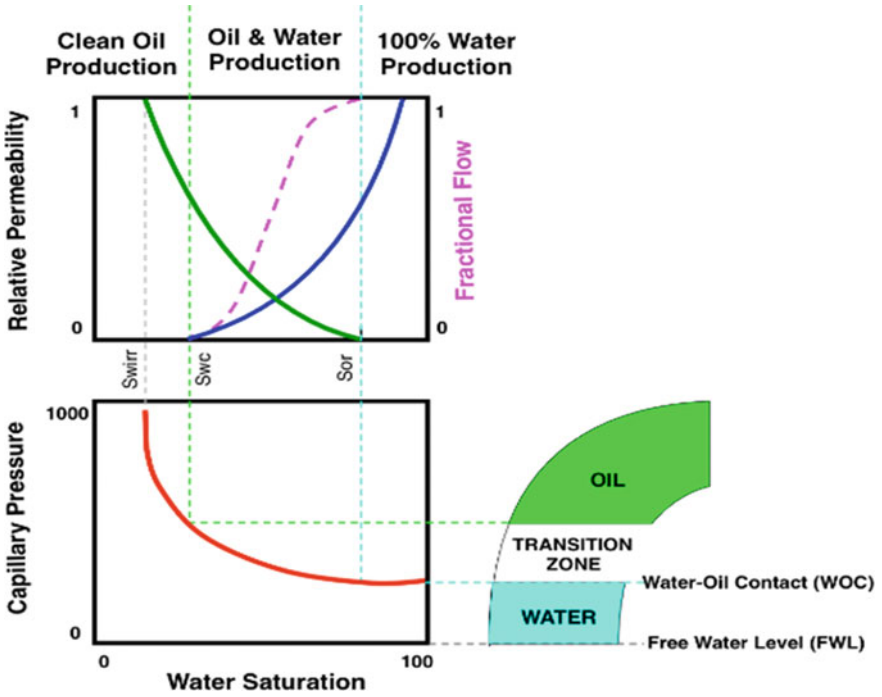
**Fig. 6.6** Illustrate the correlation between capillary pressure, relative permeability, and fractional flow (after Francisco 2017)

| The core |  | The fluids |  |
|---|---|---|---|
| Sandstone |  | Brine | 60,000 ppm |
| Length | 2.30 cm | Oil | 40°API |
| Diameter | 1.85 cm | $\mu_w$ | 1.07 cP |
| Area | 2.688 cm$^2$ | $\mu_o$ | 5.50 cP |
| Porosity | 25.5% |  |  |

| Oil rate (cc/s) | Water rate (cc/s) | Inlet pressure (psig) | Outlet pressure (psig) | Voltage drop (V) | Current (A) |
|---|---|---|---|---|---|
| 0.0000 | 1.1003 | 38.4 | 7.7 | 1.20 | 0.01 |
| 0.0105 | 0.8898 | 67.5 | 13.5 | 2.10 | 0.01 |
| 0.0354 | 0.7650 | 88.1 | 17.6 | 2.80 | 0.01 |
| 0.0794 | 0.3206 | 78.2 | 15.6 | 4.56 | 0.01 |
| 0.1771 | 0.1227 | 85.6 | 17.1 | 08.67 | 0.01 |
| 0.2998 | 0.0000 | 78.4 | 15.7 | 30.00 | 0.01 |

**Solution**

(1) $k = \dfrac{q_w \mu_w L}{A \Delta P}$

$$k = \frac{(1.1003)(1.07)(2.30)}{(2.688)(38.4 - 7.7)(14.696)}$$

$$k = 0.482 \, Darcy$$

(2) $k_o = \dfrac{q_o \mu_o L}{A \Delta P}$

$$k_o = \frac{(0.0105)(5.50)(2.30)}{(2.688)(67.5 - 13.5)(14.696)}$$

$$k_o = 0.0134 \, Darcy$$

$$k_w = \frac{q_w \mu_w L}{A \Delta P}$$

$$k_w = \frac{(0.8898)(1.07)(2.30)}{(2.688)(67.5 - 13.5)(14.696)}$$

$$k_w = 0.2217 \, Darcy$$

(3) $k_{ro} = \dfrac{k_o}{k} = 0.028$

$$k_{rw} = \frac{k_w}{k} = 0.460$$

(4)    $E_o = 1.2$ V (current across core saturated with 100% wetting phase)
    $E_t = 2.10$ V (current across core saturation with less than 100% wetting phase)

$$S_w = (\frac{E_O}{Et})^{1/2}$$

$$S_w = (\frac{1.20}{2.10})^{\frac{1}{2}} = 0.756$$

(5)  .

| Water saturation $S_w$ | Oil relative permeability $k_{ro}$ | Water relative permeability $k_{rw}$ | $k_o/k_w$ |
|---|---|---|---|
| 1.000 | 0.000 | 1.000 | 0.000 |
| 0.756 | 0.028 | 0.460 | 0.061 |
| 0.655 | 0.072 | 0.303 | 0.238 |
| 0.513 | 0.182 | 0.143 | 1.273 |
| 0.372 | 0.371 | 0.050 | 7.419 |
| 0.200 | 0.686 | 0.000 | – |

Sw, % pore space
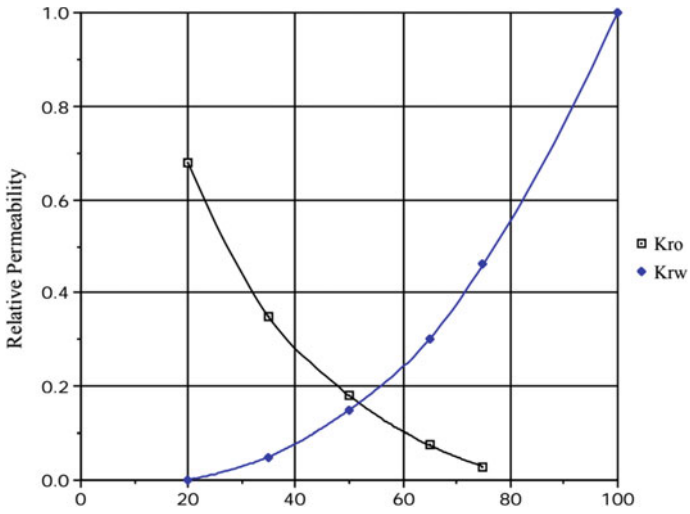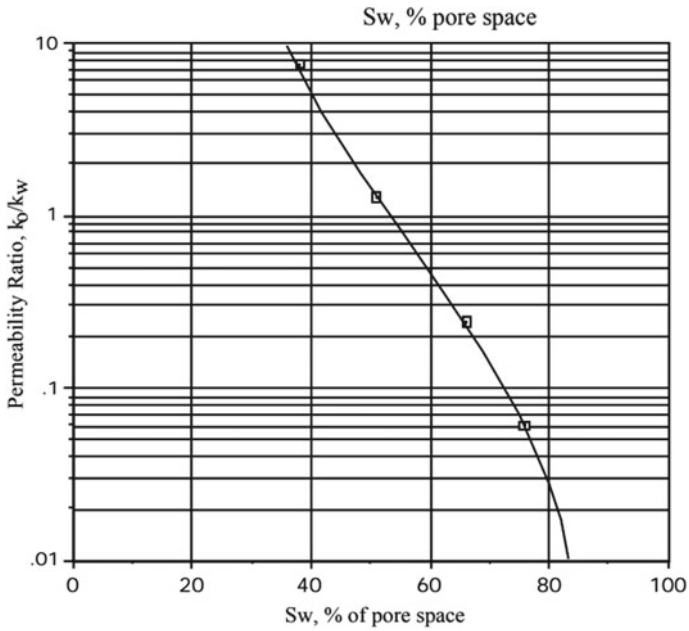
Example 6.2

For a water-wet reservoir with residual gas saturation equal to 0.05 and $S_{wi} = 0.16$, apply the below capillary pressure records to determine the relative permeability:

| $P_c$ ($S_w$) | $S_w$ | $P_c$ ($S_w$) | $S_w$ |
|---|---|---|---|
| 0.5 | 0.965 | 8 | 0.266 |
| 1 | 0.713 | 16 | 0.219 |
| 2 | 0.483 | 32 | 0.191 |
| 4 | 0.347 | 300 | 0.16 |

1. Calculate normalized water Saturation ($S_w$*),
2. Determine $\lambda$ by plotting $LogP_c$ versus $LogS_w$*.
3. Calculate relative permeability of the non-wetting phase at irreducible wetting phase Saturation ($k_{ro}$).
4. Calculate relative perm values at various water saturations.

**Solution**

Step1:

Use Eq. (6.8) to estimate normalized water saturation ($S_w$*).

| $P_c$ ($S_w$) | $S_w$ | $S_w$* | $P_c$ ($S_w$) | $S_w$ | $S_w$* |
|---|---|---|---|---|---|
| 0.5 | 0.965 | 0.958 | 8 | 0.266 | 0.126 |
| 1 | 0.713 | 0.658 | 16 | 0.219 | 0.070 |
| 2 | 0.483 | 0.385 | 32 | 0.191 | 0.037 |
| 4 | 0.347 | 0.223 | 300 | 0.16 | 0.000 |

(1) Step 2:

Determine $\lambda$ by plotting $LogP_c$ versus $LogS_w$*
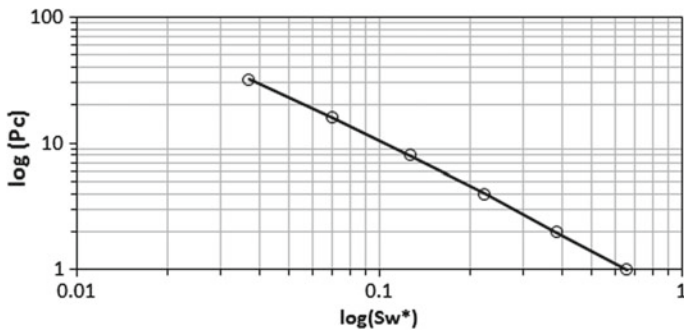


Recall Eq. (6.8), Slope is $-1/\lambda = -1.25$, so, $\lambda = 0.8$

(2) Step 3:

Determining relative permeability of the non-wetting phase at irreducible wetting phase saturation ($k_{ro}$),

Recall Eq. (6.7), $k_r^o = 0.919$ and $S_m = 0.95 = 1 - S_{rg}$.

(3) Step 4:

Determining relative permeability values, recall Eqs. (6.4) and (6.5) to determine the relative permeability of the respective phases at different water saturations:

| $S_g$ | $S_w$ | $S_w$* | $K_{rg}$ | $K_{rw}$ |
|---|---|---|---|---|
| 0.050 | 0.950 | 0.940 | 0.000 | 0.715 |
| 0.080 | 0.920 | 0.905 | 0.000 | 0.578 |
| 0.110 | 0.890 | 0.869 | 0.002 | 0.464 |
| 0.140 | 0.860 | 0.833 | 0.006 | 0.369 |

(continued)

(continued)

| $S_g$ | $S_w$ | $S_w*$ | $K_{rg}$ | $K_{rw}$ |
|-------|-------|--------|----------|----------|
| 0.170 | 0.830 | 0.798 | 0.012 | 0.290 |
| 0.230 | 0.800 | 0.762 | 0.020 | 0.226 |
| 0.260 | 0.740 | 0.690 | 0.047 | 0.132 |
| 0.290 | 0.710 | 0.655 | 0.065 | 0.099 |
| 0.320 | 0.680 | 0.619 | 0.087 | 0.073 |
| 0.350 | 0.650 | 0.583 | 0.112 | 0.052 |
| 0.380 | 0.620 | 0.548 | 0.141 | 0.037 |
| 0.410 | 0.590 | 0.512 | 0.172 | 0.026 |
| 0.440 | 0.560 | 0.476 | 0.207 | 0.017 |
| 0.470 | 0.530 | 0.440 | 0.245 | 0.011 |
| 0.500 | 0.500 | 0.406 | 0.285 | 0.007 |
| 0.530 | 0.470 | 0.369 | 0.329 | 0.004 |
| 0.560 | 0.440 | 0.333 | 0.375 | 0.002 |
| 0.590 | 0.410 | 0.298 | 0.423 | 0.001 |
| 0.620 | 0.380 | 0.262 | 0.474 | 0.001 |
| 0.650 | 0.350 | 0.226 | 0.527 | 0.000 |
| 0.680 | 0.320 | 0.190 | 0.583 | 0.000 |
| 0.710 | 29.000 | 0.155 | 0.640 | 0.000 |
| 0.740 | 0.260 | 0.119 | 0.701 | 0.000 |
| 0.770 | 0.230 | 0.083 | 0.763 | 0.000 |
| 0.800 | 0.200 | 0.048 | 0.828 | 0.000 |
| 0.830 | 0.170 | 0.012 | 0.896 | 0.000 |

Then plot $k_{rg}$ and $k_{rw}$ versus $S_w$ to show the information in its most representative form: Relative permeability.
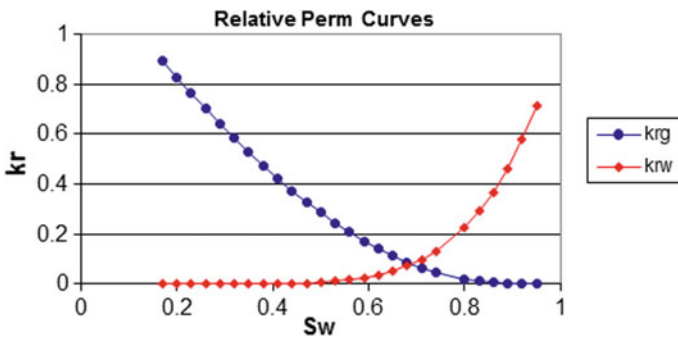
# References

Brooks RH, Corey AT (1964) Hydraulic properties of porous media. Hydrology Paper 3, Colorado State University, Fort Collins, pp 27

Brooks RH, Corey AT (1966) Properties of porous media affecting fluid flow. Proc Am Soc Civ Eng 92[IR2]:61–87

Burdine NT (1953) Relative permeability calculations from pore size distribution data. J Pet Technol 5(3):71–78. https://doi.org/10.2118/225-G

Corey AT (1954) The interrelation between gas and oil relative permeabilities. Producers Mon 19:38–41

DiCarlo D, Sahni A, Blunt M (2000) Three-phase relative permeability of water-wet, oil-wet, and mixed-wet sandpacks. SPE J 5(1): 82–91. SPE-60767-PA. http://dx.doi.org/10.2118/60767-PA. Accessed Mar 2000

Francisco C (2017) Fractional flow, relative permeability & capillarity: real example of basic concepts. https://www.linkedin.com/pulse/fractional-flow-relative-permeabilitycapillarity-real-caycedo/

Islam M, Berntsen R (1986) A dynamic method for measuring relative permeability. J Can Pet Technol 25(1):39–50. 86-01-02. https://doi.org/10.2118/86-01-02

Jerry L (2007) Carbonate reservoir characterization. https://doi.org/10.1007/978-3-540-72742-2. Accessed 2007

John H, Black J (1983) Fundamentals of relative permeability: experimental and theoretical considerations. In: SPE annual technical conference and exhibition, San Francisco, California, 5–8 Oct. https://doi.org/10.2118/12173-MS

MacAllister D, Miller K, Graham S (1993) Application of X-Ray CT scanning to determine gas/water relative permeabilities. SPE Form Eval 8(3): 184–188. SPE-20494-PA. http://dx.doi.org/10.2118/20494-PA

Oak M, Baker L, Thomas D (1990) Three-phase relative permeability of Berea sandstone. J Pet Technol 42(8):1054–1061. SPE-17370-PA. https://doi.org/10.2118/17370-PA

Qingjie L, Hongzhuang W, Wu P (2010) Improvement of flow performance through wettability modification for extra-low permeability reservoirs. Publisher; Society of Petroleum Engineers. In: International oil and gas conference and exhibition in China, 8–10 June, Beijing, China. SPE-131895-MS. https://doi.org/10.2118/131895-MS

Richard L, Susan M (1995) Literature review and recommendation of methods for measuring relative permeability of anhydrite from the Salado formation at the waste isolation pilot plant. Sandia National Laboratories. SAND93-7074 • UC-72129

Standing M (1974) Notes on relative permeability relationships. Unpublished report, Department of Petroleum Engineering and Applied Geophysics, The Norwegian Institute of Technology, The University of Trondheim

Tarek A (2010) Reservoir engineering handbook, 4th edn. TN871.A337 2010. ISBN 978-1-85617-803-7

# Chapter 7
# Overburden Pressure
# and Compressibility of Reservoir Rock

## 7.1   Overburden Pressure

The overall pressure at any formation depth, as a result of the weight of fluid-saturated rock column, is known as overburden pressure, $P_{ov}$. The whole pressure at any reservoir depth is the total of the fluid column pressure, $P_f$, and the overlaying grain column pressure. $P_m$, as seen in Fig. 7.1 and Eq. (7.1):

$$P_{ov} = P_f + P_m \qquad (7.1)$$

The total weight of the overburden is basically applying a compressive force to the formation rock. The pressure in the aperture of the reservoir rock does not come close to the overburden pressure. Normally, pore pressure is known as the reservoir pressure, is approximately 0.5 psi/ft, considering that the reservoir is adequately consolidated, therefore, the overburden pressure is not passed to the fluids in the pore

**Fig. 7.1** Overburden pressure as the combined matrix and fluid column pressure
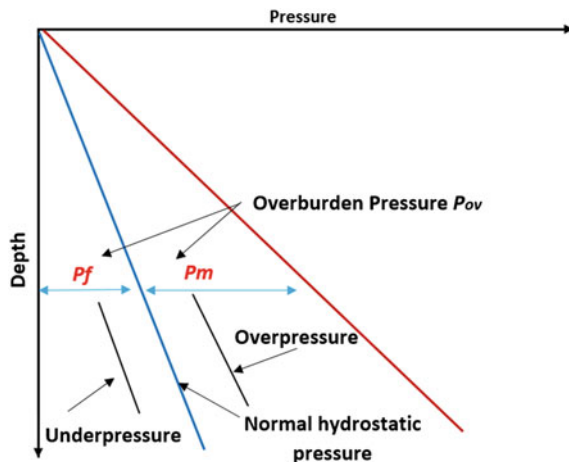
spaces (Tarek 2009). The difference between internal pore pressure and overburden is known as the effective overburden pressure. Through pressure depletion, the internal pore pressure declines and, then, the effective overburden pressure raises. The increase of the effective overburden pressure creates the following effects:

- Decrease the reservoir rock bulk volume.
- Enlarge the sand grains within the aperture.

It should be noted that this pressure is not isotropic but activates vertically. The pressures horizontally depend upon the overburden pressure, but are changed by extra-large scale sub-horizontal tectonic forces, and are affected by local in homogeneities in the crust, such as fractures. Though, to a first an approximation the pressure at depth can commonly be considered to be hydrostatic.

On other words, the pressure in the water phase is depending on the extent to which the fluid column is linked to the Earth's surface. In an open system, the fluid pressure is equal depth × density of the fluid and it's identified as a hydrostatic pressure gradient shown in Fig. 7.2, usually, the pressure gradient is 0.435 psi/ft. Overburden pressure gradient equals the load of the overburden deposit and has a pressure gradient of 1 psi/ft.

Generally, the deviations from hydrostatic pressure take place once the formation fluid is restricted and cannot equilibrate with surface pressure. Usually, the overpressuring is created by:

1. Compaction during fast burial
2. Tectonic compression
3. Hydrocarbon creation and migration (Osborne and Swarbrick 1997).

In very excessive condition, fluid pressure can be either same or go beyond overburden pressures. Unusually, pressures can be lesser than hydrostatic. An underpres-
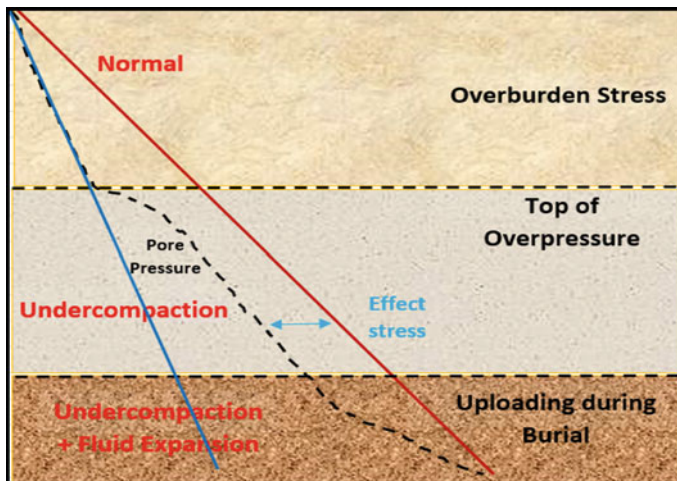


**Fig. 7.2** Effect of vertical effective stress to different subsurface conditions

sure is based on the erosional unloading that consequences in raise in pore volume caused by the elastic rebound of the deposit as the overburden are decreased (Arps 1964).

The overburden pressure can be identified as the hydrostatic pressure applies by the weight of fluid-saturated rock column and grain column overlying the depth of rock (Eq. 7.2):

$$P_{ov} = 0.052 \times \rho b \times D \qquad (7.2)$$

where:

$P_{ov}$   overburden pressure (psi)
$\rho_b$   formation bulk density (ppg)
D   vertical depth (ft)

Equation 7.3 below, its key equation for determining the overburden gradient pressure in field conditions of changing lithological and pore fluid density:

$$P_{ov} = 0.433[(1 - \emptyset)\rho_{ma} + (\emptyset\rho b)] \qquad (7.3)$$

where:

$\emptyset$   Porosity
$\rho_f$   Formation fluid density, gm/cc
$\rho_{ma}$   Matrix density, gm/cc

### 7.1.1   Pore Pressure

Normally, pore pressure is referring to the overburden pressure which is not supported by rock matrix, but rather by the fluids or gases exist in the formation. Commonly, pore pressure is same as hydrostatic pressure of water column extended from the bottom of the well to the surface. If the reservoir pressure is less than the hydrostatic pressure, in this case, the reservoir called subnormal pressure. Therefore, if the reservoir pressure more than the hydrostatic pressure then it's known as abnormal pressure reservoir depicted in Fig. 7.3.

### 7.1.2   Effective Pressure

The overburden pressure applies upon a rock to crush it. Consequently, the fluids existing in the pore spaces would be compressed. Therefore, the fluid pressure applies to the rock to stop the rock crushing. In reality, the rock does not crush under the effect of the overburden pressure, but it is a result of the strength of the rock particles
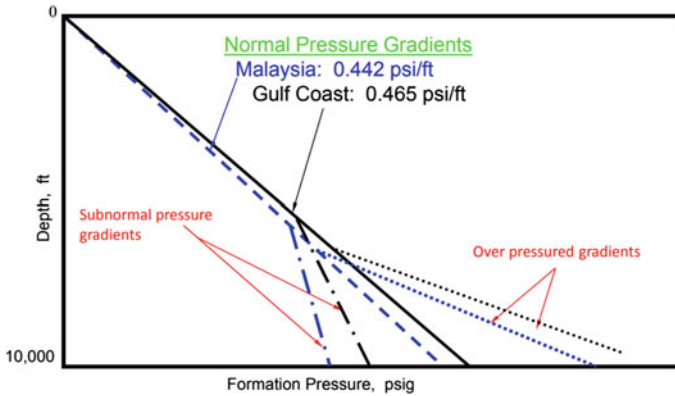
**Fig. 7.3**  Illustrates normal and abnormal reservoir pressure

and any cementation and the support effect of the fluid pressure. A total effective pressure might be identified as the overburden pressure minus the fluid pressure. Commonly, there are available evidence that the effective pressure the overburden pressure minus around 80% of the fluid pressure.

## 7.2  Compressibility of Reservoir Rock

Compressibility is a physical fact, which has a major function in the petroleum production system. Therefore, it's an important "drive mechanism" in the production system. Since the pressure drops with fluids production, then, rock grains will be closer and reduces the rock porosity. This phenomenon called rock compressibility.

The rock compressibility has a major effect on the computation of oil initially in place in undersaturated volumetric reservoirs when the edges of the field are unidentified and studies of natural water drive performance.

Almost all hydrocarbons production and formation water is a function of volume expansion when the reservoir pressure drops because of the produce of reservoir fluids. When outer forces exerted on the reservoir rocks, inner stresses are increased and if the stresses are strong enough, this will cause deformation the rock volume and shape. In general, the main compressibility effective on reservoir rock is due to two factors, known as, expansion of the rock grains, because the in situ fluid pressure drops, and the extra formation compaction brought about (Howard 2013). Both of these factors tend to decrease porosity. Rock compressibility is identified as the decrease in pore volume per unit of rock volume with a unit change in reservoir pressure, presented as (Eq. 7.4);

$$C = \frac{1}{V}\left(\frac{dP}{dV}\right)T \tag{7.4}$$

where c is the coefficient of isothermal compressibility, $c \geq 0$, V is Volume ($ft^3$), P is the pressure exerted of material (Psi), and T is the temperature (°F).

The total compressibility of any formation rock is an effect of two main factors, expansion of the single rock grains, and the extra compaction due to overburden pressure as reservoir pressure declines. In the same time, these factors tend to reduce porosity. The experiments were conducted in a way that would give compressibility measurements reflecting the combination of the two factors and would duplicate the performance of the rock under reservoir conditions. Figure 7.4 displays the apparatus used to estimate rock compressibility.

Typically, the reservoirs overburden pressure is constant but the fluid pressure in pores media changes, which causes changes in the pore volume. During the experimental work, the confining pressure ($P_f$) on the core sample will change while keeping the pore pressure constant. The gross compaction pressure is the difference between the pore pressures and overburden. This way helps to achieve valuable results during the experiment. The experiment procedure: Core sample is 100% saturated with brine. Core sample is sited in a rubber sleeve. Once pressure outside the rubber sleeve is increased, pore volume decreases and the volume of seeped brine is measured.

In 1953, Hall (1953) presented correlations between porosity and rock compressibility see Fig. 7.5 for numerous reservoirs (sandstone and limestone). All experiments were carried out with an external pressure of 3000 psi and internal pressures from 0 to 1500 psi. In 1958, Fatt (1958) stated that there is no correlation between compressibility and porosity, though the studied porosity was very narrow (10–15%).
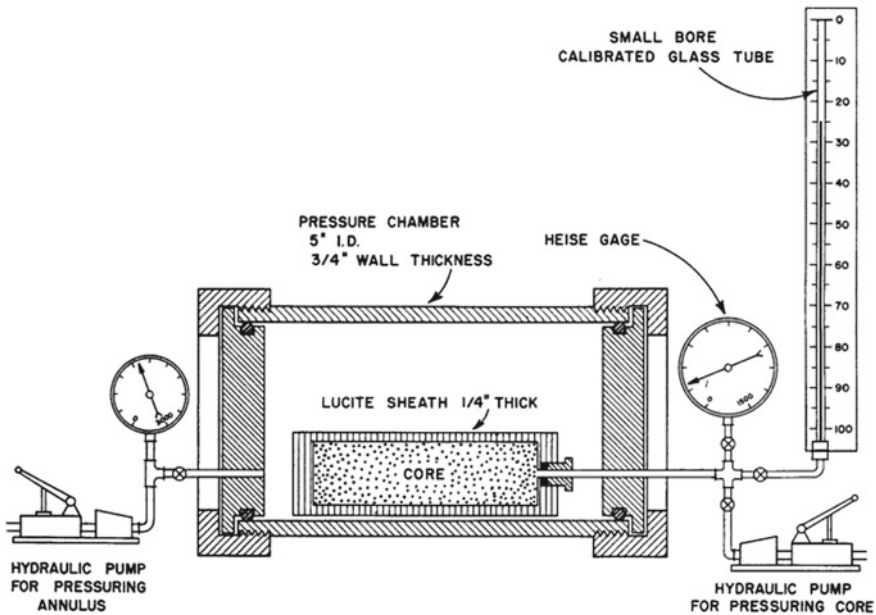


**Fig. 7.4** Effective rock compressibility versus porosity. *Source* Hall (1953)
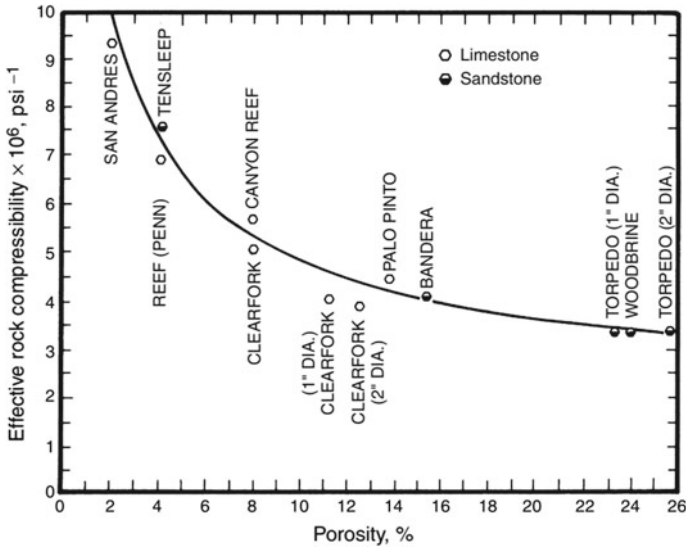
**Fig. 7.5** Effective rock compressibility versus porosity. *Source* Hall (1953)

For limestone reservoir, Knapp (1959) noticed that both pore compressibility and porosity are related to the simple empirical formula. However, in a very detailed study, Newman (1973) proposed that any correlation between rock compressibility and porosity does not use to a big range of reservoir rocks.

### 7.2.1   Effects of Rock Compressibility on Field Development

Even though rocks may be appearing inflexible and incompressible when buried at high depth and are succumbed to high pressures they might deform. This activity is captured by compressibility, a parameter that may be obtained in particular labs. The reservoir Rock compressibility is considered as extra energy or drive mechanisms that support to extract fluids from the reservoir rock and compressibility can decrease the porosity and permeability of the reservoir. If fluids can not discharge out of the rock, an overpressured reservoir is formed. Therefore, Rock compression has both negative and positive impacts of hydrocarbon production. Compression process can make sand grains to be closer and this can decrease reservoir rock permeability. Consequently, this compaction can reduce the reservoir overall production. This effect is shown in Fig. 7.6.

**Example 7.1**
Calculate the hydrostatic pressure of 10.5 ppg mud in a well at depth 5000 ft?
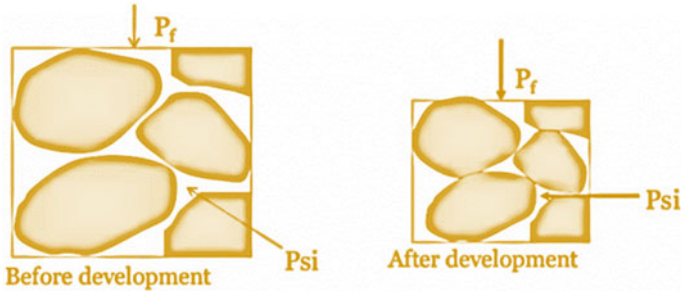
**Fig. 7.6** Illustrates the compaction effects before and after development

**Solution**

$$P_{ov} = 0.052 \times \rho b \times D$$
$$= 0.052(10.5)(5000)2730\,\text{Psi}$$

**Example 7.2**
Calculate the hydrostatic pressure of 40° API oil in a well at depth 5000 ft?

**Solution**

$$SG = 141.5/(131.5 + 40) = 0.825$$

$$Phyd = 0.433(SG)h$$
$$= 0.433(0.825)(5000) = 1786\,\text{Psi}$$

**Example 7.3**
Determine the normal reservoir pressure at depth 9000 ft if the Normal pore pressure gradient in the region is 0.422 psi/ft?

**Solution**  P = 0.422 psi/9000 ft = 3978 Psi

**Example 7.4**
A formation has a pressure of 4000 Psi at reservoir depth of 7500 ft. The operator likes to use a safety allowance of 300 Psi opposite the formation, what is the required density of the mud?

**Solution**

$$P_{ov} = 0.052 . \rho b . D$$

P = 4000 + 300/(0.052) (7500) = 11.0 ppg

**Example 7.5**
Utilize the below reservoir rock data to estimate the volume change in reservoir rock if the pressure dropped 100 psi only:

Porosity = 15%
Total reservoir area = 2,000,000 ft$^2$
Formation thickness = 150 ft
Reservoir rock compressibility = 3 × 10$^{-6}$ 1/psi

**Solution**
Reservoir rock volume = 2,000,000 × 150 = 300 × 10$^6$ ft$^2$.
   Pore volume ($V_p$) = reservoir rock volume × porosity
$V_p$ = 300 × 10$^6$ × 0.15 = 45 × 10$^6$ ft$^3$

$$\frac{dV_p}{dp} = C_f * V_p$$

$$\frac{dV_p}{dp} = 3 \times 10^{-6} * 45 * 10^6 = 135 \, \text{ft}^3/\text{psi}$$

dp = 100 psi
$dV_p$ = 13,500 ft$^3$
The percentage (%) change in reservoir pore volume @ 100 psi decline is:

$$\frac{dV_p}{dp} = \frac{13,500}{45 \times 10^6} = 0.03\%$$

# References

Arps JJ (1964) Engineering concepts useful in oil finding. AAPG Bull 43(2):157–165
Fatt I (1958) Pore volume compressibilities of sandstone reservoir rock. J Pet Tech, 64–66
Hall HN (1953) Compressibility of reservoir rocks. Trans AIME 198:309–311
Howard N (2013) Compressibility of reservoir rocks. https://doi.org/10.2118/953309-g. Accessed Apr 2013
Newman G (1973) Pore-volume compressibility of consolidated, friable, and unconsolidated reservoir rocks under hydrostatic loading. J Pet Tech, 129–134

Osborne MJ, Swarbrick RE (1997) Mechanisms for generating overpressure in sedimentary basins: a reevaluation. AAPG Bull 81(6):1023–1041

Tarek A (2009) Working guide to reservoir rock properties and fluid flow. ISBN:978-1-85617-825-9

Van der Knapp W (1959) Nonlinear behavior of elastic porous media. Trans AIME 216:179–187

# Chapter 8
# Unconventional Petroleum Reservoirs

In this chapter will present an overview of unconventional natural resources definitions and assessment. In this chapter will present an overview of unconventional natural resources definitions and assessment. Whereas, a different characterization have been presented to defined most of the unconventional reservoirs. The chapter covers most of the geological reservoirs include tight gas, tight oil, oil sands, oil shale, bitumen, gas shales, coalbed methane, and gas hydrates formations. This chapter discussed petroleum accumulation, reservoir fluids quantifications (porosity, permeability, and fluid saturations, Total oil contents), formation evaluation, and applications used to develop unconventional reservoirs.

## 8.1 Introduction

Unconventional petroleum studies have established intensely in the recent years. There are many studies were conducted in the sections of reservoir geology, geophysics, engineering, and economic evaluation. Unconventional petroleum is known as continuous or sub-continuous accumulations of hydrocarbons resources (Zhao et al. 2016a). Typically, unconventional petroleum is split into unconventional oil and natural gas resources. There is no specific definition of unconventional petroleum resources. Some researchers defined unconventional resources based only on the permeability values and others their definition was based either on the understanding of the petroleum system or product type. For instance, shale and tight sand reservoirs contain gas, wet gas, Heavy oil, and oil sands and oil fairways were classified as unconventional resources, where the permeability for such reservoirs can be above 500 nD. Besides, the unconventional reservoir can be either high or low permeability reservoir with both high and low viscosity fluids (Harris 2012). These resources can't produce by using conventional techniques. Therefore, new methods are required to increase reservoir permeability and fluid viscosity. Geologically extensive accumulations of petroleum are trapped in low permeability rock such as shale and siltstone with widespread boundaries and no clear traps or hydrocarbon-water contacts.

Unconventional resources include shale gas, tight oil, tight gas, coalbed methane, Bitumen, and gas hydrates (Gruenspecht 2011).

To make these Unconventional resources produce petroleum, the reservoir needs to exhibit very high hydrocarbon saturation, $S_o$ or $S_g$ and small $S_w$. Normally, the natural fracture may also take place, either sub-vertical fracture or horizontal fracture. These reservoirs have very low Permeability, often within nanodarcy range. Generally, the cost of the Unconventional oil production is usually more than conventional oil production and is possible can make additional environmental damage.

## 8.2   Unconventional Petroleum Geology

Unconventional hydrocarbon accumulation is referring to oil and gas continuous diffusion. Because of Pore-throats at the nanometer measure control, there is no clear trap and source rock description; also there are no identical contacts between gas and oil or between oil and water. Besides, the oil and gas saturation differs significantly with coexisting oil, gas, and water. Where, the diameter of the pore-throats is between the ranges of 100–500 nm, which will impact the unconventional hydrocarbon accumulation mechanism. In the unconventional system, there is no identical pressure system or clear bottom water boundary, also the hydrocarbon volume of each pore-cavity is differing significantly. Generally, the geological characteristics, evaluation methods, and classification systems between unconventional and conventional hydrocarbon resources are completely differences. Figure 8.1 below displays the petroleum systems of conventional resources and unconventional resources (Zou et al. 2011).
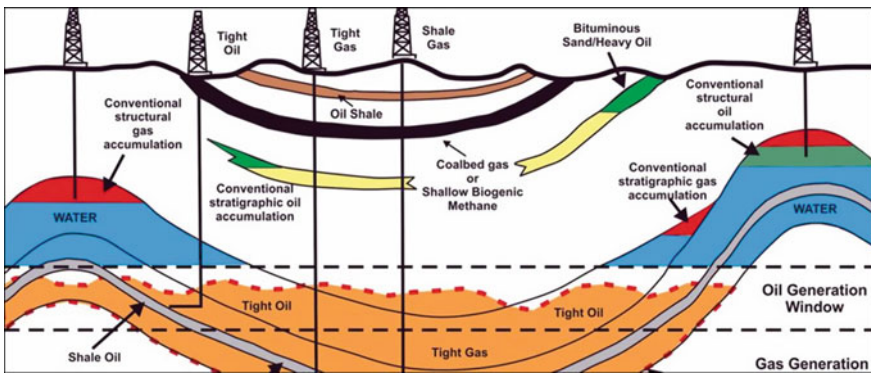


**Fig. 8.1**   Schematic shows the multiple different types of petroleum systems. *Source* Steve Sonnenberg1 and Larry Meckel (2016)

## 8.3   Types of Continuous Petroleum Accumulation

Currently, there is no accessible classification system for continuous petroleum accumulation as a way that classified for conventional petroleum accumulation. In this section, we present some classification schemes based on the features of the accumulations (Table 8.1). According to the previous exploration regions, unconventional petroleum accumulations may be classified into seven unconventional formations. Also, the deposits can be classified into the thermal genetic hydrocarbon, bio-genetic hydrocarbon, and mixture genetic hydrocarbon. The oil and gas existence type can be also absorption, isolated, or combination.

**Table 8.1**  Classification for continuous petroleum accumulation

| Basis of classification | | Type |
|---|---|---|
| Reservoir type | | Tight-sandstone gas, tight-sandstone oil, shale gas, shale oil, fractured-vuggy carbonate petroleum deposits, volcanic and metamorphic petroleum deposits, CBM, gas hydrate, and others |
| Oil and gas origin | | Thermal, biogenetic, mixed cause petroleum deposits |
| Source-reservoir-seal assemblage | Source-reservoir assemblage | Self-generated-reservoir (CBM, shale gas, shale oil, and others), non-self-generated-reservoir (tight-sandstone oil, tight sandstone gas) |
| | Petroleum source | Self-source deposits (CBM, shale gas, shale oil, and others), nonself-source deposits (tight-sandstone oil, tight-sandstone gas) |
| Oil and gas occurrence | | Adsorption type, free type, adsorption-free type |
| Continuity | | Gas deposits with continuous accumulation processes, continuous accumulation areas, and continuous exploitation processes |

*Source* ZOU (2011)

## 8.4   Methods and Technologies

The main geological principle of unconventional hydrocarbon is the reservoir and diffusion of continuous petroleum accumulations. Superior technologies are required during the study of the unconventional hydrocarbon accumulations, such as reservoir prediction, micro-seismic, large-scale fracturing etc. Furthermore, resource evaluation approaches are totally different.

The exploration methods and technologies used for conventional resources can't be used for unconventional hydrocarbon accumulations. Normally, the porosity is less than 10% and the air permeability is lower than $1 \times 10^3$ mm$^2$.

## 8.5   Defining Unconventional Oil and Gas Resources

Unconventional oil contains a broader range of liquid sources comprising oil sands, extra heavy oil, gas to liquids and other liquids.

1. **Oil sands**

Heavy oil and bituminous sands are available worldwide seen in Fig. 8.2. Oil sands usually comprise of extra heavy oil or crude bitumen trapped in an unconsolidated sandstone formation. Such petroleum is forms of crude oil which are very dense and viscous at room temperature making extraction process challenging. Occasionally, the density of the heavy crude oils close or even above water density. Accordingly, this crude seldom produced by applying conventional approaches. The major modification needs to be made on the production system to handle the production process. This type of crude oils contains heavy metals and sulphur at high concentrations level, which affect the refining processes. Such type of unconventional oil does existing in Canada's and Venezuela (Bergerson and Keith 2006).

To extracting a large amount of oil from oil sands will be difficult as the production process need high capital cost, manpower, and landscape along with the source of restricted energy for production systems such as heat and power generation (Gardiner 2009).

2. **Tight Oil**

Tight oil, comprising of light tight oil is crude oil existing in hydrocarbon bearing formations that have low permeability, normally tight sandstone or shale (Mills 2008). To improve the production performance from tight oil formations the process needs hydraulic fracturing. Commonly, oil shale is shale rich in kerogen, or synthetic oil extracted from oil shales (World Energy Resources 2013).

3. **Oil Shale**

Oil shale is sedimentary rock rich with large amounts of kerogen from see Fig. 8.3. The kerogen in oil shale can be transformed into shale oil by the chemical processes

**Fig. 8.2** Oil sand (Alberta, Canada). *Source* https://www.strausscenter.org/energy-and-security/tar-sands.html



**Fig. 8.3** An outcrop of oil shale. *Source* Smith et al. (2007)

such as hydrogenation, pyrolysis, or thermal dissolution. The temperature when decomposition of oil shale happens, at 300 °C, rely on the time scale of the pyrolysis, however, it can occur more rapidly at higher temperatures (480 °C). The ratio of shale gas to shale oil subject on the distillation temperature and as a rule, the ratio rises as temperature increase. This process is reliant on the properties of oil shale and the processing technology used. In 2016 the World Energy Council estimated the total global shale oil resources are about 6.05 trillion barrels (World Energy Council 2016).

4. **Tight Gas**

Tight gas its gas located in hard and impermeable formations. Besides, tight gas can be located in sandstone or limestone reservoirs which are nonporous, also identified as tight sand. The production process of tight gas needs more work to extract it from the tight reservoir. This means that the pores in the reservoir rock are either irregularly scattered or poorly connected with too thin capillaries, low permeability, or the capability of the gas to mobile over the rock. The secondary recovery process, such as fracturing and acidizing, is required to produce more gas from a tight reservoir at a highly economical production rate. Typically, tight gas reservoirs are discovered in Palaeozoic formations and because of cementation, compaction, and recrystallization of the formation, the permeability was extremely decreased which can be measured in the millidarcy or microdarcy range (Dan 2008).

5. **Shale Gas**

Shale gas is natural gas (mainly methane) that is located within shale reservoirs. As shales normally have extremely low permeability to produce gas at a high flow rate, shales are not commercial sources. The risk of discovering shale gas is low in resource plays, also the possible profits per successful well are lower. Since shale has small matrix permeability, the shale formation needs fractures to add more permeability either natural fractures or apply advanced technology to generate hydraulic fracturing to make widespread artificial fractures around the wellbore. Commonly, horizontal wells are used with horizontal lengths exceed 3500 m, to increase the production area at the wellbore (Dan 2008).

Shale formations that contain profitable amounts of gas have some common properties. They are rich in organic material (0.5–25%), and are mature hydrocarbon source rocks, where heat and pressure have transformed hydrocarbons to natural gas. Shale is sufficiently hard enough to keep open fractures (US Department of Energy 2009).

6. **Gas Hydrates**

Gas hydrates are crystalline water-based solids formed of water and gas molecules. It looks like ice but it comprises massive quantities of methane. It's available everywhere around the world, and it occurs in marine sediments right beneath the sea floor and in association with permafrost in the Arctic. The gas hydrate layer extends into the seafloor where temperature goes above gas hydrate stability, typically some 10–100 m under the seafloor (Sloan 1990). Normally, hydrocarbons and freons will

form hydrates at specific temperatures and pressures. The gas hydrates are massive energy resource; however, the extraction technique has up to now proven elusive. Hydrates create difficulties for the oil and gas industry because they blockage gas pipelines depicted in Fig. 8.4.

7. **Coal-Bed Methane**

Coalbed methane (CBM) is a natural gas produced from coal beds. Recently, CBM becomes the main source of energy in the producer countries. Normally, methane adsorbed into the coal matrix. Commonly It is named 'sweet gas' due to lack of hydrogen sulfide. CBM is different from any conventional gas reservoir since the methane is trapped within the coal by adsorption process. Usually, methane is close to liquid state, stored inside pores of the coal matrix. Also, the open fractures in the CBM can store free gas or saturated with water. CBM holds a little heavier hydrocarbon such as propane or butane, but no gas condensate. CBM naturally contains a few amounts of carbon dioxide. The CBM reservoirs are defined as a dual porosity reservoir in which porosity related to fractures are in charge of flow performance and the matrix porosity controls the gas storage. The range of CMB porosity can vary from 10 to 20%, but, the fracture porosity is within the range of 0.1–1% (Clarkson 2013). As mentioned early, the fracture permeability plays the major role of flow performance of CBM formation. Where, CMB permeability is within the range of 0.1–50 milliDarcys (McKee et al. 1988).



**Fig. 8.4** Hydrate Plug Formed in a Subsea Hydrocarbon Pipeline. *Source* Irmann (2013)

8. **Bitumen**

Bitumen is petroleum that presents in semi-solid or solid stage in the reservoir. It usually holds sulfur, metals, and other non-hydrocarbons contents. Usually, the Bitumen density is below 10 °API and viscosity is bigger than 10,000 cP (at reservoir temperature and atmospheric pressure on a gas-free basis). To extract Bitumen at commercial amounts needs improved applications and developed recovery approaches such as steam injection. Commonly, Near-surface bitumen deposits can be extracted through mining techniques. This type of petroleum needs refining with light hydrocarbons prior to export (Dusseault et al. 2008).

## 8.6   Nanopore System Reservoirs

Commonly, unconventional formations are mainly nanoscale pore throat structures. The following are the ranges of the pore throat diameter for unconventional formations which are measured in nanoscale:

- Shale gas from 5 to 200 nm
- Shale oil from 30 to 400 nm
- Tight limestone oil from 40 to 500 nm
- Tight sandstone oil from 50 to 900 nm
- Tight sandstone gas from 40 to 700 nm

In the pore throats, there are substantial viscous and molecular forces. Hydrocarbon is adsorbed on the minerals surfaces or kerogens in an adsorbed state or inside solid organisms in a diffused state see Fig. 8.5. Differential pressure and diffusion are the main drivers of hydrocarbon movement and accumulation. Pore connectivity is used to characterize the flow capacity (Curtis et al. 2011).

## 8.7   Formation Evaluation and Reservoir Characterization of Unconventional Reservoirs

Usually, gas or oil shale formations are known as unconventional resources formations, which are very complex in terms of depositional environment descriptions and petrophysical interpretations. Such reservoirs need to be hydraulically fractured to extract a high rate of gas or oil at economic amounts. Besides, High technology is required for increasing the production performance of these reservoirs by using horizontal laterals.

The most of clay matrix particle size available in these unconventional rock reservoirs includes many heterogeneous structural components. These reservoirs contain complex pore throat structures that are mostly nanoscale pores (Loucks et al. 2012). To produce oil and gas, the formation must show very high oil and gas saturations
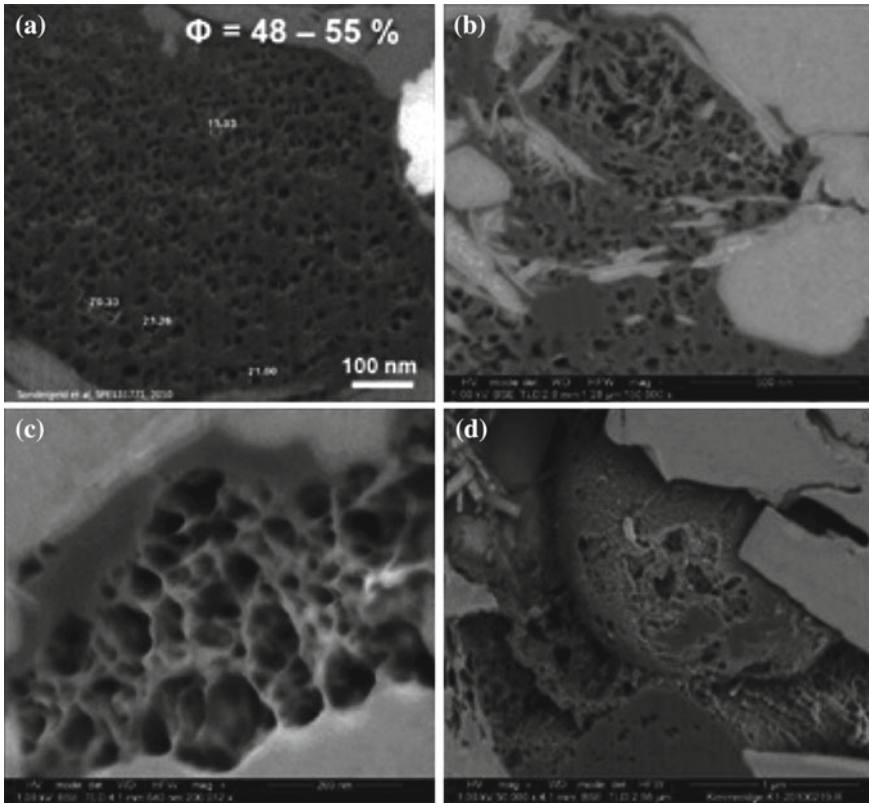
**Fig. 8.5** Nanoscale Kerogen organic porosity. *Source* Curtis et al. (2011)

with very low water saturation. Commonly, the permeability is very low and usually, it's measured in the nanodarcy scale which is very complex and challengeable for formation evaluation. Fractures can occur naturally, and distributed either vertically or horizontally. Mobile hydrocarbons can exist within the pores and also existing as absorbed hydrocarbons to the clay and kerogen surfaces. Generally, acquiring high technical data from different sources is essential to have better formation evaluation of reservoir characterization.

1. **Rock Composition Quantification**

The quantification of the mineral composition and lithology of the Reservoir is the first stage to understand the characterization of unconventional reservoirs. Where, the mineral composition is the main important property that has an influence on the productivity of the reservoir (Walles and Cameron 2009). Term shale is normally used to describe very fine-grained deposited rocks composed of clay grains with some silt. Typically, the grain size is alike in most shale reservoirs, mineralogy differs considerably, both vertically and horizontally inside a single shale reservoir and

between shale reservoirs. The formation could have varying amounts of minerals such as quartz, feldspars, dolomite, and clay. Where, the variations in reservoir mineralogy are related to the variations in the mechanical properties of the reservoir rock. The obtained data from wireline, logging while drilling Lithology, core study, and mud log can be utilized to quantify the lithology and mineral composition of the reservoir. Correct lithology and mineralogy interpretations permit more accurate porosity estimation that can help to make accurate stimulation and completion design.

2. **Total Organic Carbon Quantification**

The best clear characteristic of a source rock is that it holds a high quantity of total organic carbon (TOC). TOC has 3 main components, gas or oil, kerogen, and residual carbon (Jarvie 1991). Naturally, the hydrocarbon is generated from kerogen at high temperature and pressure. Normally, in source rock some of the hydrocarbons migrated into reservoir rock to become conventional reservoirs, however, in unconventional shale reservoirs a significant amount of the hydrocarbon is not migrated and in this case, the source rock becomes a reservoir. Several physical characteristics about the TOC and kerogen need be to quantified (Passey et al. 2010).

3. **Porosity and Permeability Quantification**

As Discussed early, shale reservoirs hold complex pore throat structures composed of very small interparticle and intraparticle. Besides, natural fractures are exists and distributed vertically and horizontally in the reservoir (Loucks et al. 2012). Conventional laboratory approaches for porosity and permeability determination are inappropriate in shale reservoirs. Typically, total shale porosities are low (5–12%). The variable amount of TOC and inorganic mineral components in the reservoir will make the determination of shale porosity by using conventional log technology very difficult. By using elemental spectroscopy and nuclear magnetic resonance logging equipment can improve accuracy. Porosity must be measured from the core and verified with the log derived porosities. Numerous laboratory approaches are used for porosity such as include mercury injection capillary pressure (MICP), gas research institute technique (GRI) standard crushed porosity, and scanning electron microscopy (SEM), and focused ion beam (FIB) tomography depicted in Fig. 8.6. Shale Permeability is very low, and measured in the nanodarcy scale and must be measured in the laboratory using core analysis measurements and calibrated with core responses. Typical laboratory approaches applied to obtain shale permeability include pressure decay, pressure pulse decay, and MICP (Passey et al. 2010).

4. **Fluid Saturation Quantification**

In conventional reservoirs, hydrocarbons are stored only in the pores of the matrix. The hydrocarbon saturations are calculated from laboratory analyses or from the wireline or LWD log measurements of resistivity and porosity. Usually, in unconventional reservoirs, hydrocarbons are trapped as free oil and gas in the fractures and shale matrix pores. Also, the sorbed gas and oil either adsorbed to the kerogen
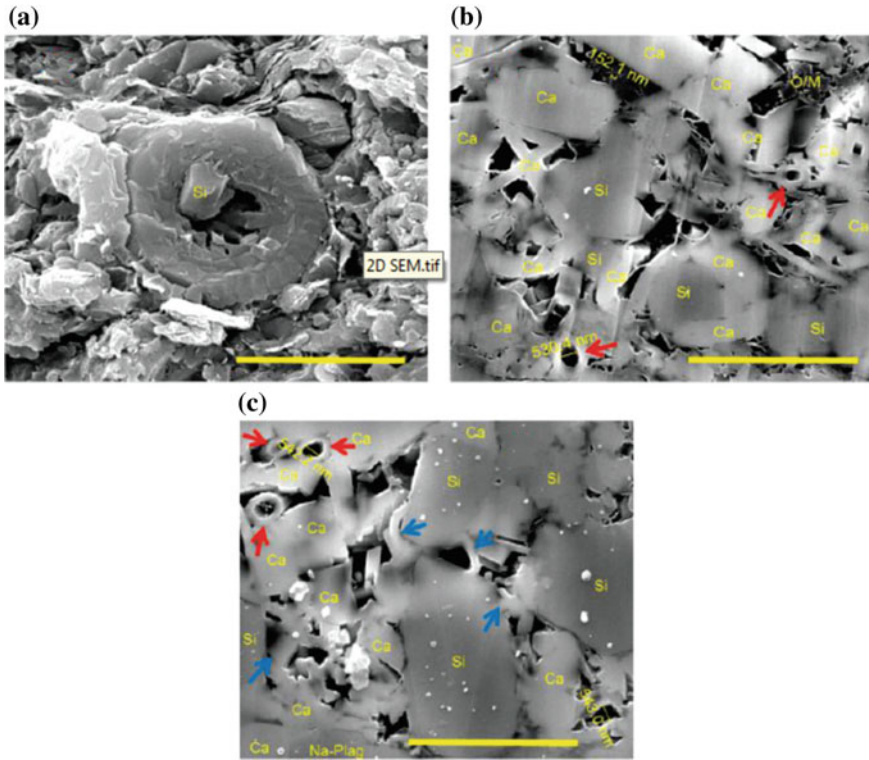
**Fig. 8.6** Differences in a resolution of the grain-related, organic matter and pore types and distribution that can be identified from ion milled SEM samples (**b**, **c**) compared to a standard SEM image. *Source* Driskill et al. (2013)

and mineral surfaces inside the fractures or absorbed to the kerogen and mineral surfaces inside the matrix rock. The dissolved gas can be stored also in the hydrocarbon liquids existing in the bitumen.

In unconventional reservoirs, a mixture of laboratory studies is the primary technique applied to determine volumes and saturation of gas or oil. For crushed core samples, Wise Retort or Dean-Stark analysis are applied to determine fluid saturations. Adsorption and desorption isotherm studies are used in gas shale reservoirs to estimate adsorbed gas volumes and total gas volumes (Bustin et al. 2009). Normally, water saturation is determined by applying the same methodology and techniques used for conventional reservoirs, such as resistivity and porosity log using a shaly sand equation or Archie equation. Adequate core saturation measurement needs to be used to compare with log derived fluid saturations.

## 8.8   Determination of Kerogen Contained Fluid Saturations

Comprehending the nature of storage and transporting the hydrocarbon in unconventional reservoirs, still under investigation. In free and gas adsorbed system, already taking into account the nanoscale porosity and non-darcy flow systems, with varieties of pore throats scale, together with dispersion methods. It's very important to develop unconventional models for molecularly dynamic kerogen adsorption surfaces with variable adsorption volumes for hydrocarbons. Researchers have developed the concept of understanding free and adsorbed hydrocarbon components through developing model methodologies comprising CBM molecular dispersion model(s) methods for gas quantification by desorption and adsorption studies (Xu et al. 2012). Hydrocarbon liquid-rich mudrock resource plays are currently the least understood with respect to these complex transport mechanisms and adsorption systems. Existing methods (Shabro et al. 2012) include developing novel numerical algorithms that concurrently considered gas dispersion in kerogen, slip flow, Knudson diffusion, and Langmuir desorption.

1. **Langmuir Isotherm Formulation**

The relief of adsorbed gas is usually defined by a pressure relationship known as "Langmuir Isotherm". The Langmuir adsorption isotherm proposed that the gas adheres to the surface of the shale or coal, and covers the surface as a single layer of gas (Fekete Associates 2012).

The typical formulation of Langmuir isotherm is (Eq. 8.1):

$$C_{gi} = \frac{V_L * P}{P_L + P} \tag{8.1}$$

where $V_L$ is Langmuir volume; $p_L$ is Langmuir pressure; $p$ is gas pressure; $C_{gi}$ is adsorbed gas content per unit mass of shale. $P_L$ and $V_L$ are indispensable parameters to describe the adsorption, which can be obtained by isothermal adsorption experiments.

The Eq. 8.1 applied for pure coal/shale. For application to coalbed methane reservoirs, Eq. 8.2 below is modified to consider ash and moisture content of the coal.

$$V(P) = (1 - C_a - C_w)\frac{V_L * P}{P_L + P} \tag{8.2}$$

where, $C_a$ is ash content of the coal, scf/ton; $C_w$ is moisture content of the coal, scf/ton.

2. **Free Gas and Adsorbed Gas Equations in Shale reservoirs**

Unconventional hydrocarbon accumulation analysis is a method that applied based on geological observations and information to calculate original oil and gas in place. The approach used to estimate the dynamic contributions of free and adsorbed gas (Eq. 8.3) in shale gas production (Fekete Associates 2012).

$$V(OGIP) = (V_{\text{free}} + V_{adsorbed}) \tag{8.3}$$

## 2.1   Adsorbed Gas Equations

Usually, shale gas formations hold adsorbed gas more than free gas. So, oil initial in place (OGIP) estimations for shale formations must also account for adsorption. The following equations can be applied to estimate the Original Adsorbed Gas-in-Place (OGIP) (Eq. 8.4) for shale gas reservoirs (Fekete Associates 2012).

$$OGIP = 43{,}560 * A * h * \rho_b * \frac{V_L * P}{P_L + P} \tag{8.4}$$

where h is thickness, ft; A is the area, acres; $\rho_b$ is adsorbed gas density, ton/ft$^3$.

## 2.2   CBM Reservoir Calculations

For coalbed methane formation, adsorbed gas is the most significant influence factor when estimating OGIP (Eq. 8.5). Normally, free gas accounts as a small amount of the entire gas-in-place. Typically, the used approach to estimate the adsorbed gas in coalbed methane is similar to that for shale gas, only a few additional parameters are included (Fekete Associates 2012).

$$OGIP = 43{,}560 * A * h * \rho_b * C_{gi} * (1 - C_a - C_w) \tag{8.5}$$

where:

$C_{gi}$ is gas content measured in coal or shale, scf/ton.

## 2.3   Free Gas Equations

Free gas equation is the same for all gas reservoirs (Eq. 8.6)

$$OGIP = 43{,}560 * A * h * \emptyset * \left(S_{gi}\right) * \frac{1}{B_{gi}} \tag{8.6}$$

where, $S_{gi}$ is gas saturation, %; $B_{gi}$ is gas formation Volume Factor, ft$^3$/scf; $\emptyset$ is porosity, %.

# 8.9   Factors Affecting Unconventional Oil and Gas Recovery

Unconventional Oil and Gas (UOG) reservoirs normally spread across large areas and therefore represent very large hydrocarbons in place. But, even by using very developed unconventional technologies, the recovery factor still very low, Typically, 10% or less for liquid-rich shales and 25–35% for gas-rich shales (Energy Information Administration 2013). Furthermore, because the recovery is greatly reliant on the technology used, per-well production is not carefully determined from geologic

evidence such as in conventional reservoirs. Instead, production is extremely sensitive to the effectiveness of the stimulation process and in situ reservoir conditions. Assessment of unconventional oil and gas production, mainly in shale formations, is more complex because the reservoir engineering models and approaches work very well for nanoscale formations (Javadpour et al. 2007). Besides, the nature, efficacy, and possible environmental influences of unconventional oil and gas development will vary considerably among and within unconventional oil and gas resource regions because of geographical, geological, and operational changeability (GAO 2012).

# References

Bergerson J, Keith D (2006) Life cycle assessment of oil sands technologies Proc. Alberta Energy Futures Project Workshop available from http://www.iseee.ca/files/iseee/ ABEnergyFutures-11.pdf

Bustin R, Bustin A, Ross D et al. (2009) Shale gas opportunities and challenges. AAPG Search Discovery Article 40382, Feb

Cai-neng ZOU, Shi-zhen TAO, Lian-hua HOU et al (2011) Unconventional petroleum geology. Geological Publishing House, Beijing, pp 201–210

Clarkson CR (2013) Production data analysis of unconventional gas wells: review of theory and best practices. Int J Coal Geol 109(2013):101–146. ISSN 0166-5162. https://dx.doi.org/10.1016/j.coal.2013.01.002

Curtis M, Ambrose R, Sondergeld C et al. (2011) Investigating the microstructure of gas shales by FIB/SEM tomography & STEM imaging. University of Oklahoma

Dan J (2008) Worldwide shale resource plays, PDF file, NAPE Forum, 26 Aug

Driskill B, Walls J, Sinclair SW et al. (2013) Applications of SEM imaging to reservoir characterization in the eagle ford shale, South Texas, USA. In: Camp W, Diaz E, Wawak B (eds) Electron microscopy of shale hydrocarbon reservoirs, vol 102. AAPG Memoir, pp 115–136

Dusseault M, Zambrano A, Barrios, J, Guerra C (2008) Estimating technically recoverable reserves in the Faja Petrolifera del Orinoco: FPO. Paper WHOC08 2008-437, world heavy oil congress

Energy Information Administration (2013) Technically recoverable shale oil and shale gas resources. http://www.eia.gov/analysis/studies/worldshalegas/pdf/overview.pdf

Fekete Associates Inc. (2012) Langmuir Isotherm. http://fekete.com/SAN/TheoryAndEquations/HarmonyTheoryEquations/Content/HTML_Files/Reference_Material/General_Concepts/Langmuir_Isotherm.htm

GAO (2012) Information on shale resources, development, and environmental and public health risks. Government Accounting Office, GAO712–732. http://www.gao.gov/products/GAO-12-732

Gardiner T (2009) Canada oil sands emit more $CO_2$ than average: report. Reuters. Retrieved 3 June 2012

Gruenspecht H (2011) International energy outlook 2011. US Energy Information Administration

Harris C (2012) What are unconventional resources? A simple definition using viscosity and permeability. AAPG Annual Convention and Exhibition, Long Beach, California. http://www.searchanddiscovery.com/documents/2012/80217cander/ndx_cander

Jarvie D (1991) Total organic carbon (TOC) analysis. In: Merill RK (ed) Treatise of petroleum geology: handbook of petroleum geology, source and migration processes and evaluation techniques, AAPG, pp 113–118

Javadpour F, Fisher D, Unsworth M (2007) Nano-scale gas flow in shale gas sediment. J Can Pet Tech 46(10):55–61

Loucks R, Reed R, Ruppel S et al (2012) Spectrum of pore types and networks in mudrocks and a descriptive classification for matrix-related mudrock pores. AAPG Bull 96(6):1071–1078

McKee C, Bumb A, Koenig R (1988) Stress-dependent permeability and porosity of coal and other geologic formations. Society of Petroleum Engineers. https://doi.org/10.2118/12858-pa

Mills RM (2008) The myth of the oil crisis: overcoming the challenges of depletion, geopolitics, and global warming. Greenwood Publishing Group. pp. 158–159. ISBN 978-0-313-36498-3

Passey Q, Bohacs K, Esch W et al. (2010) From oil-prone source rock to gas-producing shale reservoir–Geologic and petrophysical characterization of unconventional shale-gas reservoirs. Paper SPE 131350 presented at the international oil and gas conference and exhibition in China, Beijing, China. 8–10 June

Shabro V, Javadpour F, Torres-Verdín C, Sepehrnoori K (2012) Finite-difference approximation for fluid-flow simulation and calculation of permeability in porous media. Transp Porous Med 94:775–793

Sloan ED (1990) Clathrate hydrates of natural gases. Marcel Bekker, New York, pp 641

Walles F, Cameron M (2009) Evaluation of unconventional gas reservoirs: tornado charts and sidebars. Poster presented at the AAPG 2009 annual convention

World Energy Council (2016) World energy resources. Oil 2016 (PDF). World-energy-resources-full-report, p 116. ISBN 978-0-946121-62-5

World Energy Resources (2013) Survey (PDF). World energy council. 2013. ISBN 9780946121298

Zhao JZ, Cao Q, Bai YB et al (2016) Petroleum accumulation from continuous to discontinuous: concept, classification and distribution. Acta Pet Sin 37:145–159 (in Chinese)

# Chapter 9
# Naturally Fractured Reservoirs

Currently, there are numerous of authors defined the fracture from a different perspective, However, from the geo-mechanical viewpoint; a fracture is defined as a surface in which a loss of solidity has taken place. Generally, the noticeable displacement fracture is termed as a "fault", and unnoticeable displacement is termed as a "joint" depicted in Fig. 9.1.

A fracture can also be defined, in a more general way, as the discontinuity which breaks the rock beds into blocks along cracks, fissures, joints or whatever they may be referred to as, and along which there is no displacement parallel with the planes of discontinuity. Basically, whether a fracture is considered a joint or a fault depends on the scale of investigation, but in general, that which is called a fracture corresponds to a joint.

Understanding the geology of a fractured reservoir needs the know the link between the fracturing process and the geological activities which happened during this time. commonly, rock fracturing has a tectonic source, evolving in folded beds or in linking with faulting or joint forms. Generally, the study of the fracturing mechanism has lately advanced from an experiential to some more technical method.
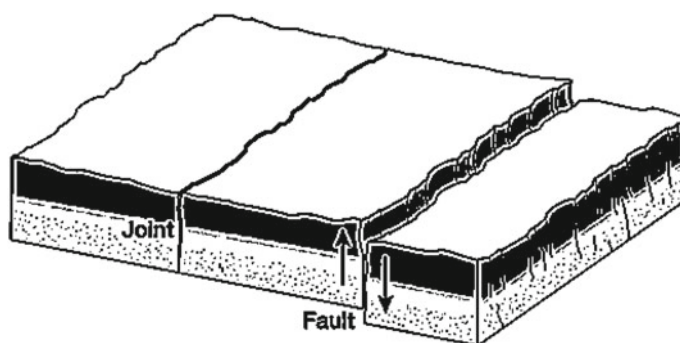


**Fig. 9.1** Diagram showing a joint and a fault

The crust of the earth is almost fractured to some extent. The fractures are mechanical failures of the rock solidity due to tectonic movement or to any other reasons such as thermal stresses and high fluid pressure, as fluid partially supports the load of the overburden rock. The overburden pressure at deeper formations can cause plastic deformation for the sedimentary rocks. these rocks are incapable to bear shear stresses for a long period of time, so it will move towards an equilibrium condition. Normally, the assessment of fracturing reservoir rock properties is very complex than conventional reservoir properties. Actually, the fracturing reliant on the form of mechanical stresses of both rock material and properties. Then, the fracture openings, distribution, orientation, etc., will be linked to stresses and rock type, depth, lithology, etc. Geologically, the naturally fractured formations can be classified into three types. The following are the fracture classifications based on their porosity systems:

1. Intercrystalline-intergranular.
2. Fracture-matrix.
3. Vugular-solution.

## 9.1  Rock Mechanics Versus Fracturing

Normally, at reservoir conditions, an initial bulk volume of the rock is under stresses forced by confining pressure, overburden pressure, fluid pressure, and tectonic movement forces. Typically, considering the forces at three directions and describing the three normal vectors as the main stresses, the stress components $\bar{\sigma}_1, \bar{\sigma}_2, \bar{\sigma}_3$ are defined as the highest, middle and lowest stresses, respectively shown in Fig. 9.2. The vertical stress, $\bar{\sigma}_1$, generated by overburden pressure, however, horizontal stresses, $\bar{\sigma}_2$, and $\bar{\sigma}_3$, defined as compressive stresses.

The link of the normal stress ($\sigma$) and shear stress ($\tau$) performing across a plane perpendicular to $\sigma_1$ and $\sigma_3$ is described as a function of the angle $\psi$, between the direction of the greatest main stress $\sigma_1$ and the plane AB see Fig. 9.3. The following equations show the equilibrium forces performing on a triangular ABC (Eq. 9.1).

$$\sum_i F_{i,n} = 0; \quad \sum_i F_{i,t} = 0$$

$$\sigma = \frac{\sigma_3 + \sigma_1}{2} + \frac{\sigma_3 - \sigma_1}{2} \cos 2\psi + \tau_{3,1} \sin 2\psi \tag{9.1}$$

And in direction t (Eq. 9.2):

$$\tau = \frac{\sigma_1 - \sigma_3}{2} \sin 2\psi + \tau_{3,1} \cos 2\psi \tag{9.2}$$

By applying Mohr's diagram seen in Fig. 9.4 because of the variation of angle $\psi$,

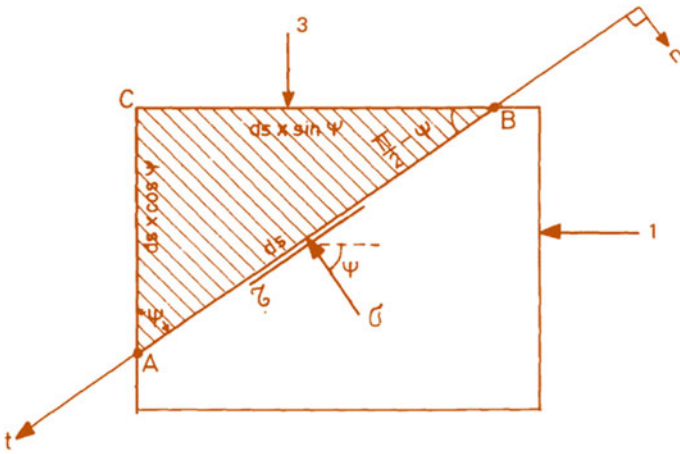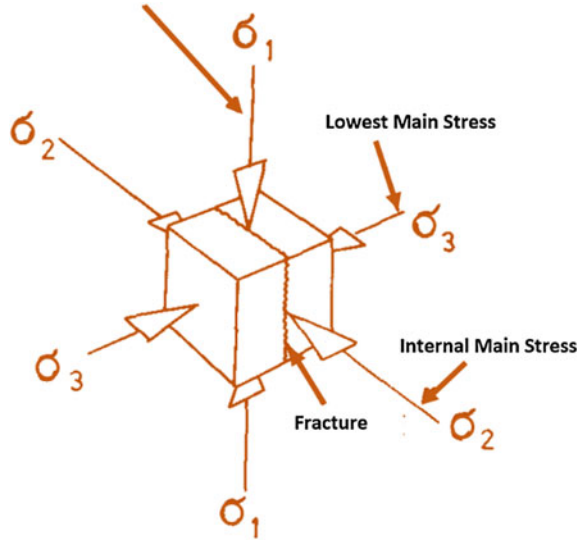**Fig. 9.2** Stress components on the plane of fracturing



**Fig. 9.3** Normal stress ($\sigma$) and shear stress ($\tau$) on a plane of angle $\psi$ (*Source* King Hubert, Courtesy AAPG)

Eqs. 9.1 and 9.2 may be modified as a function of principal stresses of $\sigma_1^*$ and $\sigma_3^*$ indicated by the directions

$$\Psi = \psi_1 \text{ and } \Psi = \psi_2 = +90°$$

If $\psi_1$, $\psi_2$, directions of the main stresses and the principal stresses, $\sigma_1^*$ and $\sigma_3^*$, are known, Eqs. 9.1 and 9.2 will become (Eq. 9.3).
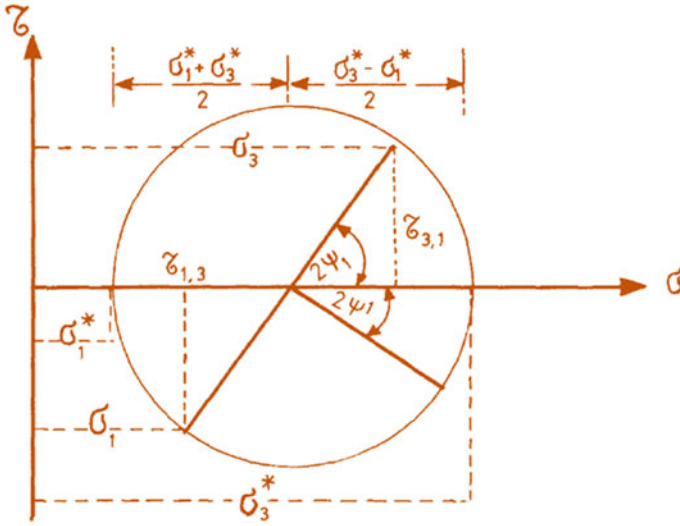
**Fig. 9.4** Mohr's diagram for σ and τ, on a plane of orientation ψ, (King Hubert', Courtesy AAPG)

$$\sigma = \frac{\sigma_1^* + \sigma_3^*}{2} + \frac{\sigma_1^* + \sigma_3^*}{2} \cos 2\psi^1 \qquad (9.3)$$

$$\tau = \frac{\sigma_1^* + \sigma_3^*}{2} \sin 2\psi^1 \qquad (9.4)$$

where,

$$\psi = \psi^1 + \psi' \qquad (9.5)$$

## 9.2  Deformational Properties

There are many significant factors what needs to be taking into consideration once we need to fracture behavior. These factors are time expressed by loading rate, formation temperature, confining pressure and rock type. The hard ductility relationship should be linked fundamentally to the rock type which will present a different behavior under similar natural conditions.

1.  Loading rate

A reduction in the strain rate will make an increase in flexibility; however, the strain rate is a function of temperature confining pressure, and rock distortion mechanism. Test observation has revealed in any circumstance that for sandstone and compressed

limestone the long period strength of formation will not differ much from the laboratory experimental data.

2. Temperature effect

Temperature impact was studied by Handin (1966). He studied rock samples in the laboratory under a different temperature ranging from 25 to 300 °C. Handin concluded that the increase in temperature is followed by a decrease in yield and final strength and an increase in flexibility. The temperature impact also appeared to be very sensitive in carbonate formations than in silicate rocks. The impact of temperature on limestone is shown in Fig. 9.5.

3. Rock Type

Numerou studies were conducted to understand the mechanical properties of sedimentary rocks, however still need more investigations to defined the relationship for different rock materials (McQuillan 1973). Generally, by increasing the confining pressure and the temperature with reducing the strain rate, an increase in flexibility will result. Both sandstone and dolomite never become flexible in the same environment as limestone. So, the change in flexibility is insignificant at shallow depth, but it's very significant at high depth.
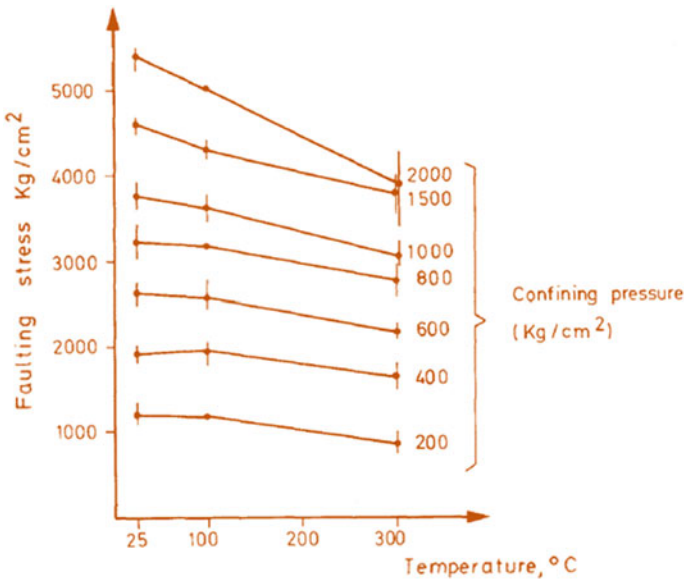


**Fig. 9.5** The impact of faulting stress and temperature on limestone formation at different confining pressures

## 9.3  Quantitative Assessment of Fracturing

Recently, there are some studies developed the quantitative evaluation procedure of fracturing. The studies focused on fracture density or the fundamental of fractures physical parameters. Two significant studies addressed the relationship between folding on fracture parameters through a mathematical mode (Murray 1977), and another studied the assessment of fracture density in certain reservoir and stress conditions (Ramstads 1977).

1. **Fractured reservoir productivity**

The reservoir productivity is depending on the fracture density in the reservoir rock. Many investigators studied the relationship between fracture porosity and permeability at bed thickness and structural curvature.

   If the thickness, h, of the folded layer is known, then the curvature of radius R can be calculated, a series of stresses should develop in the reservoir. If the cross section depicted in Fig. 9.6 displays that the fractures take place due to structural folding, then a fracture at every zone $\Delta S$ will result with increasing radius R.

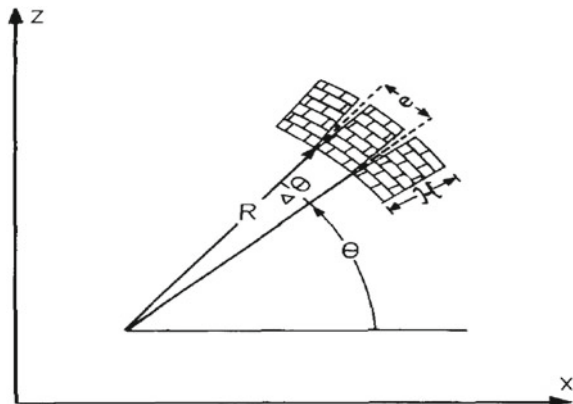(a) **Porosity of fractured formation**

Porosity is defined as pore volume divided by bulk, which could be stated by using the notations from Fig. 9.6. The fracture pore volume is (Eq. 9.6):

$$V_{pf} = \frac{[(R+H)\Delta\theta - R\Delta\theta].H}{2} = \frac{H^2\Delta\theta}{2} \tag{9.6}$$

while the bulk volume is (Eq. 9.7):

$$V_B = \frac{[(R+H)\Delta\theta - R\Delta\theta].H}{2} = \frac{2RH\Delta\theta + H^2\Delta\theta}{2} \tag{9.7}$$

**Fig. 9.6** Simplified folding cross-section (*Source* Murray 1977)

then the fracture porosity is (Eq. 9.8):

$$\emptyset_f = \frac{V_f}{V_{fB}} = \frac{H}{2R + H} \tag{9.8}$$

As R is always much larger than pay H, $(R \gg H)$ then,

$$\emptyset_f = \frac{H}{2R} \tag{9.9}$$

If $R$ is defined as the reciprocal derivative of the structural curvature slope then,

$$R = \frac{1}{\frac{d_z^2}{d_x^2}} \tag{9.10}$$

The fracture porosity can be written as (Eq. 9.11),

$$\emptyset_f = \frac{1}{2}H\left(\frac{d_z^2}{d_x^2}\right) \tag{9.11}$$

The variation of fracture porosity, $(\emptyset_f)$, is 0.1–5%, reliant on the status of solution channeling, as presented in Fig. 9.7, and also depend on the fracture spacing and width.

Sometimes, fracture porosity value can reach 7%. Correct measurement of fracture porosity is very important for the reservoir development plan. If oil is accumulated in both the matrix and fractures, then the entire original oil in place ($N_{ot}$) in the reservoir
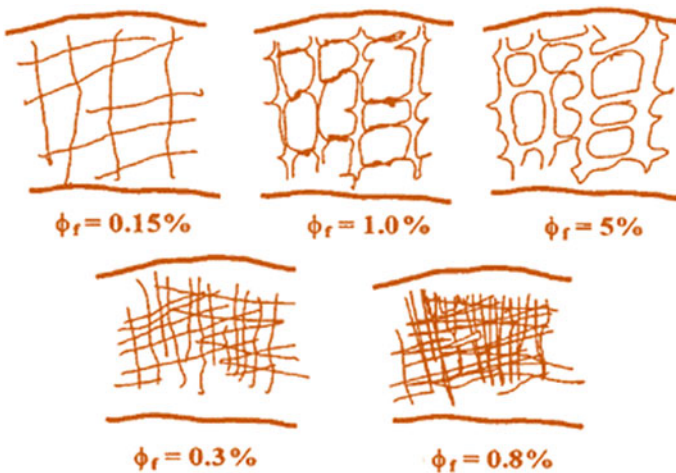


**Fig. 9.7** Variation of fracture porosity in carbonate reservoir rocks

rock can be calculated using the following equation (Eq. 9.12):

$$N_{ot}(STB) = N_{om} + N_{of} \tag{9.12}$$

where $N_{om}$ is oil volumes trapped in the matrix and $N_{Of}$ is oil volumes trapped in the fractures. As volumetric system, these two trapped accumulations can be calculated as following in STB (Eqs. 9.13 and 9.14).

$$N_{om} = \frac{7758\, A\, h\, \varnothing_m (1 - S_{wm})\left(1 - \varnothing_f\right)}{B_o} \tag{9.13}$$

$$N_{of} = \frac{7758\, Ah\, \varnothing_f \left(1 - S_{wf}\right)}{B_o} \tag{9.14}$$

where A is the surface area of the reservoir, acres; h is the average reservoir thickness, $f_t$; $\varnothing_f$ the fracture porosity, fraction; $\varnothing_m$ is the matrix porosity, fraction; Swf is the water saturation in fractures, fraction; Swm is the water saturation in matrix, fraction, and $B_o$ is the oil formation volume factor, bbl/STB.

### (b) **Permeability of fractured formation**

The fundamentals of permeability recognized in the conventional reservoir rock, still valid in the fractured reservoir case. However, in the existence of two systems (matrix and fussers), permeability termed as matrix permeability, fissure permeability and, system (fracture-matrix) permeability. These permeabilities caused misperception mainly about fracture permeability, which can be defined also as single fracture permeability or as fracture network permeability, or as fracture permeability of fracture-bulk volume.

Fracture Permeability can be estimated by using the fluid flow in a particular fracture with a variable "b" opening. The total flow rate for the whole pay zone changes from zero to H. Therefore, Q is (Eq. 9.15),

$$Q = \int_0^H dH = -\frac{1}{12\mu}\frac{dp}{dy}\int_0^H b^3 dH \tag{9.15}$$

If "$b$" differs with the pay zone via a constant "$a$". The output will be (b = aH) (Eq. 9.16),

$$Q = a\frac{a^3}{12\mu}\frac{dp}{dy}\int_0^H H^3 dH = \frac{a^3 H^4}{48\mu}\frac{dp}{dy} \tag{9.16}$$

And filtration velocity "V" for flowing section S is (Eq. 9.17),

$$V = \frac{Q}{S} = \frac{1}{S}\frac{a^3 H^4}{48\mu}\frac{dp}{dy} \tag{9.17}$$

Equations 9.11 and 9.14, the permeability can be written as (Eq. 9.18),

$$K_f = \frac{S^2}{48H^2}(H.\frac{d^2 Z}{dx^2})^3 = \frac{1}{48}e^2(H\frac{d^2 Z}{dx^2})^3 \tag{9.18}$$

Which can be further adjusted in dimensional factors (Eq. 9.19),

$$K_f = 2x10^{11}[(\frac{H}{\frac{d^2 Z}{dx^2}})]^3(H.\frac{d^2 Z}{dx^2})^3 e^2 \tag{9.19}$$

where, $K_f$ fracture permeability (md) and fracture bed interval e (feet). There are various expressions of fractures permeability that need to addressed clearly.

1. **Intrinsic fracture permeability, $K_{ff}$**

This permeability defined as measured fracture permeability during the fluid flow in a single fracture or in a fracture network. It is, actually, the conductivity of a single fracture or a group fracture network. Therefore, the flow cross section was from the open fractures areas only, but not from the surrounding matrix extent. If the fracture is parallel to the flow direction depicted in Fig. 9.8, fracture 1 is parallel to the horizontal flow direction), then flow rate in the fracture can be expressed as follows (Eq. 9.20):
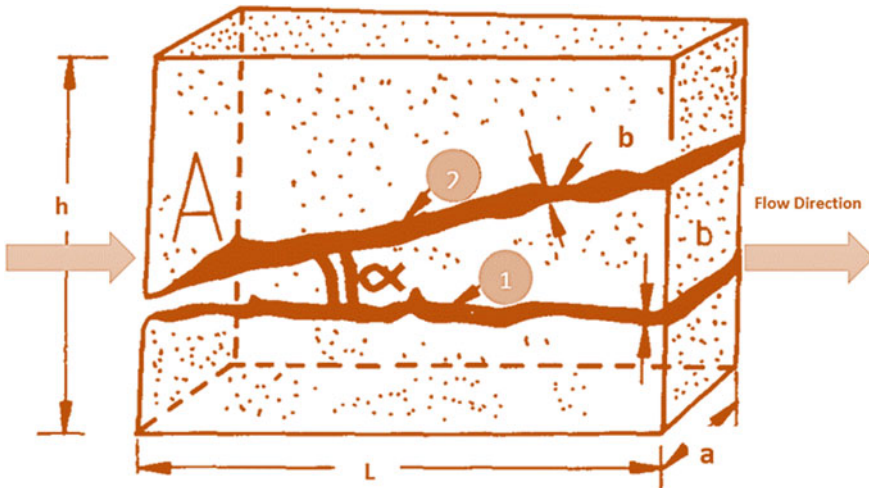


**Fig. 9.8** Fracture and matrix block having a single fracture

$$q_f = ab \frac{b^2 \cos^2 \alpha}{12\mu} \frac{\Delta P}{1} \tag{9.20}$$

Following Darcy concept, if limited to the whole cross flow section (A = ab), the flow rate is expressed by (Eq. 9.21),

$$q = A \frac{K_f}{\mu} \frac{\Delta P}{\Delta L} = ab \frac{K_f}{\mu} \frac{\Delta P}{1} \tag{9.21}$$

The additional comparison of Eqs. 9.20 with 9.21 will result the following equation (Eq. 9.22):

$$K_{ff} = \frac{b^2}{12} \cos^2 \alpha \tag{9.22}$$

For a fracture network, the intrinsic permeability is given by the following Eq. 9.23:

$$K_{ff} = \frac{1}{12} [\cos^2 \alpha \sum_1^{n\alpha} b_{\alpha i}^2 + \cos^2 \beta \sum_1^{n\beta} b_{\beta i}^2 + \cdots] \tag{9.23}$$

## 2.   Conventional fracture permeability, $K_f$

The concept of conventional fracture permeability is different from the intrinsic fracture permeability method, where this method the bulk volume of the rock associated with the single fracture or net of fractures is considered. Therefore, the flow cross section A depicted in Fig. 9.8, is not defined as A = ab, but as (Eq. 9.24),

$$A_B = ah \tag{9.24}$$

So (Eq. 9.25),

$$q = A_B \frac{K_f}{\mu} \frac{\Delta P}{1} = ah \frac{K_f}{\mu} \frac{\Delta P}{1} \tag{9.25}$$

## 3.   Permeability of fracture-matrix system

Typically, this type of permeability system may be characterized by the simple adding of the permeability of the matrix K, and the permeability of the fractures $K_f$ (Eq. 9.26),

$$K_t = K_m + K_f \tag{9.26}$$

If Eq. 9.27 denotes to the schematic defined in Fig. 9.8, it is obvious that the total permeability will subject to the flow direction. Any alteration in flow direction will change $K_f$.
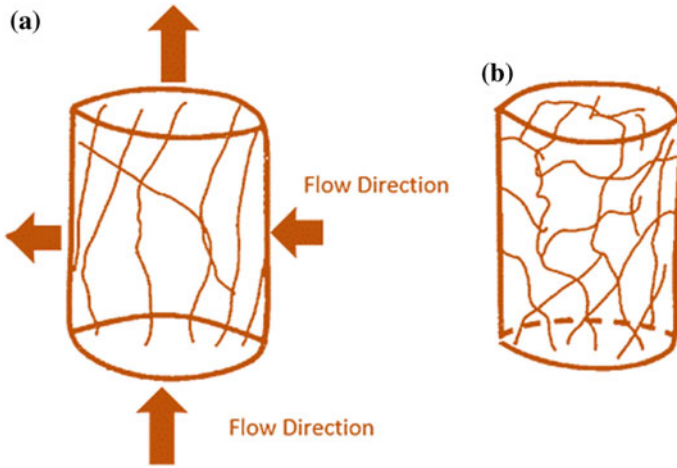
**Fig. 9.9** Core sample. **a** Oriented fractures, **b** random orientation of fractures

4. **Fracture permeability from cores**

Based on Darcy's law, the permeability of the core samples can be obtained by the following Eq. 9.27:

$$K_t = \frac{Q\mu L}{A\Delta P} \qquad (9.27)$$

By using Eq. 9.27 to determine the total permeability of the core plug showing in Fig. 9.9a, the result will be incorrect due to the existing of vertical fracture in the sample. While, for randomly fracture orientation, as showing in Fig. 9.9b, the obtained total permeability from Eq. 9.27 is more represents to the fracture-matrix system, without considering flow direction.

5. **Fracture permeability from well testing**

Typically, at radial steady-state flow to the wellbore, the permeability value can be determined by using the following classic Eq. 9.28:

$$K_t = \frac{Q\mu[\ln\left(\frac{r_e}{r_w}\right) + S]}{2\pi h \Delta P} \qquad (9.28)$$

The total permeability $K_t$ against individual permeabilities K, and $K_f$ will reliant on the reservoir model selected. The following are the most common idealized models currently used to estimate the relationship between $K_t$ and $K_m$, $K_f$. See Fig. 9.1:

1. Kazemi model (Kazemi 1969): modeled by different horizontal layers of matrix and fractures as seen in Fig. 9.10a.
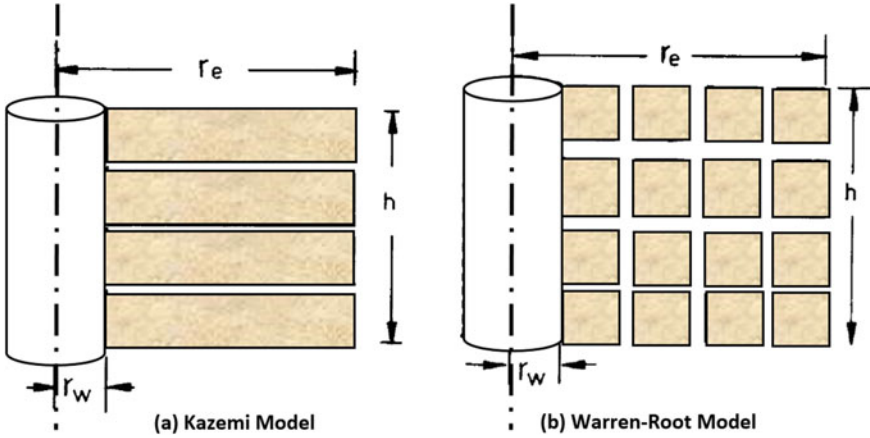
Fig. 9.10   Radial flow models. **a** Kazemi model, **b** Warren-Root model

2. Warren-Root model (Warren 1963): modeled by a number of matrix blocks crossed by an orthogonal network of fractures as shown in Fig. 9.10b.

In the Kazemi model the flow through the beds with different permeabilities will use the following Eq. 9.29:

$$K_t = K_m + K_f = K_m + K_{ff} \frac{n\,b}{h} \qquad (9.29)$$

In the Warren-Root model, the flow mechanism is very different. The matrix blocks always feed the fractures, then the fluid flows to the wellbore over the fracture network. In this case, the total permeability is the same fracture permeability (Eq. 9.30):

$$K_t = K_f \qquad (9.30)$$

(c) **Minimum fracturing stress**

The lowest stress required (Van Golf-Racht and Ramstad 1976) to progression fractures is described by the following relationship (Eq. 9.31):

$$\sigma_1 > E\left(\frac{d^2 Z}{d_{X^2}}\right) \qquad (9.31)$$

where:

E = Elasticity modulus.

## 9.4  Indicators of Natural Fractures

Numerous researchers indicated that fractures can change the matrix porosity and the permeability of the formation. If the natural fractures or interconnected vugs are occupied with secondary minerals, they may confine the flow. But, normally open fractures improve the isolated rock porosity which eventually increases the hydro-carbon recovery. Therefore, it's very important to determine the fracture distribution to evaluate reservoir performance. Typically, fractures can create about 1% of the porosity.

Estimating the reservoir rock porosity and permeability at early stages of the project will improve the selection of the locations and number of wells required in the field development plan. There are some researchers (Friedman and Stearns 1978) studied several methods to identify and evaluate naturally fractured reservoirs. Some of these approaches are as follow refer to Fig. 9.11:

1. Mud Loss circulation and a rise in drilling penetration rate (Fig. 9.11).
2. The availability of fractures and solution channels in cores give valuable information about the nature of a reservoir rock.
3. Logging tools are used to identify the lithology, fluid saturations, and porosity, but not to natural fractures.
4. Pressure buildup and drawdown tests in naturally fractured provide a good indication of fractures availability in the reservoir depicted in Fig. 9.12.
5. High amplitude feature which penetrates different zones, is an identification of present natural vertical fractures in a non-deviated borehole.
6. Downhole cameras and photographic, are applied to identify fractures and solution channels.
7. Productivity index is a very good indicator to prove the presences of natural fracture in the reservoir.
8. The significant improvement in well production when stimulation the well is the best indication of a naturally fractured reservoir.

There is no single approach applied alone to proof of the existence of fractures in the formation. Wellbore logs and televiewers normally provide a good indication of the attendance of features. However, they do not indicate the minor fracture systems.
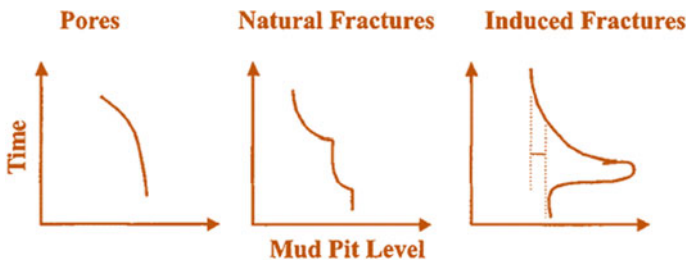


**Fig. 9.11**  Mud pit loss indication in pores, natural fractures, and induced fractures
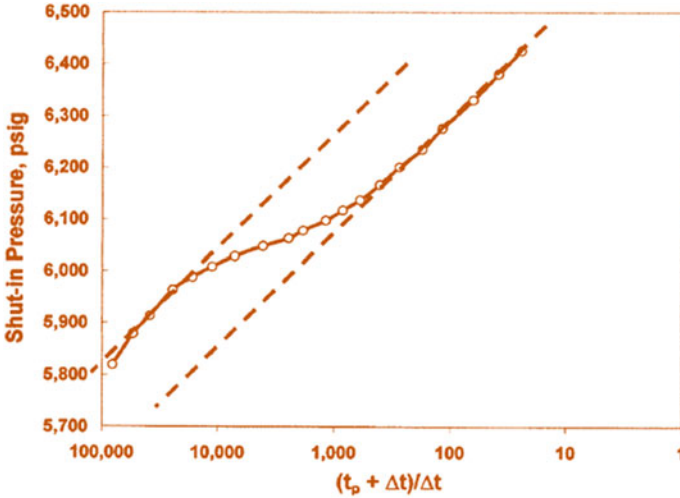
Fig. 9.12 An indication of existing natural fracture using pressure buildup test analysis

## 9.5 Area of Fractures

Typically, the internal surface area of the fracture is donated as $S_{pv}$, and the surface area for the number of fractures is defined as:

$$n(2w_fL + 2h_fL) = 2n(w_f + h_f)L \text{ and}$$

The pore volume is $n(w_f \, h_f \, L)$, assuming the fracture delivers all of the storing and permeability shown in Fig. 9.13. The particular surface area of the fracture per unit pore volume is expressed as (Eq. 9.32):

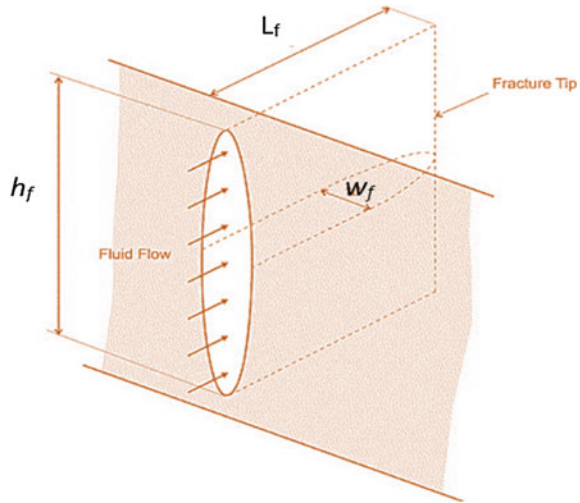$$S_{vp} = \frac{2n(w_f + h_f)L}{2nw_fh_fL} = 2\left(\frac{1}{h_f} + \frac{1}{w_f}\right) \tag{9.32}$$

By applying the same assumptions, the surface area per unit grain volume is (Eq. 9.33):

$$S_{gv} = \frac{2n(w_f + h_f)L}{AL(1 - \emptyset)} \tag{9.33}$$

The equation can be simplified by multiplying and dividing by $W_f \, h_f$ (Eq. 9.34):

$$S_{gv} = \frac{2nw_fh_f}{AL(1 - \emptyset)}\left(\frac{1}{h_f} + \frac{1}{w_f}\right) \tag{9.34}$$

**Fig. 9.13** Diagram shows
the fracture shape



## 9.6   Fluid Saturation in a Fractured Reservoir

Typically, the matrix fluid saturation in a fractured reservoir has the same challenges
to that of not a fractured reservoir. The methodology used to determine the fluid
saturation in the fractured reservoir is the same procedure either using logs or in the
laboratory.

The low the secondary porosity value (dual porosity) compared with the primary
porosity, does not affect hydrocarbons saturation. Normally, the saturation in frac-
tures can be assumed 100% with the fluids (100% oil zone or 100% water zone).
However, the issue here is the fluid saturation in a fractured must be tested as a dou-
ble porosity system. Therefore, the link between matrix saturation versus fracture
saturation is demonstrated by a series of characteristics.

1. **Absent of transition zones in a fractured formation**

In fractured formation, the identification of the zones in the reservoir is obtained
by the fluid distribution in the fracture system. The gravity forces in the fractured
reservoir are more significant than the capillary pressure forces (neglected). There-
fore, the fluid contacts in the fracture network system will be identified by a distinct
horizontal level over the whole reservoir seen in Fig. 9.14.

2. **High water saturation zones in the fractured reservoir are unrelated to
   water-oil contact**

If the reservoir rock fractured before the hydrocarbon migration, then this might
cause variations in water saturation within the hydrocarbon zone which are separate
from the water table and transition zone.

To display the inconsistent characteristic of water saturation versus depth,
Fig. 9.14 demonstrates the locations of the two well penetrating fractured network
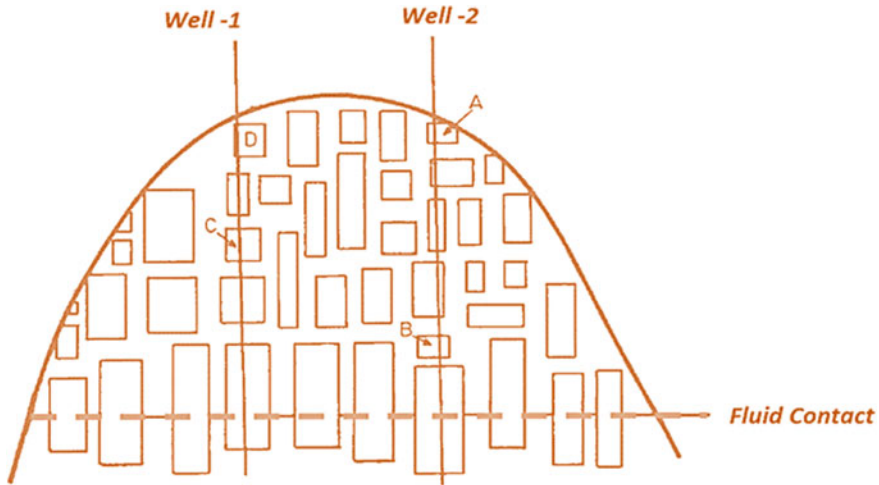
**Fig. 9.14** Schematic showing fractured networks with different type of matrix

reservoirs. Matrix porosity is considered to be constant, but due to the fracture process, the average height of the matrix blocks is different. In this example, the higher water saturation is found in the small blocks (A, B, C, and D). As the blocks are far away from the transition zone, then it's useless to do any correlation of fluid contacts between the wells (Van Golf-Racht 1982).

On the other hand, the gravity forces in the larger blocks that have bigger heights, are greater than capillary forces where their matrix are fully saturated with hydrocarbons. It is clear that the capillary pressure force, the height of the matrix block, and fracture density are governing the fluid saturation distribution over a fractured reservoir system.

## 9.7 Relationship of Permeability Versus Porosity in a Fracture Network System

Typically, the rock properties in the fractured reservoir are completely different from a conventional reservoir, then the reservoir evaluation process must be different. this is because the fractured reservoir has a different form of permeability and porosity relationship (primary and secondary properties). Therefore, the relationship between the porosity and permeability in the fracture network system need other methods.

To categorize this problem, a simplified model which may be related to any particular reservoir flowing problems or might be observed from the results obtained from well testing depicted in Fig. 9.15.
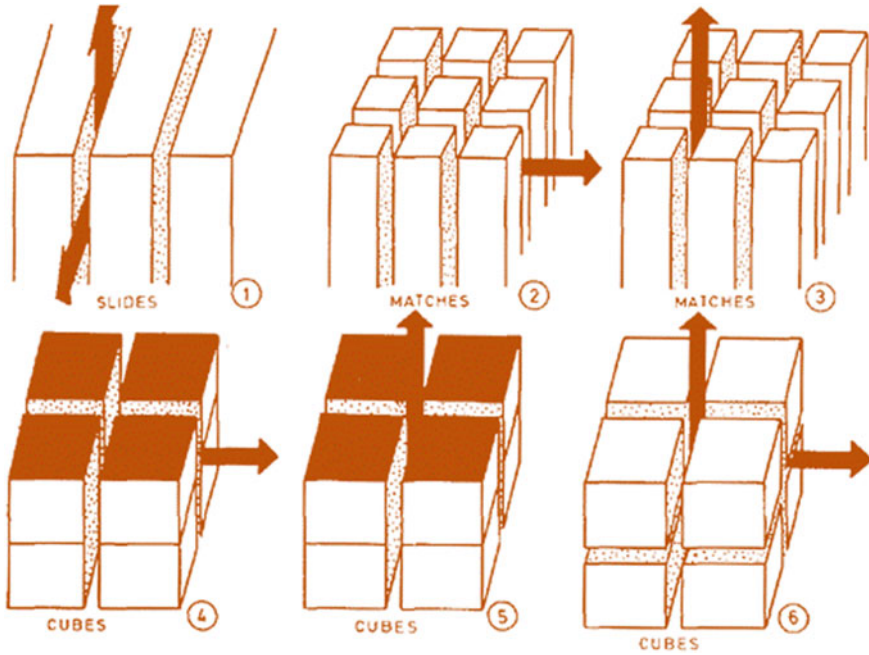
**Fig. 9.15** Simplified models of matrix blocks (*Source* Reiss 1976)

## 9.8 Compressibility in a Fractured Rock

Compressibility is a very important parameter in fractured reservoir system mostly because of the large difference between the matrix and fractures porosities. The compressibility is very important in the analysis of the transient pressure performance obtained from well testing. In this case, compressibility related to the double porosity system is defined by the storage capacity parameter which strongly controls pressure performance.

In a fractured reservoir system, both primary porosity [matrix (m)] and secondary Porosity [Fractures (f), vugs (v), and cavities (c)] are considered in the fractured rock compressibility as follows (Eq. 9.35):

$$C_t = C_m + \emptyset_c C_c + \emptyset_f C_f + \emptyset_v C_v \tag{9.35}$$

Commonly, the compressibility of vugs and caverns are approximated as, $C_V \approx 3C_m$. The following equation (Eq. 9.36) describe the compressibility for secondary porosity in carbonate reservoir rock ($C_{psp}$)

$$C_{psp} \approx \left[ \left( \frac{\emptyset_f}{\emptyset_{ts}} \frac{1350}{\sigma - P} \right) - 0.09 \right] 10^{-4} \tag{9.36}$$
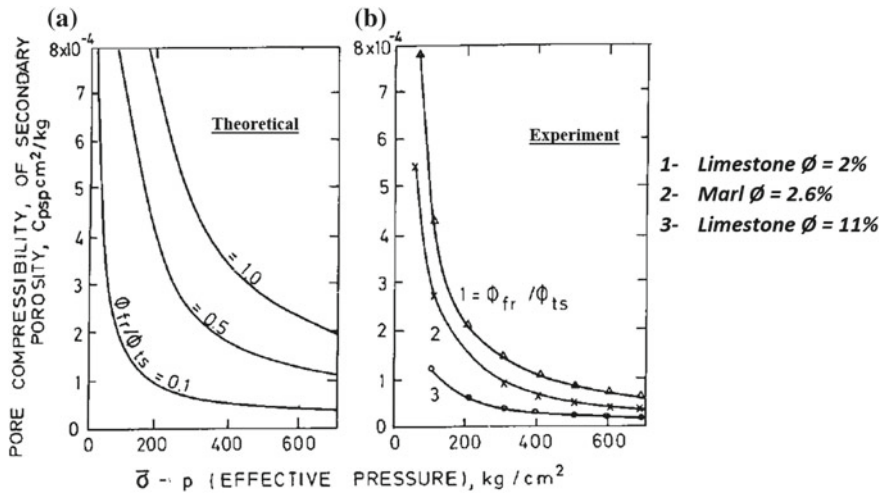
**Fig. 9.16**  Pore compressibility versus effective pressure, **a** theoretical relationship, **b** experimental relationship

where: $Q_{ts}$ is total secondary porosity, fraction, and P is the pressure, kg/cm$^2$. The $\varnothing_f/\varnothing_{ts}$ is described as a fraction of the total secondary porosity versus $C_{psp}$ (Eq. 9.36). The experimental trend approves the theoretical method, Fig. 9.16.

## 9.9   Relative Permeability in a Fractured Reservoir

Normally, the fluid relative permeabilities in a conventional reservoir rock are determined from special core analysis. But, in a fractured reservoir system, assessment of relative permeability curves more complex due to the presence of the double porosity in the reservoir system. There are numerous of relative permeability studies were conducted on heterogeneity reservoir, but not many studies were carried out on the fractured reservoir system.

As the performance of relative permeability versus heterogeneity can be applied as a standard method of a fractured reservoir system, then it is interesting to test in the laboratory the effect of flooding rate and wettability in a heterogeneous reservoir (Huppler 1970). By using water flooding to assess the relative permeability in heterogeneous reservoir rocks, shows a sort of uncertainty if water breakthrough occurs at the early stage of the production time. Therefore, the form of the fracture-matrix relative permeability curve will look like an anomalously shaped curve shown in Fig. 9.17.

In the case of continuity of fluid flow in matric and in the fractures, the relative permeability shape curve will be similar to the shape shown in Fig. 9.18 (Braester 1972). Where the shape shows a variation of relative permeability curves of oil and
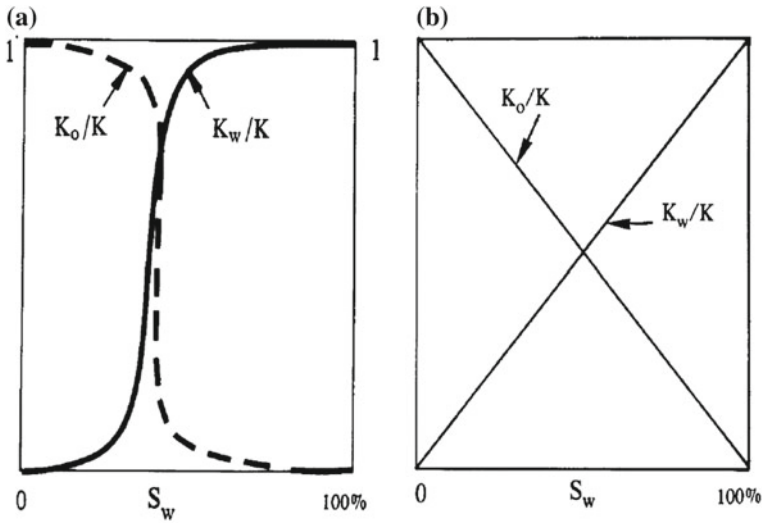
**Fig. 9.17** Relative permeability curve for fracture reservoir rocks. **a** Fractures not along core axis; **b** fractures along the core axis (*Source* Van Golf-Racht 1982)
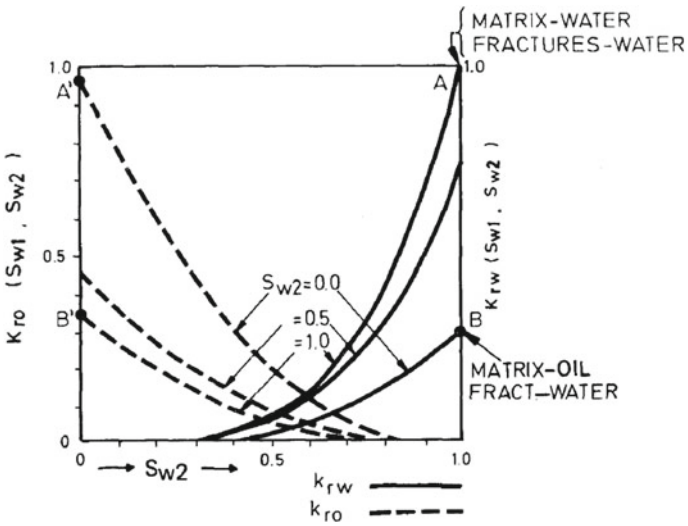


**Fig. 9.18** Relative permeability of a matrix-fracture reservoir unit (*Source* Braester 1972)

water as a function of water saturation, and the relationship between permeabilities is similar to the Corey equations as seen the following equations (Eqs. 9.37 and 9.38):

$$K_{ro} = \left[\frac{K_2}{K} + \left(1 - \frac{K_2}{K}\right)(1 - s_{w1})^2(1 - s_{w1})^2\right](1 - s_{w2})^2(1 - s_{w2})^2 \qquad (9.37)$$

$$K_{rw} = \left[\frac{K_2}{K} + \left(1 - \frac{K_2}{K}\right)s_{w2}^4\right]s_{w2}^4 \qquad (9.38)$$

## 9.10  Capillary Pressure Curve in Fracture Formation

Capillary pressure force is another important parameter in a fractured reservoir system. Capillary forces are very fundamental component of the reservoir flow driving mechanism. The capillary pressure play strong role in the displacement process in either imbibition process, or in drainage displacement process. Normally, the capillary reservoir controls the fluid distribution in the reservoir, where the transition layer is located between the water oil contact and the oil layer. However, this phenomenon does not exist in the fracture reservoir system.

The break of the small individual matrixes in the fracture network reservoir clarifies why the water table is only connected to the fracture network. Besides, as the fractures are big channels with insignificant capillary forces, the transition zone vanishes in a fractured reservoir system, and water-oil contact turns into a horizontal plane. Also, the static and dynamic equilibrium of the matrix blocks is controlled by both capillary forces and gravitational forces. Water-oil contacts in fractures, along with the oil water contacts inside the matrix blocks, are important reference planes for the assessment of the reservoir driving mechanism of both capillary pressure and gravity forces. As an example, Fig. 9.19 shows the clarification of reference levels in fractures and matrix through imbibition displacement process.

## 9.11  Summary

A strong basis in reservoir rock properties is the backbone for most of the engineering activities in the petroleum industry. A reservoir rock property gives a well-balanced illustration of basic perception that includes this huge subject area. This book covers a variety of rock properties, and various laboratory measurement techniques.

This book reviews the properties of reservoir rocks, to the degree that of direct relevance for oil and gas reservoirs engineering. The main purpose is to introduce the rock properties and therefore, emphasis placed on concepts and underlying physics. The chapter describes how the ability of reservoir rocks to store and transmit fluids,
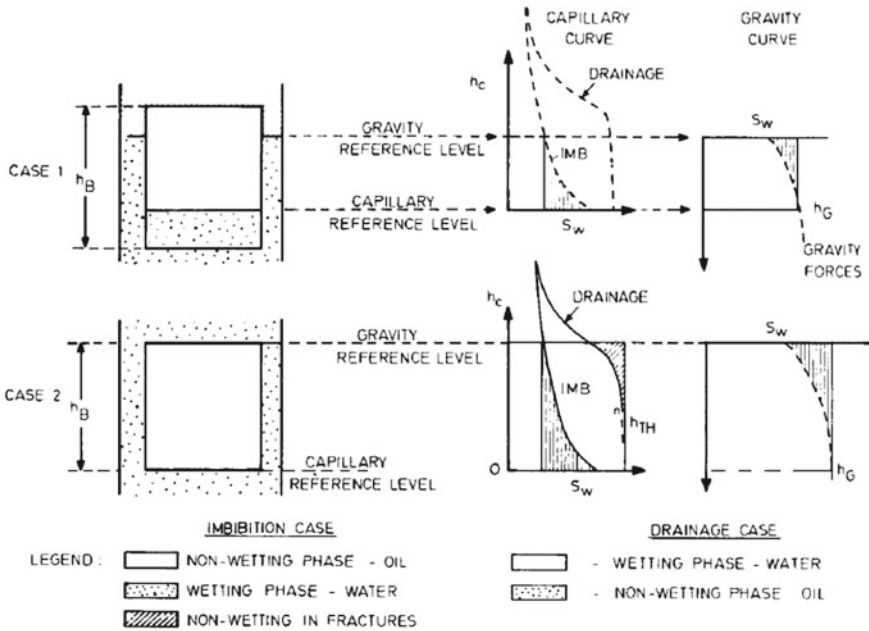
**Fig. 9.19** Diagram showing reference levels in fractures and matrix through imbibition displacement process (*Source* Van Golf-Racht 1982)

it shows how the petrophysical rock properties of porosity, permeability, relative permeability, and fluid saturations are connected together through aperture size. Where aperture size is linked to the size and sorting of the grains that form the structure of the rock. Oil and water saturations are dependent on the aperture size, porosity, and capillary pressure. Where, the capillary pressure is a function of reservoir height through the density difference of the existing fluids. Also, the permeability is related to the porosity and aperture size. Relative permeability is related to the absolute permeability and fluid saturation, which are both related to aperture size.

The book also reviews the Relationship between Relative Permeability, Capillary Pressure, and Fractional Flow.

The book covers most of the unconventional natural resource definitions and assessment, and discussed petroleum accumulation, reservoir fluids quantifications, formation evaluation, and applications used to develop unconventional reservoirs. Finally, last part of the book addressed the fracture reservoir and explains the most types of fractures along with the fracture rock properties. In general, the book is practical to everyone has engineering experience.

The text describes the significancy of rock properties in petroleum engineering systems. Input references, mathematical terms, and laboratory measurement methodology demonstrate the major influence and relationships between all rock properties.

# References

Braester C (1972) Simultaneous flow of immiscible liquids through porous fissured media. J Pet Technol 297–303

Friedman G, Sanders J (1978) Principles of sedimentology. Wiley, New York

Handin J (1966) Strength and ductility. In: Handbook of physical constants, vol 97. Geol Soc America Mem, pp 223–289

Huppler J (1970) Numerical investigations of the effects of core heterogeneities on waterflood relative permeabilities. Soc Pet Eng J 10(4):381–392

Kazemi H (1969) Pressure transient analysis of naturally fractured reservoir with uniform fracture distribution. Soc Pet Eng J 90(4):451–462

McQuillan H (1973) Small- scale fracture density in Asmari formation of southwest Iran and its relation to bed thickness and structural setting. Am Assoc Pet Geol Bull V45(1):1–38

Murray G (1977) Quantitative fracture study, Sanish Pool. In: Fracture-controlled production, AAF'G Reprint Series 21

Ramstad L (1977) Geological modelling of fractured hydrocarbon reservoirs. University of Trondheim, report No. 774

Reiss L (1976) Reservoir engineering in fractured reservoirs. French Institute of Petroleum

Van Golf-Racht T, Ramstad L (1976) Modelling North Sea fractured limestone reservoir. Offshore North Sea proceedings, Stavanger, Noway

Van Golf-Racht T (1982) Fundamentals of fractured reservoir engineering—Developments in petroleum science, No. 12. Amsterdam, Elsevier Scientific Publishing Co., 710 p

Warren J, Root P (1963) The behaviour of naturally fractured reservoirs. Soc Pet Eng J 3(3):245

# Summary

A strong basis in reservoir rock properties is the backbone for most of the engineering activities in the petroleum industry. A reservoir rock property gives a well-balanced illustration of basic perception that includes this huge subject area. This book covers a variety of rock properties, and various laboratory measurement techniques.

This book reviews the properties of reservoir rocks, to the degree that of direct relevance for oil and gas reservoirs engineering. The main purpose is to introduce the rock properties and therefore, emphasis placed on concepts and underlying physics. The chapter describes how the ability of reservoir rocks to store and transmit fluids, it shows how the petrophysical rock properties of porosity, permeability, relative permeability, and fluid saturations are connected together through aperture size. Where aperture size is linked to the size and sorting of the grains that form the structure of the rock. Oil and water saturations are dependent on the aperture size, porosity, and capillary pressure. Where, the capillary pressure is a function of reservoir height through the density difference of the existing fluids. Also, the permeability is related to the porosity and aperture size. Relative permeability is related to the absolute permeability and fluid saturation, which are both related to aperture size.

The book also reviews the Relationship between Relative Permeability, Capillary Pressure, and Fractional Flow.

The book covers most of the unconventional natural resource definitions and assessment, and discussed petroleum accumulation, reservoir fluids quantifications, formation evaluation, and applications used to develop unconventional reservoirs. Finally, last part of the book addressed the fracture reservoir and explains the most types of fractures along with the fracture rock properties. In general, the book is practical to everyone has engineering experience.

The text describes the significance of rock properties in petroleum engineering systems. Input references, mathematical terms, and laboratory measurement methodology demonstrate the major influence and relationships between all rock properties.

# Bibliography

Abeysinghe K, Fjelde I, Lohne A (2012) Dependency of remaining oil saturation on wettability and capillary number. Paper SPE 160883 presented at the SPE Saudi Arabia Section technical Symposium and Exhibition, Al-Khobar, pp 8–11

Chitale V, Gbenga A, Rob K, Alistair T, Paul (2014) Learning from deployment of a variety of modern petrophysical formation evaluation technologies and techniques for characterization of a pre-salt carbonate reservoir: case study from campos basin, Brazil. Presented at the SPEWLA 55th Annual Logging Symposium Abu Dhabi, 18–22 May. SPWLA-2014-G

Geffen T, Owens W, Parrish D et al. (1951) Experimental investigation of factors affecting laboratory relative permeability measurements. J Pet Technol 3(4):99–110. SPE-951099-G. http://dx.doi.org/10.2118/951099-G

Islam M, Berntsen R (1986) A dynamic method for measuring relative permeability. J Can Pet Technol 25(1):39–50. 86-01-02. http://dx.doi.org/10.2118/86-01-02

Irmann-Jacobsen, Tine B (2013) Flow assurance—a system perspective. MEK4450-FMC Subsea technologies. [http://www.uio.no/studier/emner/matnat/math/MEK4450/h11/undervisningsmateriale/modul5/MEK4450_FlowAssurance_pensum-2.pdf]

John H, Black J (1983) Fundamentals of relative permeability: experimental and theoretical considerations. In: SPE annual technical conference and exhibition, San Francisco, California, 5–8 Oct. https://doi.org/10.2118/12173-MS

Jacco HS, Bruno A (2008) A microscopic view on contact angle selection. Phys Fluids 20:057101. https://doi.org/10.1063/1.2913675

King H, Willis D (1972) Mechanics of hydraulic fracturing. American Association of Petroleum Geologists. Reprinting series, vol 21

Lock M, Ghasemi M, Mostofi V, Rasouli (2012) An experimental study of permeability determination in the lab. WIT Trans. Eng. Sci. 81. Department of Petroleum Engineering, Curtin University, Australia. http://dx.doi.org/10.2495/pmr120201

Oak M, Baker L, Thomas D (1990) Three-Phase relative permeability of berea sandstone. J Pet Technol 42(8):1054–1061. SPE-17370-PA. http://dx.doi.org/10.2118/17370-PA

Oil sand Magazine, https://www.strausscenter.org/energy-and-security/tar-sands.html. https://www.strausscenter.org/energy-and-security/tar-sands.html

Steve S, Larry M (2017) Our current working model for unconventional tight petroleum systems: oil and gas. http://www.searchanddiscovery.com/documents/2017/80589sonnenberg/ndx_sonnenberg.pdf

Smith J, Jensen H, (2007) Oil shale. In: McGraw Hill encyclopedia of science & technology, 10th edn, vol 12. McGraw-Hill, pp 330–335

Terra G et al (2010) Carbonate rock classification applied to Brazilian sedimentary basins. Boletin Geociencias Petrobras 18(1):9–29

Van Golf-Racht T, Ramstad L (1976) Modelling North Sea fractured limestone reservoir. Offshore
    North Sea proceedings, Stavanger, Noway
Xu T, Hoffman BT (2013) Hydraulic fracture orientation for miscible gas injection EOR in
    unconventional oil reservoirs. Paper SPE 168774 / URTeC 1580226 presented at the uncon-
    ventional resources technology conference, Denver, Colorado, 12−14 Aug. http://dx.doi.org/10.
    2118/168774